ERCB

Overview of Airborne-Electromagnetic and -Magnetic Geophysical Data Collection Using the GEOTEM® Survey Near Three Hills and Cochrane, Alberta

Energy Resources Conservation Board

AGS
Alberta Geological Survey

Overview of Airborne-Electromagnetic and -Magnetic Geophysical Data Collection Using the GEOTEM® Survey near Three Hills and Cochrane, Alberta

S.R. Slattery[1] and L.D. Andriashek[2]

[1] Formerly of Alberta Geological Survey (see page ii for current address)
[2] Energy Resources Conservation Board Alberta Geological Survey

June 2012

Author address:
Shawn Slattery
Syncrude Canada Ltd.
P.O. Bag 4009, M.D. A 250
Fort McMurray, AB T9H 3L1
Canada
Tel: 780.715.9579
E-mail: slattery.shawn@syncrude.com

Contents

Table

Figures

Acknowledgements

Abstract

This report is one in a series of eight Alberta Geological Survey (AGS) Open File reports that provide an overview of airborne electromagnetic and magnetic geophysical surveys completed over the Edmonton–Calgary Corridor (ECC) by Fugro Airborne Surveys. These surveys were completed between November 2007 to February 2010 as part of a joint AGS and Alberta Environment and Sustainable Resource Development (ESRD) study to determine the usefulness of the RESOLVE®, GEOTEM® and TEMPEST® geophysical survey techniques in mapping the distribution and physical attributes of sediment- and bedrock-aquifer complexes over areas of formerly glaciated terrain.

The ECC was selected as the first test area to support the AGS-ESRD groundwater mapping program as it represents the region with the highest rates of industrial and urban growth in the province. Since this growth will exert increasing demands on water resources in the ECC, it is necessary to reassess the spatial distribution of previously mapped, as well as unmapped, aquifer complexes in the region. By doing so, Alberta may better predict and manage current and/or future stresses on existing aquifer systems caused by industrial, agricultural and urban development. Airborne geophysical survey methods were selected as one of the tools in completing this assessment.

The ECC is an ideal area to evaluate the usefulness of airborne electromagnetic and magnetic geophysical survey techniques due to the wealth of existing surficial and subsurface geological datasets (i.e., geological mapping, lithologs, petrophysical data, field observations, etc.). These datasets provide users with a means to calibrate and verify airborne geophysical data, analyses and interpretations within the ECC.

This report describes data collection methods using the Fugro Airborne Surveys' GEOTEM® survey techniques and data processing completed for two study blocks near Three Hills and Cochrane, Alberta.

1 Introduction

In recognition of increasing rates of urbanization and industrialization in Alberta, and the foreseeable pressures that this will have on existing water supplies, the Alberta Geological Survey (AGS) in partnership with Alberta Environment and Sustainable Resource Development (ESRD) has initiated a multiyear project to characterize nonsaline aquifer complexes within the province. The Edmonton–Calgary Corridor (ECC), the region with the most industrial and urban development in Alberta, was selected as the first study area by AGS and ESRD (Figure 1).

It is inevitable that future groundwater usage in the ECC will place additional stress on existing aquifer systems. Therefore, reassessing previously mapped aquifers, potentially locating unmapped aquifers and implementing management strategies that ensure groundwater resources exist for future use are essential. As management strategies and decision-making tools will require more accurate geological and hydrogeological models, innovative approaches to data collection will be required. In complicated geological terrains, such as the ECC, where hydraulic pathways within glacial sediments and between glacial sediments and underlying bedrock formations are poorly understood, continuous high-resolution geological mapping of both glacial sediments and bedrock formations is necessary to better understand and illustrate the architecture of geological strata. A better understanding of the geological architecture within the ECC will allow for improved geological modelling, which in turn will allow for a better hydrogeological model of the ECC. It is anticipated that this model will form the cornerstone for numerous applications, such as groundwater exploration programs, aquifer protection studies and significant recharge area identification. More importantly, this model will form the framework for groundwater-flow modelling exercises and future water-budget calculations leading to improved water management decisions.

Recognizing the need for high-quality regional geological data, AGS and ESRD have collaborated to obtain airborne geophysical survey data for near-continuous coverage of the ECC. A similar approach has been taken in other areas of formerly glaciated terrain by geological surveys in the United States, Europe and the United Kingdom (cf., Smith et al., 2003, 2006, 2007; Lahti et al., 2005; Wiederhold et al., 2009). Despite the success of these surveys in mapping the distribution of near-surface and subsurface aquifers, one of the main objectives of our investigation is to evaluate and compare the usefulness of these same types of airborne geophysical survey techniques in mapping the distribution of aquifers in the ECC.

Between November 2007 and February 2010, airborne-electromagnetic (AEM) and airborne-magnetic (AM) surveys were completed by Fugro Airborne Surveys over 11 study blocks in the ECC on behalf of AGS and ESRD. The airborne-geophysical surveys were undertaken using one or a combination of the following survey techniques: fixed-wing, GEOTEM® or TEMPEST® time-domain or helicopter-borne, RESOLVE® frequency-domain (Figure 2a).

This report provides an overview of data collection using the GEOTEM® time-domain survey technique, data processing and the interpretation of data completed over two study blocks near Three Hills and Cochrane, Alberta (Figure 2b). Information on GEOTEM® and TEMPEST® time-domain and/or RESOLVE® frequency-domain airborne-geophysical survey techniques completed over the remaining survey blocks in the ECC are presented in separate Open File reports (Slattery and Andriashek, 2012a–g).

2 Purpose and Scope

The reasons for completing AEM and AM geophysical surveys in the ECC are multifaceted. First, it is to evaluate the effectiveness of frequency- and time-domain geophysical surveys to determine the spatial distribution of near-surface and subsurface electrical and magnetic properties of sediments and bedrock. It
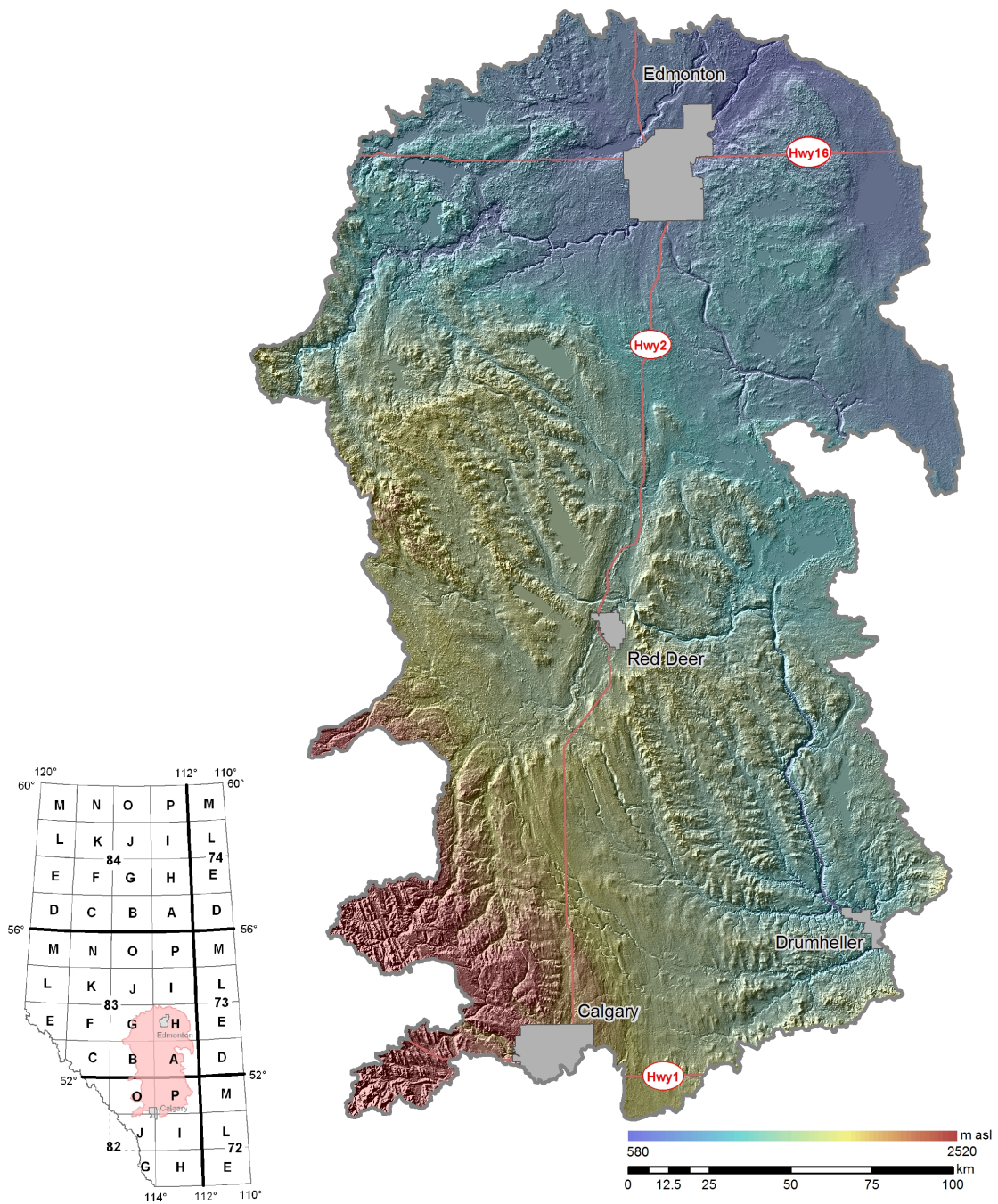
Figure 1. Digital elevation model (DEM) accented by hillshaded relief of surface topography of the Edmonton–Calgary Corridor (ECC), Alberta. Elevation of surface topography in metres above sea level is defined by colour ramp. Vertical exaggeration is 20x. Inset map depicts location of the ECC, Alberta.
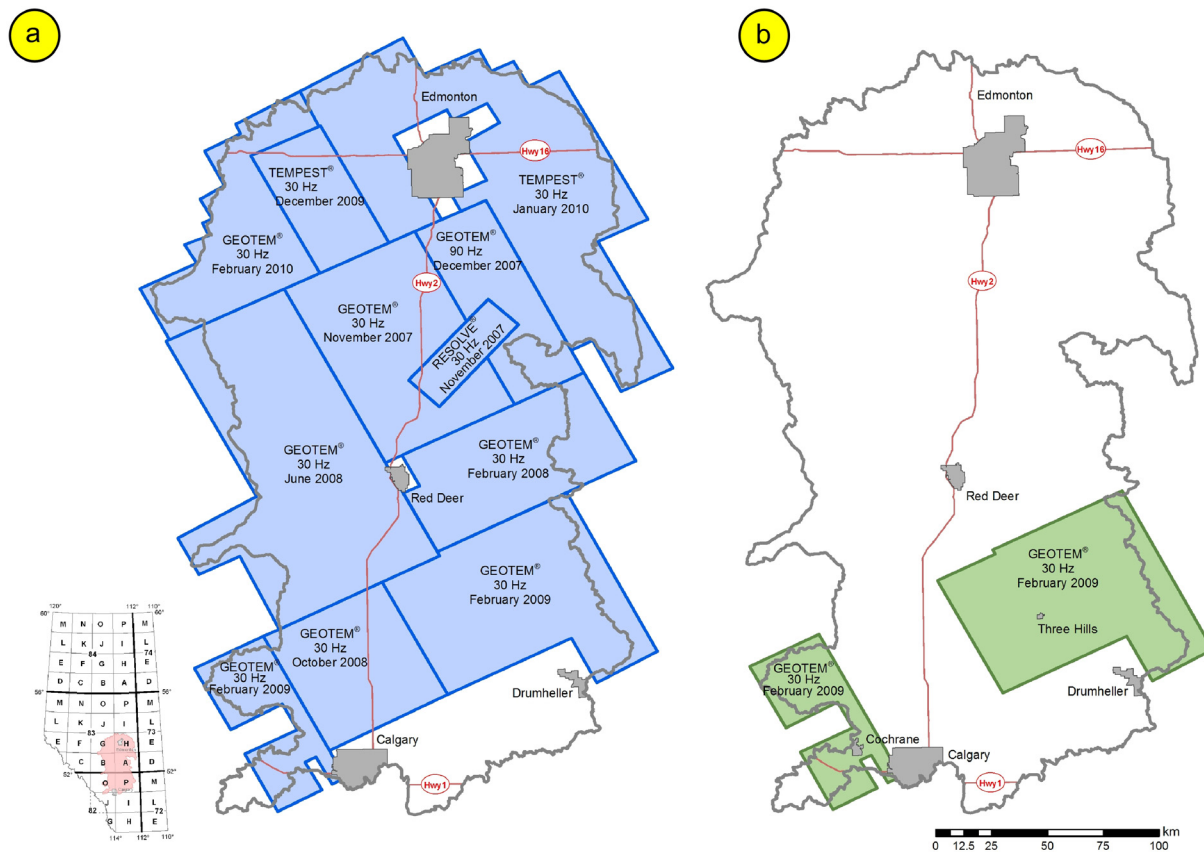
Figure 2. a) Location of the 11 geophysical survey blocks in the Edmonton–Calgary Corridor (ECC), Alberta. The type of geophysical survey completed and when it was completed are provided on each survey block. b) Location of the two survey blocks near Three Hills and Cochrane, Alberta, discussed in this report. Inset map depicts the location of the ECC, Alberta.

is anticipated that these properties will be related to geological and hydrogeological features in the ECC, which will provide a better understanding of the geological architecture. This, in turn, will allow for more accurate geological and hydrogeological models to support improved water management decisions.

Second, the selection of the ECC for AEM and AM surveying was influenced by the widespread availability of existing surface and subsurface geological and geophysical data in the region (Table 1). These data are needed to validate the results and interpretations of the AEM and AM survey data. If the interpretation of AEM and AM survey data correlates with geological data and ground and downhole geophysical data, then AEM and AM surveying techniques could be used to interpret the geological framework in those areas that have limited subsurface geological and geophysical data. In such areas, AEM and AM surveys may provide a more time- and cost-efficient means to acquire continuous, high-quality geological data than traditional drilling methods and geological mapping investigations.

Third, the geological setting of the ECC is such that aquifer complexes can occur at various depths and have a variety of sediment and rock properties. Low-frequency (30 and 90 hertz [Hz]), GEOTEM® time-domain surveys were completed to provide greater penetration depths and summary electromagnetic (EM) and magnetic data to improve the delineation of regional-scale geological strata in the ECC. The AGS and ESRD tested the RESOLVE® frequency-domain survey in areas where more detailed resolution of the near-surface geology was required. A simplified cross-section of the geological setting is depicted in Figure 3.

Table 1. Data sources and types available to validate airborne-electromagnetic (AEM) and airborne-magnetic (AM) geophysical data in the Edmonton–Calgary Corridor, Alberta. Abbreviations: ESRD, Alberta Environment and Sustainable Resource Development; AGS, Alberta Geological Survey; ERCB, Energy Resources Conservation Board.

Data Source	Data Class	Number of Data Points
ESRD digital water-well database	Water-well records and litholog records	234 902
AGS geotechnical database	Geotechnical borehole records	1202
ERCB oil-and-gas–well database	Oil-and-gas–well and petrophysical records	5161
AGS borehole database	Geological borehole and petrophysical records	363
AGS field observations	Field-based geological data	322
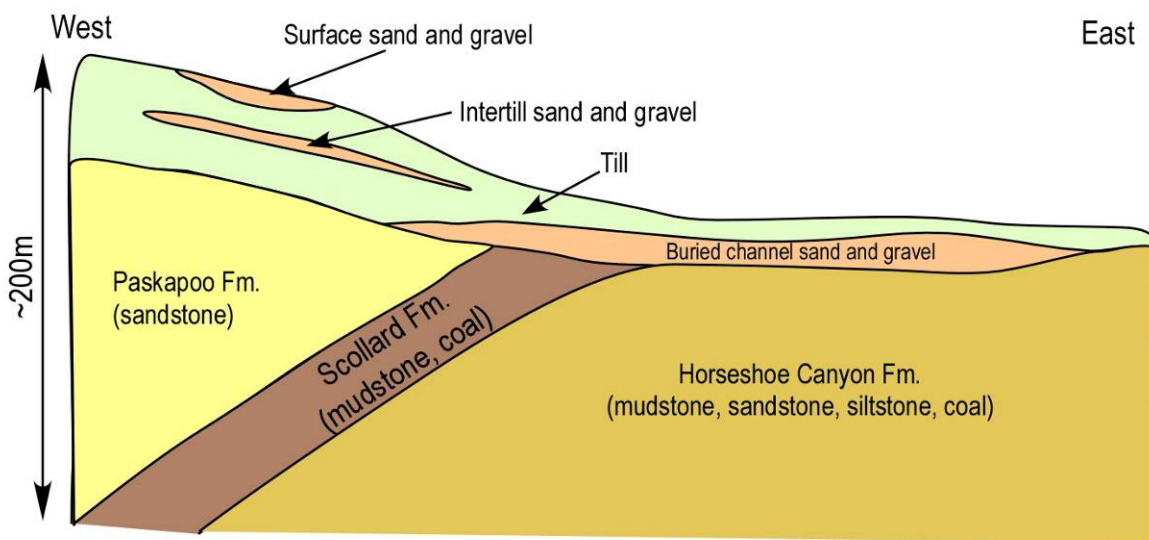
Figure 3. Simplified, regional-scale cross-section, oriented west to east, of sediments and bedrock surveyed using the low-frequency, GEOTEM® time-domain survey, central Alberta.

3 Location of Study Area and Geophysical Study Blocks

The ECC study area occupies approximately 49 500 km^2 and lies within portions of NTS 82I, J, O and P and 83A, B, G and H. Ten subwatershed boundaries define the irregularly shaped boundary of the ECC study area (Figure 1).

Between November 2007 and February 2010, AEM and AM surveys were completed over 11 study blocks in the ECC (Figure 2a). Data collection over the Three Hills and Cochrane study blocks (Figure 2b) was completed between January 27 and February 20, 2009, using a fixed-wing, GEOTEM® survey. The survey was flown over 11 057 line-kilometres (line-km) using a base frequency of 30 Hz. Data were recorded along flight lines oriented northwest to southeast that ranged in length from 14 to 82 km, with a line separation of approximately 800 m. Thirteen tie lines were completed approximately 1450 km apart in a northeast-southwest direction. Additional information on this survey technique is presented in the following section and in Appendix 1.

4 Methodology

4.1 Data Acquisition, Processing and Interpretations

Digital data from the AEM and AM surveys were acquired by the contractor, Fugro Airborne Surveys, using the GEOTEM® survey technique. This technique is briefly described below and presented in Appendix 1. For additional information the reader is referred to Fraser (1978), Smith et al. (2003, 2006, 2007), Paine and Minty (2005) and Siemon (2006).

Datasets provided to AGS and ESRD from the contractor include both unprocessed and processed tabular datasets, as well as grid-based digital maps illustrating ground resistivity in relation to depth below ground surface. AGS and ESRD did not process any of the geophysical data.

4.2 GEOTEM® Time-Domain Geophysical Survey

The fixed-wing, GEOTEM® time-domain survey technique consists of a towed-bird EM system. The survey technique is based on the premise that fluctuations in the primary EM field produced in the transmitting loop will result in eddy currents being generated in any conductors in the ground. The eddy currents then decay to produce a secondary EM field that may be sensed in the receiver coil. Each primary pulse causes decaying eddy currents in the ground to produce a secondary magnetic field. This secondary magnetic field, in turn, induces a voltage in the receiver coils, which is the EM response. Good conductors decay slowly, whereas poor conductors decay more rapidly.

The primary EM pulses are created by a series of discontinuous sinusoidal current pulses fed into a three- or six-turn transmitting loop surrounding the aircraft and fixed to the nose, tail and wing tips. For this survey, instrumentation was installed on a modified Casa 212 aircraft (Figure 4). The base frequency rate is selectable: 25, 30, 75, 90, 125, 150, 225 and 270 Hz, and the length of the pulse can be adjusted to suit specific targets. Standard pulse widths available are 0.6, 1.0, 2.0 and 4.0 ms, and the receiver is a three-axis (x, y, z) induction coil that is towed by the aircraft on a 135 m long, nonmagnetic cable (refer to Appendix 1, Figure 3). The usual mean terrain clearance for the aircraft is 120 m with the EM receiver normally being situated 50 m below and 130 m behind the aircraft. Additional information on the GEOTEM® survey technique is provided in Appendix 1.

Figure 4. a) The GEOTEM® survey technique in flight. Note the transmitting loop fixed to the aircraft's nose, tail and wing tips. Primary electromagnetic pulses are created by a series of discontinuous sinusoidal current pulses and transmitted into the transmitting loop. b) Modified Casa 212 aircraft used by Fugro Airborne Surveys in this study.

5 References

Fraser, D.C. (1978): Resistivity mapping with an airborne multicoil electromagnetic system; Geophysics, v. 43, p. 144–172.

Lahti, M., Vanhala, H., Mattsson, A., Beamish, D. and Lerssi, J. (2005): Environmental applications of airborne geophysics – groundwater and contaminated soil in Finland, Germany and United Kingdom; Geological Survey of Finland, Special Paper 39, p. 155–175.

Paine, J.G. and Minty, B.R.S. (2005): Airborne hydrogeophysics; *in* Hydrogeophysics, Y. Rubin and S.S. Hubbard (ed.), Water Science and Technology Library, v. 50, p. 333–357.

Siemon, B. (2006): Electromagnetic methods – frequency domain – airborne techniques; *in* Groundwater geophysics – a tool for hydrogeology, R. Kirsch (ed.), Springer-Verlag, p. 155–170.

Slattery, S.R. and Andriashek, L.D. (2012a): Overview of airborne-electromagnetic and -magnetic geophysical data collection using the RESOLVE[®] and GEOTEM[®] survey techniques near Red Deer, central Alberta; Energy Resources Conservation Board, ERCB/AGS Open File Report 2012-07, 246 p.

Slattery, S.R. and Andriashek, L.D. (2012b): Overview of airborne-electromagnetic and -magnetic geophysical data collection using the GEOTEM[®] survey technique in the Sylvan Lake area, central Alberta; Energy Resources Conservation Board, ERCB/AGS Open File Report 2012-08, 175 p.

Slattery, S.R. and Andriashek, L.D. (2012c): Overview of airborne-electromagnetic and -magnetic geophysical data collection using the GEOTEM[®] survey technique north of Calgary, Alberta; Energy Resources Conservation Board, ERCB/AGS Open File Report 2012-09, 169 p.

Slattery, S.R. and Andriashek, L.D. (2012d): Overview of airborne-electromagnetic and -magnetic geophysical data collection using the TEMPEST[®] survey technique near Edmonton, Alberta; Energy Resources Conservation Board, ERCB/AGS Open File Report 2012-11, 38 p.

Slattery, S.R. and Andriashek, L.D. (2012e): Overview of airborne-electromagnetic and -magnetic geophysical data collection using the GEOTEM[®] survey technique near Drayton Valley, central Alberta; Energy Resources Conservation Board, ERCB/AGS Open File Report 2012-12, 92 p.

Slattery, S.R. and Andriashek, L.D. (2012f): Overview of airborne-electromagnetic and -magnetic geophysical data collection and interpretation in the Edmonton–Calgary Corridor, central Alberta; Energy Resources Conservation Board, ERCB/AGS Open File Report 2012-13, 208 p.

Slattery, S.R. and Andriashek, L.D. (2012g): Overview of airborne-electromagnetic and -magnetic geophysical data collection using the TEMPEST[®] survey technique near Wabamun, central Alberta; Energy Resources Conservation Board, ERCB/AGS Open File Report 2012-14, 38 p.

Smith, B.D., Irvine, R., Blome, C.D., Clark, A.K. and Smith, D.V. (2003): Preliminary results, helicopter electromagnetic and magnetic survey of the Seco Creek area, Medina and Uvalde counties, Texas; Proceedings for the Symposium on the Application of Geophysics to Environmental and Engineering Problems, San Antonio, Texas, 15 p.

Smith, B.D., Thamke, J.N., Cain, M.J., Tyrrell, C. and Hill, P.L. (2006): Helicopter electromagnetic and magnetic survey maps and data, East Poplar Oil Field area, Fort Peck Indian Reservation, northeastern Montana, August 2004; United States Geological Survey, Open File Report 2006-1216, 23 p., 1 plate.

Smith, B.D., Grauch, V.J.S., McCafferty, A.E., Smith, D.V., Rodriguez, B.R., Pool, D.R., Deszcz-Pan, M. and Labson, V.F. (2007): Airborne electromagnetic and magnetic surveys for ground-water resources: a decade of study by the U.S. Geological Survey; *in* Proceedings of Exploration 07: Fifth Decennial International Conference on Mineral Exploration, B. Milkereit (ed.), p. 895–899.

Wiederhold, H., Schaumann, G. and Steuer, A. (2009): Airborne geophysical investigations for hydrogeological purposes in northern Germany; Near Surface 2009 – 15th European Meeting of Environmental and Engineering Geophysics, September 7–9, 2009, Dublin, Ireland, 5 p.

**Appendix 1 – Logistics and Processing Report Airborne Magnetic and GEOTEM®
Survey, Edmonton Calgary Corridor, Red Deer, Alberta**

LOGISTICS AND PROCESSING REPORT
Airborne Magnetic and GEOTEM® Survey

EDMONTON – RED DEER AREA
ALBERTA

Job No. 09401

Alberta Energy Resources Conservation Board

**LOGISTICS AND PROCESSING REPORT
AIRBORNE MAGNETIC AND GEOTEM® SURVEY
EDMONTON CALGARY CORRIDOR
RED DEER, ALBERTA**

JOB NO. 09401

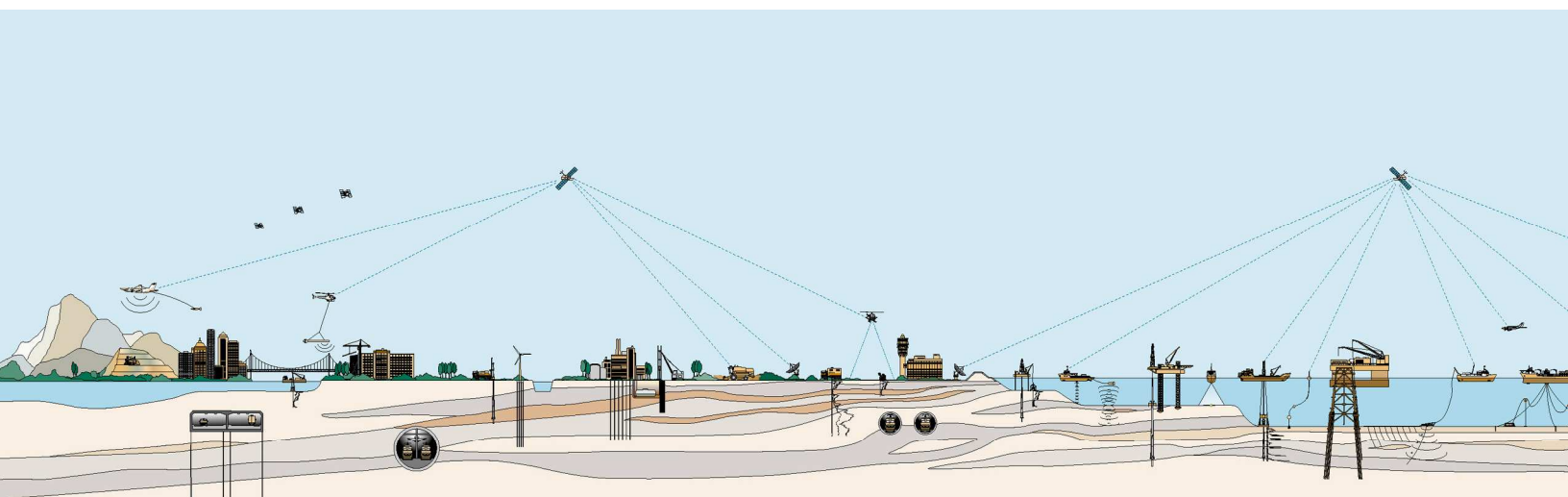Client: Alberta Energy Resources Conservation Board
Unit 402 - 4999-98 Avenue
Edmonton, Alberta
T6B 2X3

Date of Report: March, 2009

TABLE OF CONTENTS

APPENDICES

I

Introduction

Between January 27th and February 20th, 2009, Fugro Airborne Surveys conducted a GEOTEM® electromagnetic and magnetic survey of the Edmonton Calgary Corridor on behalf of Energy Resources and Conservation Board. Using Red Deer, Alberta as the base of operations, a total of 11,057 line kilometres of data was collected using a Casa 212 modified aircraft (Figure 1).

The survey data were processed and compiled in the Fugro Airborne Surveys Ottawa office. The collected and processed data are presented on colour or black and white maps, and multi-parameter profiles. The following maps were produced: Residual Magnetic Intensity (RMI), First Vertical Derivative of RMI, Resistivity Depth Slices at 10, 30, 60 and 120 m, Apparent Resistivity and Flight Path. In addition, digital archives of the raw and processed survey data in line format, and gridded EM data were delivered.

Figure 1: Specially modified Casa 212 aircraft used by Fugro Airborne Surveys.

II

Survey Operations

Location of the Survey Area

The Edmonton Calgary Corridor Block (Figure 2) was flown with Red Deer, Alberta as the base of operations. A total of 191 traverse lines were flown ranging in length from 14 km to 82 km, with a spacing of 800 m between lines, and 13 tie lines were flown with a spacing of 14500 m between tie-lines totalling 11057 km for the complete survey.
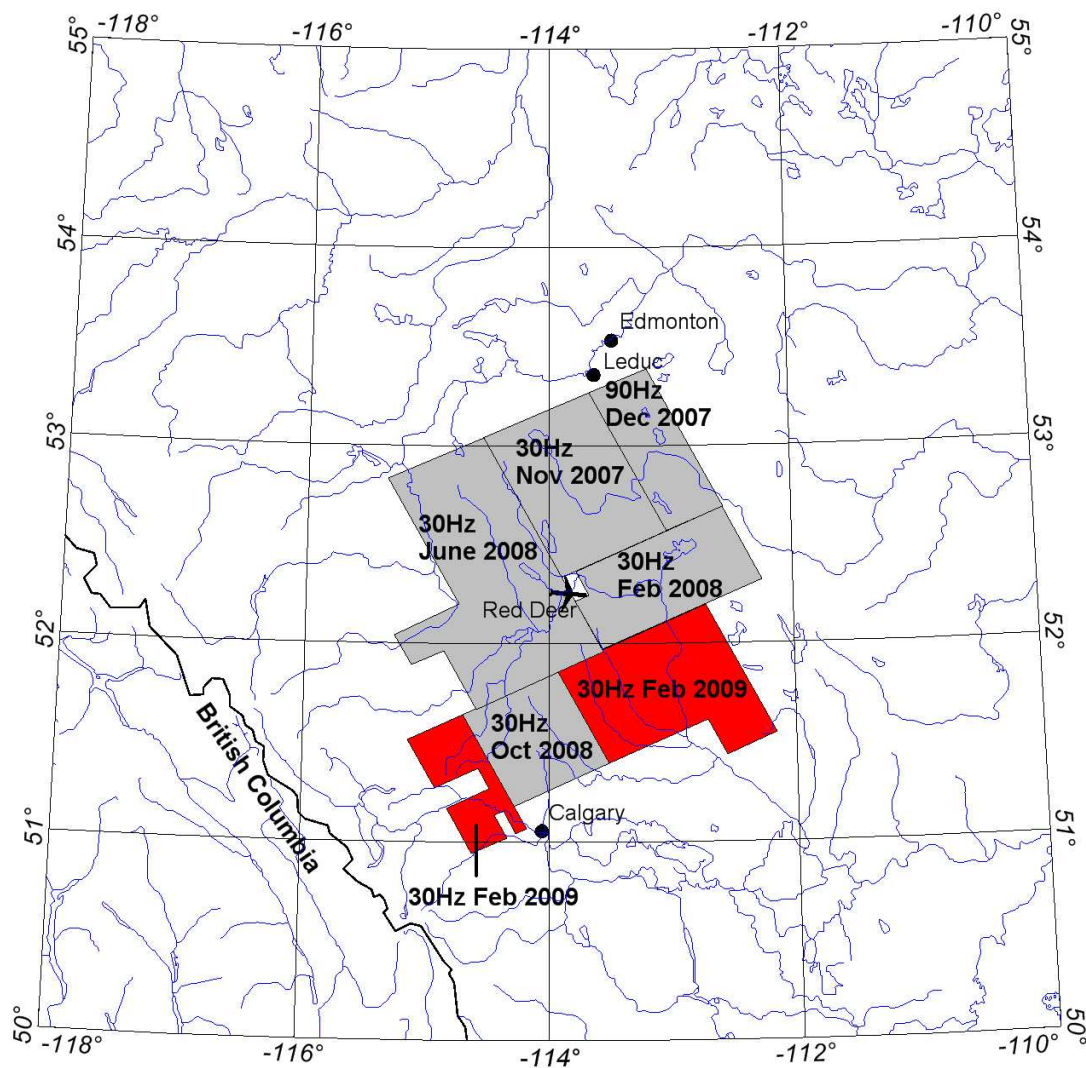
Figure 2: Survey location.

Aircraft and Geophysical On-Board Equipment

Aircraft:	Casa 212 (Twin Turbo Propeller)
Operator:	FUGRO AIRBORNE SURVEYS
Registration:	C-FDKM
Survey Speed:	125 knots / 145 mph / 65 m/s

Figure 3: Mag and GEOTEM® Receivers

Magnetometer: Scintrex Cs-2 single cell cesium vapour, towed-bird installation, sensitivity = 0.01 nT[1], sampling rate = 0.1 s, ambient range 20,000 to 100,000 nT. The general noise envelope was kept below 0.5 nT. The nominal sensor height was ~73 m above ground.

Electromagnetic system: GEOTEM 20 channel Multicoil System

Transmitter: Vertical axis loop mounted on aircraft of 231 m^2

Number of turns   6

Nominal height above ground of 120 m

Receiver: Multicoil system (x, y and z) with a final recording rate of 4 samples/second, for the recording of 20 channels of x, y and z-coil data. The nominal height above ground is ~75 m, placed ~130 m behind the centre of the transmitter loop.

Base frequency:	30 Hz
Pulse width:	4036μs
Pulse delay:	41 μs
Off-time:	12590 μs
Point value:	8.1 μs
Transmitter Current:	~635 A
Dipole moment:	~8.6x10^{5}Am²

Figure 4: Modified Casa 212 in flight.

---

1 One nanotesla (nT) is the S.I. equivalent of one gamma.

Table 1: Electromagnetic Data Windows.

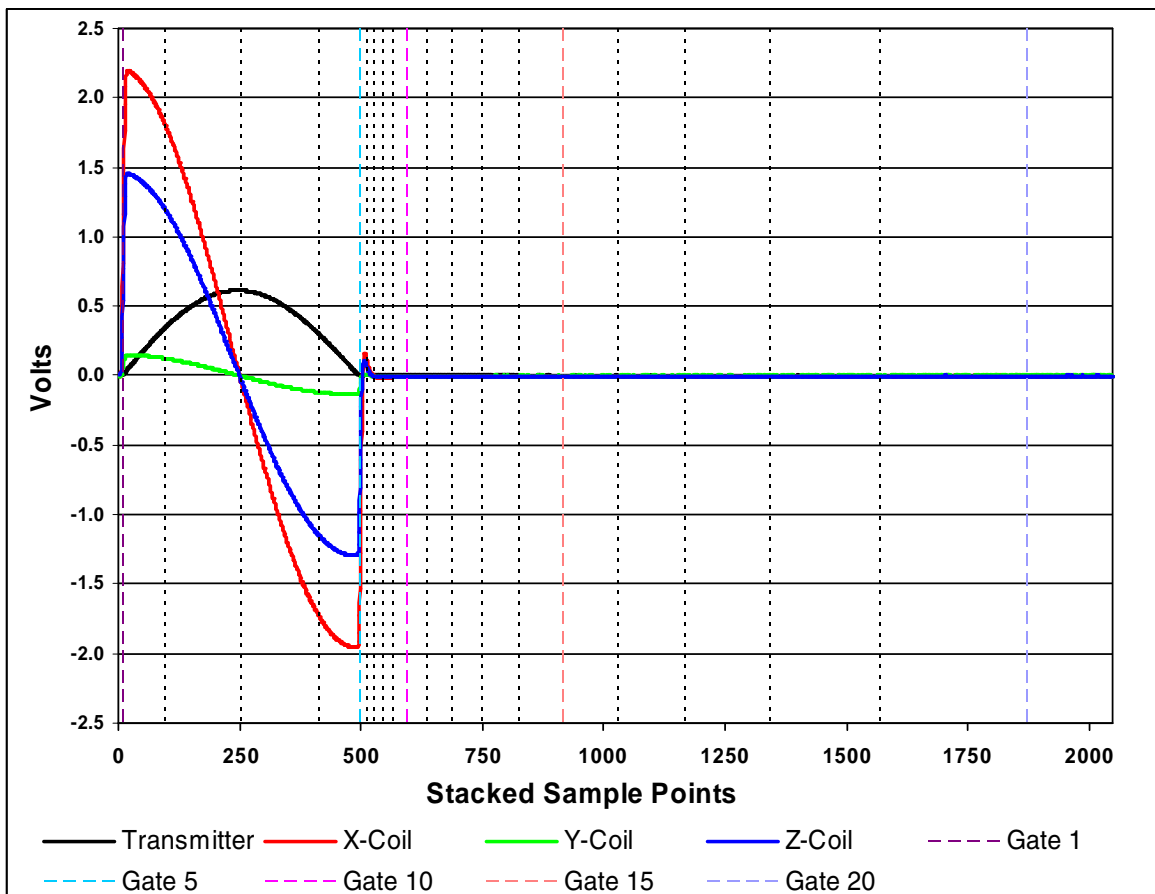| Channel	Start (p)	End (p)	Width (p)	Start (ms)	End (ms)	Width (ms)	Mid (ms)
1	6	20	15	0.041	0.163	0.122	0.102
2	21	177	157	0.163	1.440	1.278	0.802
3	178	336	159	1.440	2.734	1.294	2.087
4	337	493	157	2.734	4.012	1.278	3.373
5	494	508	15	4.012	4.134	0.122	4.073
6	509	520	12	4.134	4.232	0.098	4.183
7	521	535	15	4.232	4.354	0.122	4.293
8	536	555	20	4.354	4.517	0.163	4.435
9	556	580	25	4.517	4.720	0.203	4.618
10	581	615	35	4.720	5.005	0.285	4.862
11	616	660	45	5.005	5.371	0.366	5.188
12	661	715	55	5.371	5.819	0.448	5.595
13	715	785	71	5.811	6.388	0.578	6.099
14	786	870	85	6.388	7.080	0.692	6.734
15	871	970	100	7.080	7.894	0.814	7.487
16	971	1095	125	7.894	8.911	1.017	8.403
17	1096	1245	150	8.911	10.132	1.221	9.521
18	1246	1445	200	10.132	11.759	1.628	10.946
19	1446	1695	250	11.759	13.794	2.035	12.777
20	1696	2048	353	13.794	16.667	2.873	15.230

Figure 5: GEOTEM Waveform and response with gate centres showing positions in sample points.

Digital Acquisition:	FUGRO AIRBORNE SURVEYS GEODAS SYSTEM.
Barometric Altimeter:	Rosemount 1241M, sensitivity 1 ft, 0.5 sec recording interval.
Radar Altimeter:	King, accuracy 2%, sensitivity 1 ft, range 0 to 2500 ft, 0.5 sec recording interval.
Camera:	Panasonic colour video, super VHS, model WV-CL302.
Electronic Navigation:	NovAtel OEM4, 1 sec recording interval, with a resolution of 0.00001 degree and an accuracy of ±5m.

Base Station Equipment

Magnetometer:	Scintrex CS-2 single cell cesium vapour, mounted in a magnetically quiet area, measuring the total intensity of the earth's magnetic field in units of 0.01 nT at intervals of 0.5 s, within a noise envelope of 0.20 nT.
GPS Receiver:	NovAtel OEM4, measuring all GPS channels, for up to 12 satellites.
Computer:	Laptop, Pentium model.
Data Logger:	CF1, SBBS (single board base station).

Field Office Equipment

Computer:	Dell Inspiron 9000 Series laptop.
Printer:	Canon bubblejet printer.
DVD writer Drive:	Internal DVD+RW format.
Hard Drive:	100 GB Removable hard drive.

Survey Specifications

Traverse Line Direction:	150°- 330°
Traverse Line Spacing:	800 m
Tie Line direction:	65°- 245°
Tie Line spacing:	14500 m
Navigation:	Differential GPS. Traverse and tie line spacing was not to exceed the nominal by more than 50 m from flight plan over 3 km.
Altitude:	The survey was flown at a mean terrain clearance of 120 m. Altitude was not to exceed 140 m over 3 km.

Magnetic Noise Levels:	The noise envelope on the magnetic data was not to exceed ± 0.25 nT over 3 km.

EM Noise Levels:	The noise envelope on the raw electromagnetic dB/dt X- and Z-coil channel 20 was not to exceed ± 3500 pT/s over a distance greater than 3 km as displayed on the raw analogue traces.

Field Crew

Data Processor:	A. Jones, L. Lafrenière, E. Rooen
Pilots:	B. Gorrell, S. Savage, D. Maertens
Electronics Operator:	D. Patzer, S. Gorokhovski
Engineer:	T. Boughner, W. Werry

Production Statistics

Flying dates:	January 27th – February 20th, 2009
Total production:	11057 line kilometres
Number of production flights:	22
Days lost weather:	2

III

Quality Control and Compilation Procedures

In the field after each flight, all analogue records were examined as a preliminary assessment of the noise level of the recorded data. Altimeter deviations from the prescribed flying altitudes were also closely examined as well as the diurnal activity, as recorded on the base station.

All digital data were verified for validity and continuity. The data from the aircraft and base station were transferred to the PC's hard disk. Basic statistics were generated for each parameter recorded, these included: the minimum, maximum, and mean values; the standard deviation; and any null values located. All recorded parameters were edited for spikes or datum shifts, followed by final data verification via an interactive graphics screen with on-screen editing and interpolation routines.

The quality of the GPS navigation was controlled on a daily basis by recovering the flight path of the aircraft. The correction procedure employs the raw ranges from the base station to create improved models of clock error, atmospheric error, satellite orbit, and selective availability. These models are used to improve the conversion of aircraft raw ranges to aircraft position.

Checking all data for adherence to specifications was carried out in the field by the FUGRO AIRBORNE SURVEYS field geophysicist.

IV

Data Processing

Flight Path Recovery

GPS Recovery:	GPS positions recalculated from the recorded raw range data, and differentially corrected.
Projection:	Alberta 10 TM Projection
Datum:	NAD83
Central meridian:	115° West
False Easting:	500000 metres
False Northing:	0 metres
Scale factor:	0.9992

Altitude Data

Noise editing:	Alfatrim median filter used to eliminate the highest and lowest values from the statistical distribution of a 5 point sample window for the GPS elevation, and the two highest and lowest values from a 9 point sample window for the radar and barometric altimeters.

Base Station Diurnal Magnetics

Noise editing:	Alfatrim median filter used to eliminate the two highest and two lowest values from the statistical distribution of a 9 point sample window.
Culture editing:	Polynomial interpolation via a graphic screen editor.
Noise filtering:	Running average filter set to remove wavelengths less than 8 seconds.

Extraction of long wavelength component:

Running average filter to retain only wavelengths greater than 223 seconds.

Airborne Magnetics

Lag correction:	3.6 s
Noise editing:	4th difference editing routine set to remove spikes greater than 0.5 nT.
Noise filtering:	Triangular filter set to remove noise events having a wavelength less than 0.9 seconds.
Diurnal subtraction:	The long wavelength component of the diurnal (greater than 223 seconds) was removed from the data with a base value of 57250 nT added back.
IGRF removal date:	2009.1

Gridding: The data was gridded using an akima routine with a grid cell size of 200 m.

Residual Magnetic Intensity

The residual magnetic intensity (RMI) is calculated from the total magnetic intensity (TMI), the diurnal, and the regional magnetic field. The TMI is measured in the aircraft, the diurnal is measured from the ground station and the regional magnetic field is calculated from the International Geomagnetic Reference Field (IGRF). The low frequency component of the diurnal is extracted from the filtered ground station data and removed from the TMI. The average of the diurnal is then added back in to obtain the resultant TMI. The regional magnetic field, calculated for the specific survey location and the time of the survey, is removed from the resultant TMI to obtain the RMI. The final step is to Tie line level and microlevel the RMI data.

Magnetic First Vertical Derivative

The first vertical derivative was calculated in the frequency domain from the final grid values to enhance subtleties related to geological structures.

A first vertical derivative has also been displayed in profile form. This was calculated from the line data by combining the transfer functions of the 1st vertical derivative and a low-pass filter (cut-off value = 7 s, roll-off value = 5 s). The low-pass filter was designed to attenuate the high frequencies representing non-geological signal, which are normally enhanced by the derivative operator. This parameter is also stored in the final digital archive.

Electromagnetics

dB/dt data

Lag correction: 4.0 s

Data correction: The x, y and z-coil data were processed from the 20 raw channels recorded at 4 samples per second.

The following processing steps were applied to the dB/dt data from all coil sets:

a) The data from channels 1 to 5 (on-time) and 6 to 20 (off-time) were corrected for drift in flight form (prior to cutting the recorded data back to the correct line limits) by passing a low order polynomial function through the baseline minima along each channel, via a graphic screen display;

b) The data were edited for residual spheric spikes by examining the decay pattern of each individual EM transient. Bad decays (i.e. not fitting a normal exponential function) were deleted and replaced by interpolation;

c) Noise filtering was done using an adaptive filter technique based on time domain triangular operators. Using a 2nd difference value to identify changes in gradient along each channel, minimal filtering (3 point convolution) is applied over the peaks of the anomalies, ranging in set increments up to a maximum amount of filtering in the resistive background areas (31 points for both the x-coil and the z-coil data);

d) The filtered data from the x, y and z-coils were then re-sampled to a rate of 5 samples per second and combined into a common file for archiving.

B-field data

Processing steps: The processing of the B-Field data stream is very similar to the processing for the regular dB/dt data. The lag adjustment used was the same, followed by:

1) Drift adjustments;

2) Spike editing for spheric events;

3) Correction for coherent noise. By nature, the B-Field data will contain a higher degree of coherency of the noise that automatically gets eliminated (or considerably attenuated) in the regular dB/dt, since this is the time derivative of the signal;

4) Final noise filtering with an adaptive filter.

Note: The introduction of the B-Field data stream, as part of the GEOTEM® system, provides the explorationist with a more effective tool for exploration in a broader range of geological environments and for a larger class of target priorities.

The advantage of the B-Field data compared with the normal voltage data (dB/dt) are as follows:

1. A broader range of target conductance that the system is sensitive to. (The B-Field is sensitive to bodies with conductance as great as 100,000 Siemens);

2. Enhancement of the slowly decaying response of good conductors;

3. Suppression of rapidly decaying response of less conductive overburden;

4. Reduction in the effect of spherics on the data;

5. An enhanced ability to interpret anomalies due to conductors below thick conductive overburden;

6. Reduced dynamic range of the measured response (easier data processing and display).
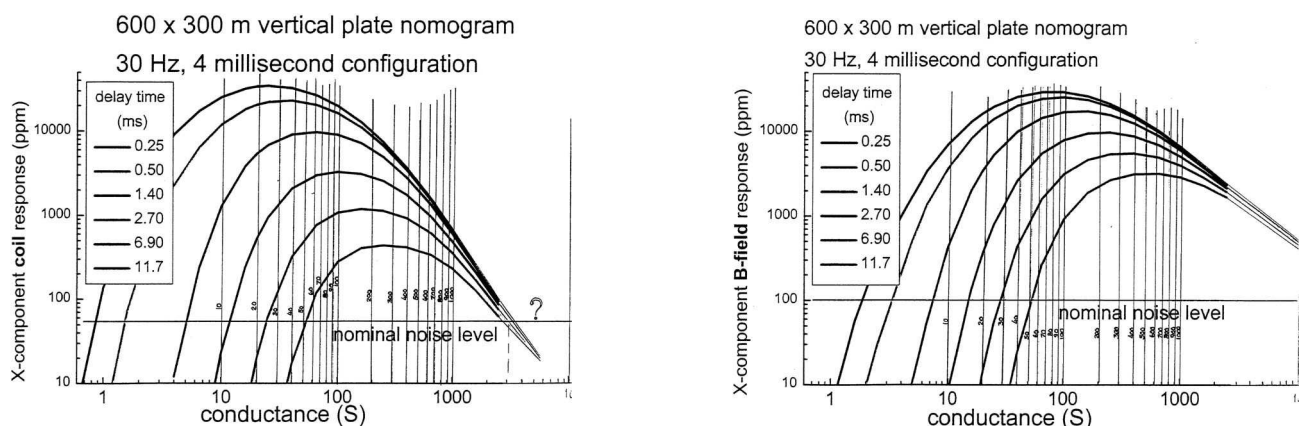

Figure 6: dB-dt vertical plate nomogram (left), B-field vertical plate nomogram (right).

Figure 6 displays the calculated vertical plate response for the GEOTEM® signal for the dB/dt and B-Field. For the dB/dt response, you will note that the amplitude of the early channel peaks at about 25 Siemens, and the late channels at about 250 Siemens. As the conductance exceeds 1000 Siemens the response curves quickly roll back into the noise level. For the B-Field response, the early channel amplitude peaks at about 80 Siemens and the late channel at about 550 Siemens. The projected extension of the graph in the direction of increasing conductance, where the response would roll back into the noise level, would be close to 100,000 Siemens. Thus, a strong conductor, having a conductance of several thousand Siemens, would be difficult to interpret on the dB/dt data, since the response would be mixed in with the background noise. However, this strong conductor would stand out clearly on the B-Field data, although it would have an unusual character, being a moderate to high amplitude response, exhibiting almost no decay.

In theory, the response from a super conductor (50,000 to 100,000 Siemens) would be seen on the B-Field data as a low amplitude, non-decaying anomaly, not visible in the off-time channels of the dB/dt stream. Caution must be exercised here, as this signature can also reflect a residual noise event in the B-Field data. In this situation, careful examination of the dB/dt on-time (in-pulse) data is required to resolve the ambiguity. If the feature were strictly a noise event, it would not be present in the dB/dt off-time data stream. This would locate the response at the resistive limit, and the mid in-pulse channel (normally identified as channel 3) would reflect little but background noise, or at best a weak negative peak. If, on the other hand, the feature does indeed reflect a superconductor, then this would locate the response at the inductive limit. In this situation, channel 3 of the dB/dt stream will be a mirror image of the transmitted pulse, i.e. a large negative.

Coil Oscillation Correction

The electromagnetic receiver sensor is housed in a bird which is towed behind the aircraft using a cable. Any changes in airspeed of the aircraft, variable crosswinds, or other turbulence will result in the bird swinging from side to side. This can result in the induction sensors inside the bird rotating about their mean orientation. The rotation is most marked when the air is particularly turbulent. The changes in orientation result in variable coupling of the induction coils to the primary and secondary fields. For example, if the sensor that is normally aligned to measure the x-axis response pitches upward, it will be measuring a response that will include a mixture of the X and Z component responses. The effect of coil oscillation on the data increases as the signal from the ground (conductivity) increases and may not be noticeable when flying over areas which are generally resistive. This becomes more of a concern when flying over highly conductive ground.

Using the changes in the coupling of the primary field, it is possible to estimate the pitch, roll and yaw of the receiver sensors. In the estimation process, it is assumed that a smoothed version of the primary field represents the primary field that would be measured when the sensors are in the mean orientation. The orientations are estimated using a non-linear inversion procedure, so erroneous orientations are sometimes obtained. These are reviewed and edited to insure smoothly varying values of orientations. These orientations can then be used to unmix the measured data to generate a response that would be measured if the sensors were in the correct orientation. For more information on this procedure, see:
http://www.fugroairborne.com/resources/technical_papers/airborne_em/atem.html

For the present dataset, the data from all 20 channels of dB/dt and B-Field parameters have been corrected for coil oscillation.

Apparent Resistivity

Fugro has developed an algorithm that converts the response in any measurement window (on or off-time) into an apparent resistivity. This is performed using a look-up table that contains the response at a range of half-space conductivities and altimeter heights.

The apparent resistivity for the present dataset was calculated using dB/dt Z Coil channels 1 - 20 to provide the maximum information on the near-surface conductivity of the ground which, when combined with the magnetic signature, provides good geological mapping.

Resistivity-Depth-Images (RDI)

The Resistivity-Depth-Images (RDI) sections were calculated from the B Field Z-coil response, using an algorithm that converts the response in any measurement window (on- or off-time) into resistivity. For on-time data, it is not straightforward to identify which depth the apparent resistivity is associated, or identify any variation in resistivity with depth. Hence, the earth is assigned a constant value from surface to depth.

However, for the off-time data, the apparent resistivity can be associated with a depth. This depth, δ, depends on the magnetic permeability μ, the delay time t of the measurement window and the estimated apparent conductivity σ_{app}, i.e.

$$\delta = 0.55 \sqrt{\frac{t}{\mu \sigma_{app}}} \; .$$

The electromagnetic method is most sensitive to conductive features so resistive features will be poorly resolved. The process of converting voltage data to resistivity as a function of depth tends to create smoother depth variations than can occur in reality.

The RDI sections, derived from each survey line, are created as individual grids. An additional set of RDI grids have been corrected for altitude variations such that the top of each section reflects the true terrain topography and it is these grids that are displayed on the multiplot profiles.

The RDI derived information is also provided as SEGY files and in a geosoft database as an array. The array consists of 151 levels of resistivity, from 0 to 300 metres depth. The resistivity values can be gridded to provide resistivity depth slices for desired depths. On this project, resistivity depth slices were created for depths of 10, 30, 60 and 120 m below the surface.

V

Final Products

Digital Archives

Line and grid data in the form of ASCII text files (*.xyz), Geosoft databases (*.gdb), SEG-Y Archives (*.sgy), Geosoft grids (*.grd), and ArcInfo ASCII grids (*.asc) have been written to DVD. The formats and layouts of these archives are further described in Appendix E (Data Archive Description). Hardcopies of all maps have been created as outlined below.

Maps

Scale:	1:250,000
Parameters:	Residual Magnetic Intensity
	First Vertical Derivative of the Residual Magnetic Intensity
	Apparent Resistivity
	Resistivity Depth Slice at 10 m Depth
	Resistivity Depth Slice at 30 m Depth
	Resistivity Depth Slice at 60 m Depth
	Resistivity Depth Slice at 120 m Depth
	Flight Path
Media/Copies:	1 Paper & 2 Digital (Geosoft *.map format & PDF Format)

Profile Plots

Scale:	1:100,000
Parameters:	Multi-channel presentation with 13 channels of both dB/dt and B-field X and Z-coil, Residual Magnetic Intensity, Calculated Magnetic Vertical Gradient, Radar Altimeter, EM Primary Field, Hz Monitor, Terrain and Terrain adjusted Resistivity Depth Section.
Media/Copies:	2 Digital (*.emf format) of Each Line

Report

Media/Copies:	2 Paper & 2 digital (PDF format)

Appendix A

Fixed-Wing Airborne Electromagnetic Systems

FIXED-WING AIRBORNE ELECTROMAGNETIC SYSTEMS

General

The operation of a towed-bird time-domain electromagnetic system (EM) involves the measurement of decaying secondary electromagnetic fields induced in the ground by a series of short current pulses generated from an aircraft-mounted transmitter. Variations in the decay characteristics of the secondary field (sampled and displayed as windows) are analyzed and interpreted to provide information about the subsurface geology. The response of such a system utilizing a vertical-axis transmitter dipole and a multicomponent receiver coil has been documented by various authors including Smith and Keating (1991, Geophysics v.61, p. 74-81). To download this paper, see the website
http://www.fugroairborne.com/resources/technical_papers/airborne_em/multicomponent_EM.html

A number of factors combine to give the fixed-wing platforms excellent signal-to-noise ratio and depth of penetration: 1) the principle of sampling the induced secondary field in the absence of the primary field (during the "off-time"), 2) the large separation of the receiver coils from the transmitter, 3) the large dipole moment and 4) the power available from the fixed wing platform. Such a system is also relatively free of noise due to air turbulence. However, also sampling in the "on-time" can result in excellent sensitivity for mapping very resistive features and very conductive features, and thus mapping the geology (Annan et al., 1991, Geophysics v.61, p. 93-99) (for download see http://www.fugroairborne.com/resources/technical_papers/airborne_em/resistive_limit.html).   The on-time and off-time parts of the half-cycle waveform are shown in Figure 1.

Through free-air model studies using the University of Toronto's Plate and Layered Earth programs it may be shown that the "depth of investigation" depends upon the geometry of the target. Typical depth limits would be 400 m below surface for a homogeneous half-space, 550 m for a flat-lying inductively thin sheet or 300 m for a large vertical plate conductor. These depth estimates are based on the assumptions that the overlying or surrounding material is resistive.

The method also offers very good discrimination of conductor geometry. This ability to distinguish between flat-lying and vertical conductors combined with excellent depth penetration results in good differentiation of bedrock conductors from surficial conductors (Appendix C).

Methodology

The Fugro time-domain fixed-wing electromagnetic systems (GEOTEM® and MEGATEM®) incorporate a high-speed digital EM receiver. The primary electromagnetic pulses are created by a series of discontinuous sinusoidal current pulses fed into a three- or six-turn transmitting loop surrounding the aircraft and fixed to the nose, tail and wing tips. The base frequency rate is selectable: 25, 30, 75, 90, 125, 150, 225 and 270 Hz. The length of the pulse can be tailored to suit the targets. Standard pulse widths available are 0.6, 1.0, 2.0 and 4.0 ms. The available off-time can be selected to be as great as 16 ms. The dipole moment depends on the pulse width, base frequency and aircraft used on the survey. Example pulse widths and off-time windows at different base frequencies are shown on Figure 2.   The specific dipole moment, waveform and gate settings for this survey are given in the main body of the report.

The receiver is a three-axis (x,y,z) induction coil. In the fixed-wing systems, this is towed by the aircraft on a 135-metre cable. The tow cable is non-magnetic, to reduce noise levels. The usual mean terrain clearance for the aircraft is 120 m with the EM bird being situated nominally 50 m

below and 130 m behind the aircraft (see Figure 3).

Each primary pulse causes decaying eddy currents in the ground to produce a secondary magnetic field. This secondary magnetic field, in turn, induces a voltage in the receiver coils, which is the electromagnetic response. Good conductors decay slowly, while poor conductors more rapidly (see Figure 1).

The measured signals pass through anti-aliasing filters and are then digitized with an A/D converter at sampling rates of up to 80 kHz. The digital data flows from the A/D converter into an industrial-grade computer where the data are processed to reduce the noise.

 Operations, which are carried out in the receiver, are:

1. *Primary-field removal:* In addition to measuring the secondary response from the ground, the receiver sensor coils also measure the primary response from the transmitter. During flight, the bird position and orientation changes slightly, and this has a very strong effect on the magnitude of the total response (primary plus secondary) measured at the receiver coils. The variable primary field response is distracting because it is unrelated to the ground response. The primary field can be measured by flying at an altitude such that no ground response is measurable. These calibration signals are used to define the shape of the primary waveform. By definition this primary field includes the response of the current in the transmitter loop plus the response of any slowly decaying eddy currents induced in the aircraft. We assume that the shape of the primary will be unchanged as the bird position changes, but that the amplitude will vary.   The primary-field-removal procedure involves solving for the amplitude of the primary field in the measured response and removing this from the total response to leave a secondary response. Note that this procedure removes any ("in-phase") response from the ground that has the same shape as the primary field. For more details on the primary-field removal procedure, see the paper on the web-site http://www.fugroairborne.com/resources/technical_papers/airborne_em/inphase.html

2. *Digital Stacking:* Stacking is carried out to reduce the effect of broadband noise on the data.

3. *Windowing of data*: The digital receiver samples the secondary and primary electromagnetic field at 64, 128 or 384 points per EM pulse and windows the signal in up to 20 time gates whose centres and widths are software selectable and which may be placed anywhere within or outside the transmitter pulse. This flexibility offers the advantage of arranging the gates to suit the goals of a particular survey, ensuring that the signal is appropriately sampled through its entire dynamic range. Example off-time windows are shown on Figure 1.

4. *Power Line Filtering:* Digital comb filters are applied to the data during real-time processing to remove power line interference while leaving the EM signal undisturbed. The RMS power line voltage (at all harmonics in the receiver passband) are computed, displayed and recorded for each data stack.

5. *Primary Field:* The primary field at the towed sensor is measured for each stack and recorded as a separate data channel to assess the variation in coupling between the transmitter and the towed sensor induced by changes in system geometry.

6. *Earth Field Monitor:* A monitor of sensor coil motion noise induced by coil motion in the Earth's magnetic field is also extracted in the course of the real-time digital processing. This information is also displayed on the real-time chart as well as being recorded for post-survey

diagnostic processes.

7. *Noise/Performance:* A monitor computes the RMS signal level on an early off-time window over a running 10-second window. This monitor provides a measure of noise levels in areas of low ground response. This information is printed at regular intervals on the side of the flight record and is recorded for every data stack.

One of the major roles of the digital receiver is to provide diagnostic information on system functions and to allow for identification of noise events, such as sferics, which may be selectively removed from the EM signal. The high digital sampling rate yields maximum resolution of the secondary field.

System Hardware

The airborne EM system consists of the aircraft, the on-board hardware, and the software packages controlling the hardware. The software packages in the data acquisition system and in the EM receiver were developed in-house, as were, certain elements of the hardware (transmitter, system timing clock, towed-bird sensor system).

Transmitter System

The transmitter system drives high-current pulses of an appropriate shape and duration through the coils mounted on the aircraft.

System Timing Clock

This subsystem provides appropriate timing signals to the transmitter, and also to the analog-to-digital converter, in order to produce output pulses and capture the ground response. All systems are synchronized to GPS time.

Towed-Bird Systems

A three-axis induction coil sensor is mounted inside a towed bird, which is typically 50 metres below and 130 metres behind the aircraft. (A second bird, housing the magnetometer sensor, is typically 50 metres below and 80 metres behind the aircraft.)
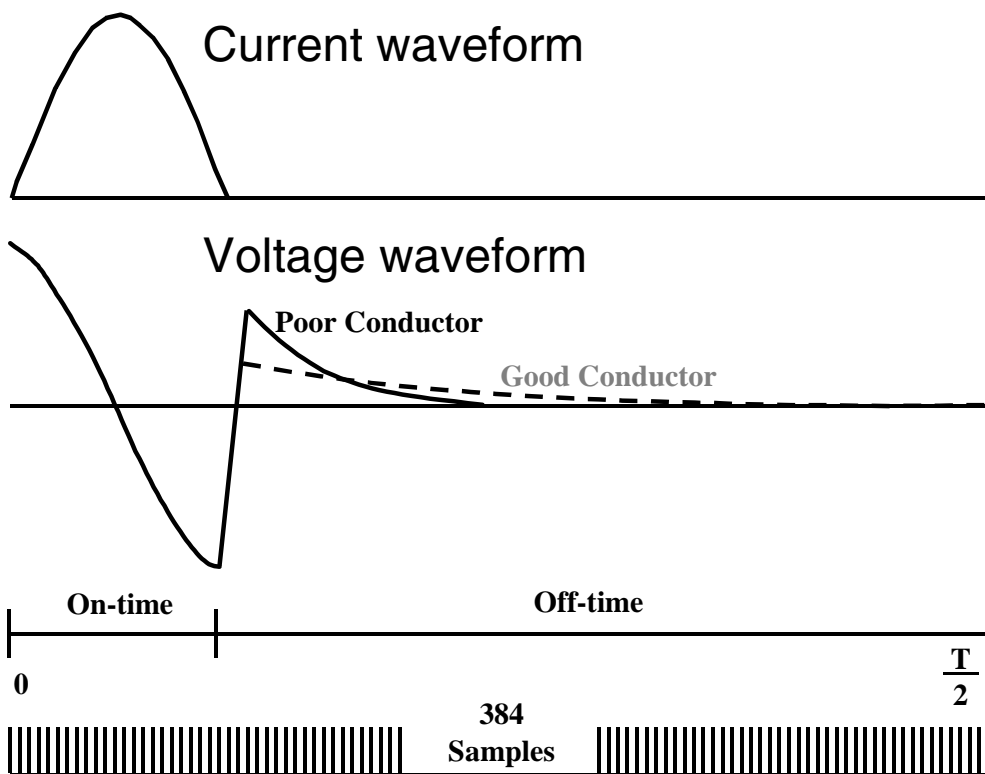
Figure 1. The waveforms and data sampling throughout the transmitter on- and off-time.
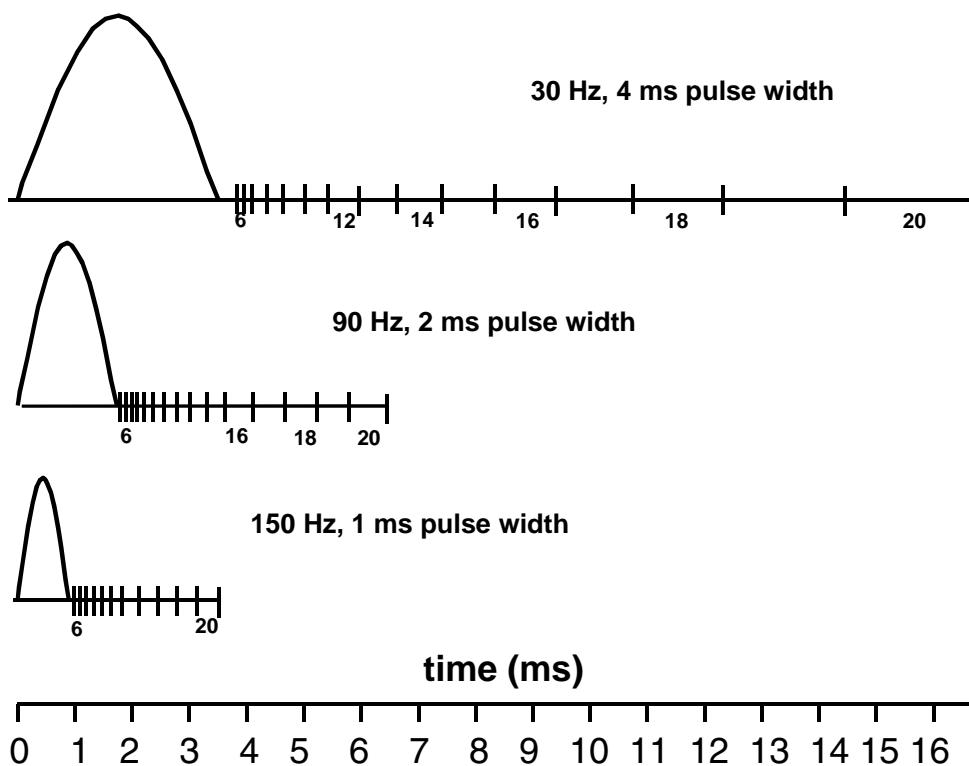

Figure 2. Pulse width and measurement windows for 150, 90 and 30 Hz base frequencies.
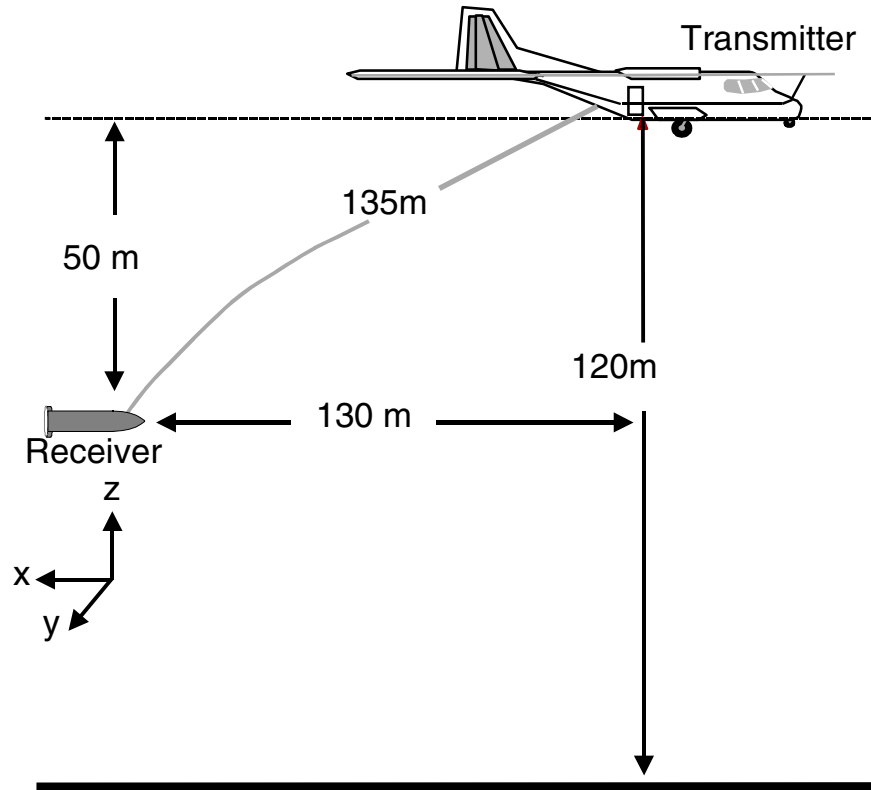
Figure 3. Nominal geometry of the fixed-wing electromagnetic system.

Appendix B

Airborne Transient EM Interpretation

Interpretation of transient electromagnetic data

Introduction

The basis of the transient electromagnetic (EM) geophysical surveying technique relies on the premise that changes in the primary EM field produced in the transmitting loop will result in eddy currents being generated in any conductors in the ground. The eddy currents then decay to produce a secondary EM field that may be sensed in the receiver coil.

MEGATEM® and GEOTEM® are airborne transient (or time-domain) towed-bird EM systems incorporating a high-speed digital receiver which records the secondary field response with a high degree of accuracy. Most often the earth's total magnetic field is recorded concurrently.

Although the approach to interpretation varies from one survey to another depending on the type of data presentation, objectives and local conditions, the following generalizations may provide the reader with some helpful background information.

The main purpose of the interpretation is to determine the probable origin of the responses detected during the survey and to suggest recommendations for further exploration. This is possible through an objective analysis of all characteristics of the different types of responses and associated magnetic anomalies, if any. If possible the airborne results are compared to other available data. Certitude is seldom reached, but a high probability is achieved in identifying the causes in most cases. One of the most difficult problems is usually the differentiation between surface conductor responses and bedrock conductor responses.

Types Of Conductors

Bedrock Conductors

The different types of bedrock conductors normally encountered are the following:

1. _Graphites_. Graphitic horizons (including a large variety of carbonaceous rocks) occur in sedimentary formations of the Precambrian as well as in volcanic tuffs, often concentrated in shear zones. They correspond generally to long, multiple conductors lying in parallel bands. They have no magnetic expression unless associated with pyrrhotite or magnetite. Their conductivity is variable but generally high.

2. _Massive sulphides_. Massive sulphide deposits usually manifest themselves as short conductors of high conductivity, often with a coincident magnetic anomaly. Some massive sulphides, however, are not magnetic, others are not very conductive (discontinuous mineralization or sphalerite), and some may be located among formational conductors so that one must not be too rigid in applying the selection criteria.

   In addition, there are syngenetic sulphides whose conductive pattern may be similar to that of graphitic horizons but these are generally not as prevalent as graphites.

3. _Magnetite and some serpentinized ultrabasics_. These rocks are conductive and very magnetic.

4. _Manganese oxides_. This mineralization may give rise to a weak EM response.

Surficial Conductors

1. Beds of clay and alluvium, some swamps, and brackish ground water are usually poorly conductive to moderately conductive.

2. Lateritic formations, residual soils and the weathered layer of the bedrock may cause surface anomalous zones, the conductivity of which is generally low to medium but can occasionally be high. Their presence is often related to the underlying bedrock.

Cultural Conductors (Man-Made)

3. *Power lines*. These frequently, but not always, produce a conductive type of response. In the case when the power line comb filter does not remove the radiated field, the anomalous response can exhibit phase changes between different windows. In the case of current induced by the EM system in a grounded wire, or steel pylon, the anomaly may look very much like a bedrock conductor.

4. *Grounded fences or pipelines*. These will invariably produce responses much like a bedrock conductor. Whenever they cannot be identified positively, a ground check is recommended.

5. *General culture*. Other localized sources such as certain buildings, bridges, irrigation systems, tailings ponds etc., may produce EM anomalies. Their instances, however, are rare and often they can be identified on the visual path recovery system.

Analysis Of The Conductors

The conductance of a plate is generally estimated assuming the plate is vertical and 600m by 300m. Hence the conductance alone is not generally a decisive criterion in the analysis of a conductor. In particular, one should note:

- Its shape and size,
- All local variations of characteristics within a conductive zone,
- Any associated geophysical parameter (e.g. magnetics),
- The geological environment,
- The structural context, and
- The pattern of surrounding conductors.

The first objective of the interpretation is to classify each conductive zone according to one of the three categories which best defines its probable origin. The categories are cultural, surficial and bedrock. A second objective is to assign to each zone a priority rating as to its potential as an economic prospect.

Bedrock Conductors

This category comprises those anomalies that cannot be classified according to the criteria established for cultural and surficial responses. It is difficult to assign a universal set of values that typify bedrock conductivity because any individual zone or anomaly might exhibit some, but not all, of these values and still be a bedrock conductor. The following criteria are considered indicative of a bedrock conductor:

1. An intermediate to high conductivity identified by a response with slow decay, with an anomalous response present in the later windows.

2. For vertical conductors, the anomaly should be narrow, relatively symmetrical, with a well-defined x-component peak.

3. If the conductor is thin, the response should show the characteristics evident in Figures 2 to 4. These figures illustrate how the response varies as a function of the flight direction for three bodies with different dips. The alternating character of the response as a result of line direction can be diagnostic of conductor geometry.

4. A small to intermediate amplitude. Large amplitudes are normally associated with surficial conductors. The amplitude varies according to the depth of the source.

5. A degree of continuity of the EM characteristics across several lines.

6. An associated magnetic response of similar dimensions. One should note, however, that those magnetic rocks that weather to produce a conductive upper layer would possess this magnetic association. In the absence of one or more of the characteristics defined in 1, 2, 3, 4 and 5, the related magnetic response cannot be considered significant.

Most obvious bedrock conductors occur in long, relatively monotonous, sometimes multiple zones following formational strike. Graphitic material is usually the most probable source. Massive syngenetic sulphides extending for many kilometres are known in nature but, in general, they are not common. Long formational structures associated with a strong magnetic expression may be indicative of banded iron formations.

In summary, a bedrock conductor reflecting the presence of a <u>massive sulphide</u> would normally exhibit the following characteristics:

- A high conductivity,
- A good anomaly shape (narrow and well-defined peak),
- A small to intermediate amplitude,
- An isolated setting,
- A short strike length (in general, not exceeding one kilometre), and
- Preferably, with a localized magnetic anomaly of matching dimensions.

Surficial Conductors

This term is used for geological conductors in the overburden, either glacial or residual in origin, and in the weathered layer of the bedrock. Most surficial conductors are probably caused by clay minerals. In some environments the presence of salts will contribute to the conductivity. Other possible electrolytic conductors are residual soils, swamps, brackish ground water and alluvium such as lake or river-bottom deposits, flood plains and estuaries.

Normally, most surficial materials have low to intermediate conductivity so they are not easily mistaken for highly conductive bedrock features. Also, many of them are wide and their anomaly shapes are typical of broad horizontal sheets.

When surficial conductivity is high it is usually still possible to distinguish between a horizontal plate

(more likely to be surficial material) and a vertical body (more likely to be a bedrock source) thanks to the asymmetry of the fixed-wing system responses observed at the edges of a broad conductor when flying adjacent lines in opposite directions. The configuration of the system is such that the response recorded at the leading edge is more pronounced than that registered at the trailing edge. Figure 1 illustrates the "edge effect". In practice there are many variations on this very diagnostic phenomenon.

One of the more ambiguous situations as to the true source of the response is when surface conductivity is related to bedrock lithology as for example, surface alteration of an underlying bedrock unit. At times, it is also difficult to distinguish between a weak conductor within the bedrock (e.g. near-massive sulphides) and a surficial source.

In the search for massive sulphides or other bedrock targets, surficial conductivity is generally considered as interference but there are situations where the interpretation of surficial-type conductors is the primary goal. When soils, weathered or altered products are conductive, and in-situ, the responses are a very useful aid to geologic mapping. Shears and faults are often identified by weak, usually narrow, anomalies.

Analysis of surficial conductivity can be used in the exploration for such features as lignite deposits, kimberlites, paleochannels and ground water. In coastal or arid areas, surficial responses may serve to define the limits of fresh, brackish and salty water.

Cultural Conductors
The majority of cultural anomalies occurs along roads and is accompanied by a response on the power line monitor. (This monitor is set to 50 or 60 Hz, depending on the local power grid.) In some cases, the current induced in the power line results in anomalies that could be mistaken for bedrock responses. There are also some power lines that have no response whatsoever.

The power line monitor, of course, is of great assistance in identifying cultural anomalies of this type. It is important to note, however, that geological conductors in the vicinity of power lines may exhibit a weak response on the monitor because of current induction via the earth.

Fences, pipelines, communication lines, railways and other man-made conductors can give rise to responses, the strength of which will depend on the grounding of these objects.

Another facet of this analysis is the line-to-line comparison of anomaly character along suspected man-made conductors. In general, the amplitude, the rate of decay, and the anomaly width should not vary a great deal along any one conductor, except for the change in amplitude related to terrain clearance variation. A marked departure from the average response character along any given feature gives rise to the possibility of a second conductor.

In most cases a visual examination of the site will suffice to verify the presence of a man-made conductor. If a second conductor is suspected the ground check is more difficult to accomplish. The object would be to determine if there is (i) a change in the man-made construction, (ii) a difference in the grounding conditions, (iii) a second cultural source, or (iv) if there is, indeed, a geological conductor in addition to the known man-made source.

The selection of targets from within extensive (formational) belts is much more difficult than in the case of isolated conductors. Local variations in the EM characteristics, such as in the amplitude,

decay, shape etc., can be used as evidence for a relatively localized occurrence. Changes in the character of the EM responses, however, may be simply reflecting differences in the conductive formations themselves rather than indicating the presence of massive sulphides and, for this reason, the degree of confidence is reduced.

Another useful guide for identifying localized variations within formational conductors is to examine the magnetic data in map or image form. Further study of the magnetic data can reveal the presence of faults, contacts, and other features, which, in turn, help define areas of potential economic interest.

Finally, once ground investigations begin, it must be remembered that the continual comparison of ground knowledge to the airborne information is an essential step in maximizing the usefulness of the airborne EM data.
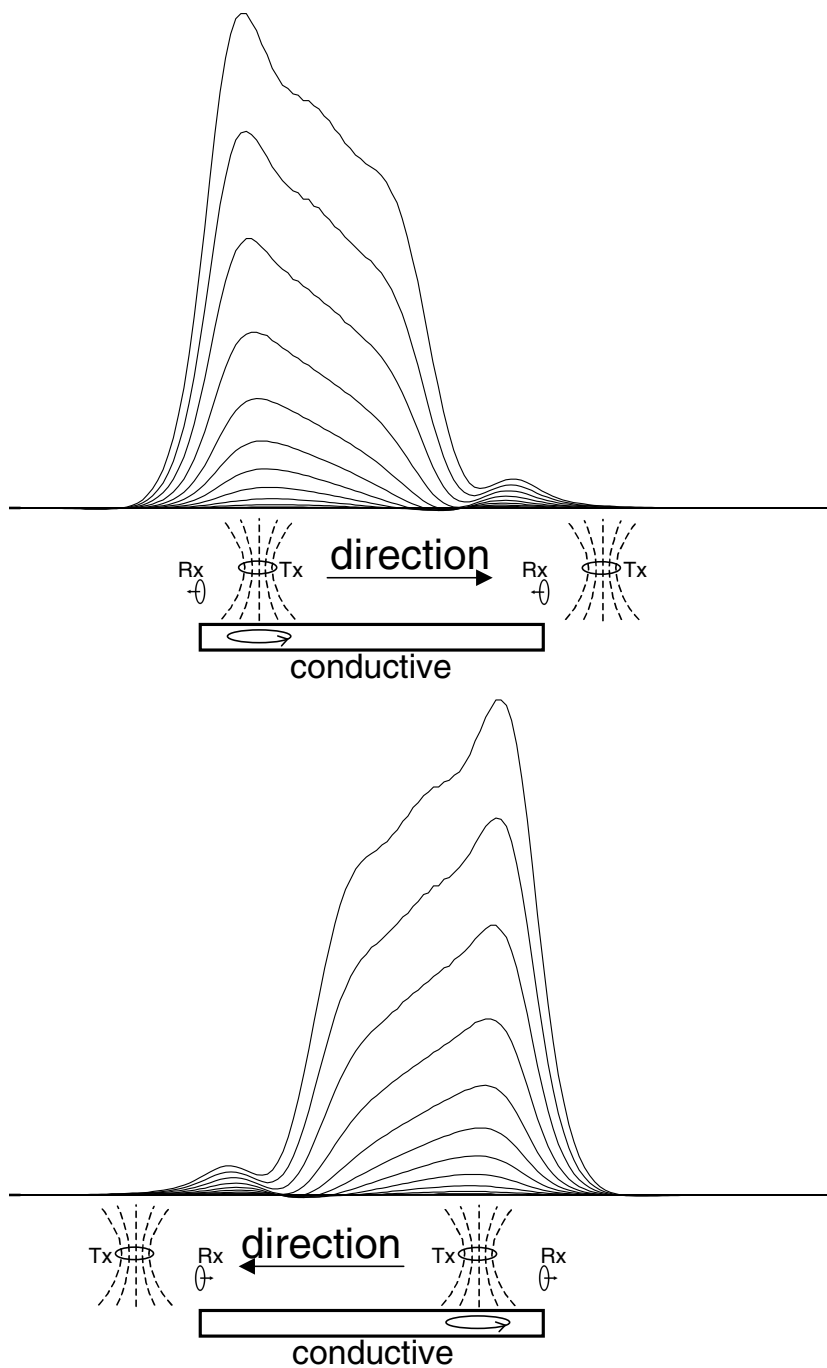
Figure 1. Illustration of how the x-component response varies depending on the flight direction. When the receiver flies onto the conductor, the transmitter is over the conductor and current is induced in the conductive material, resulting in a large response. When the receiver flies off the conductor, the transmitter is not over conductive material, so the response is small.
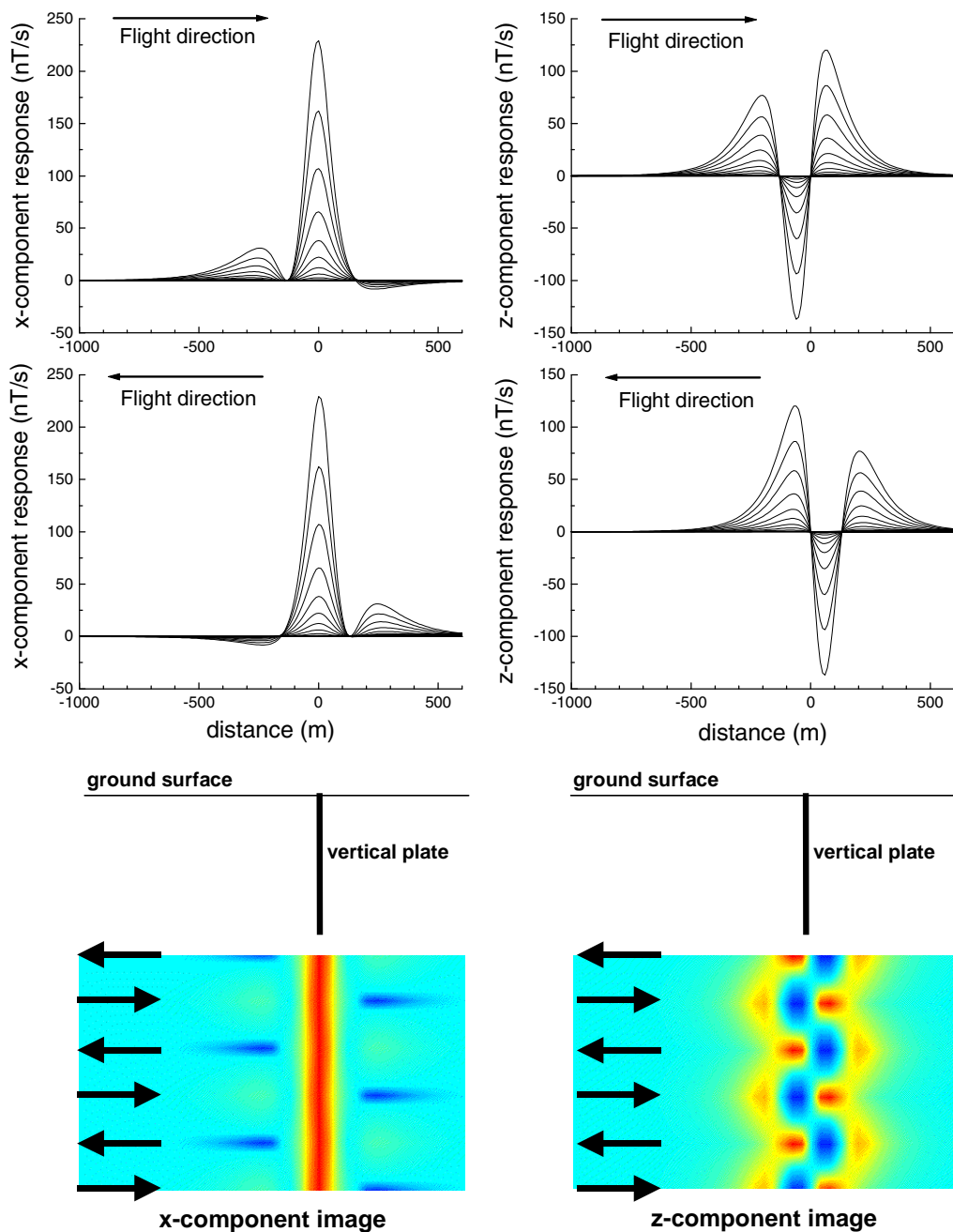
Figure 2. The response over a vertical plate. The left panels show the x-component, the right panels the z component. The top is flying left to right, the middle is right to left, the bottom is a plan image with the alternating flight directions shown with arrows.
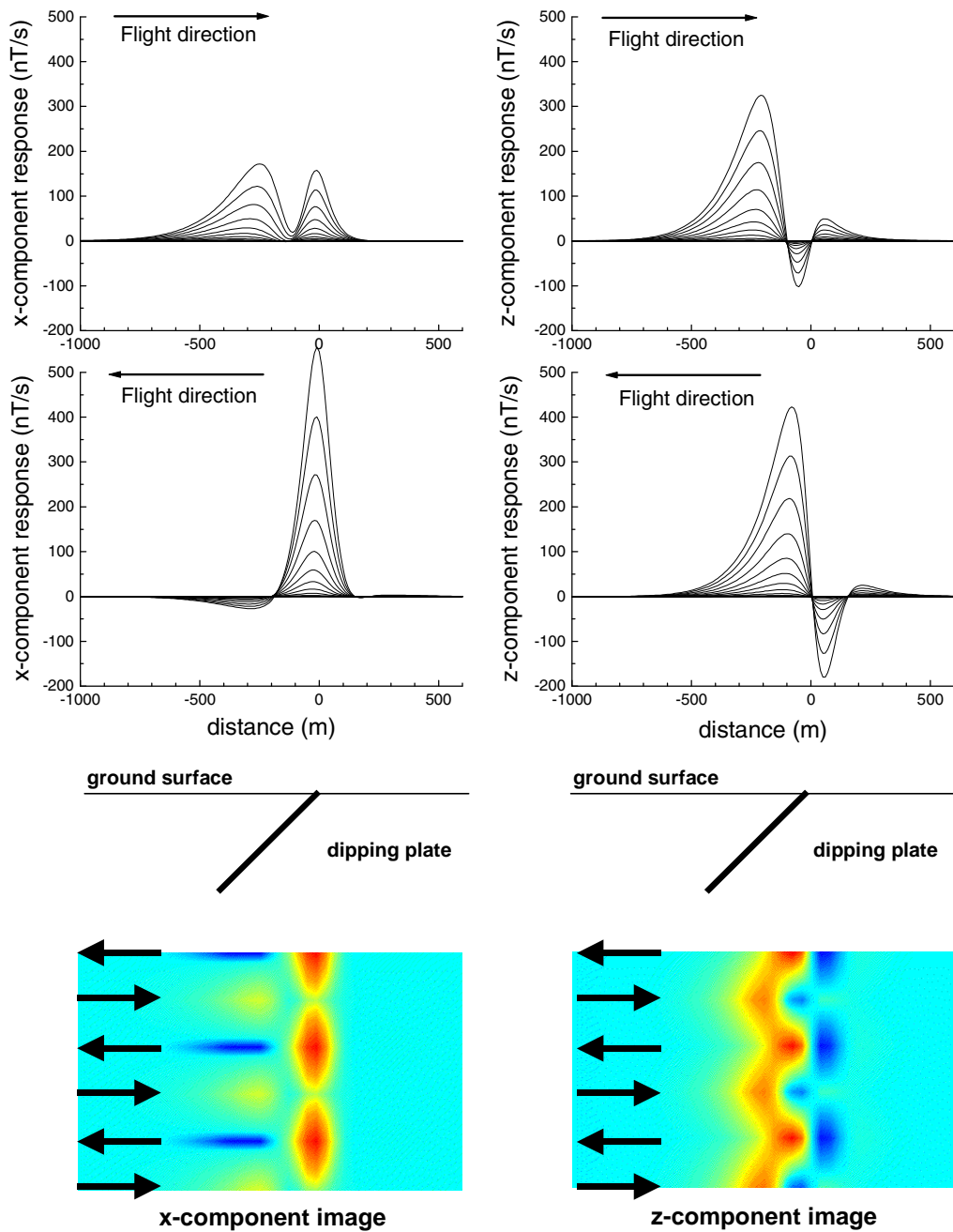
Figure 3. The response over a 45 degree dipping plate. The left panels show the x-component, the right panels the z component. The top is flying left to right, the middle is right to left, the bottom is a plan image with the alternating flight directions shown with arrows.

—
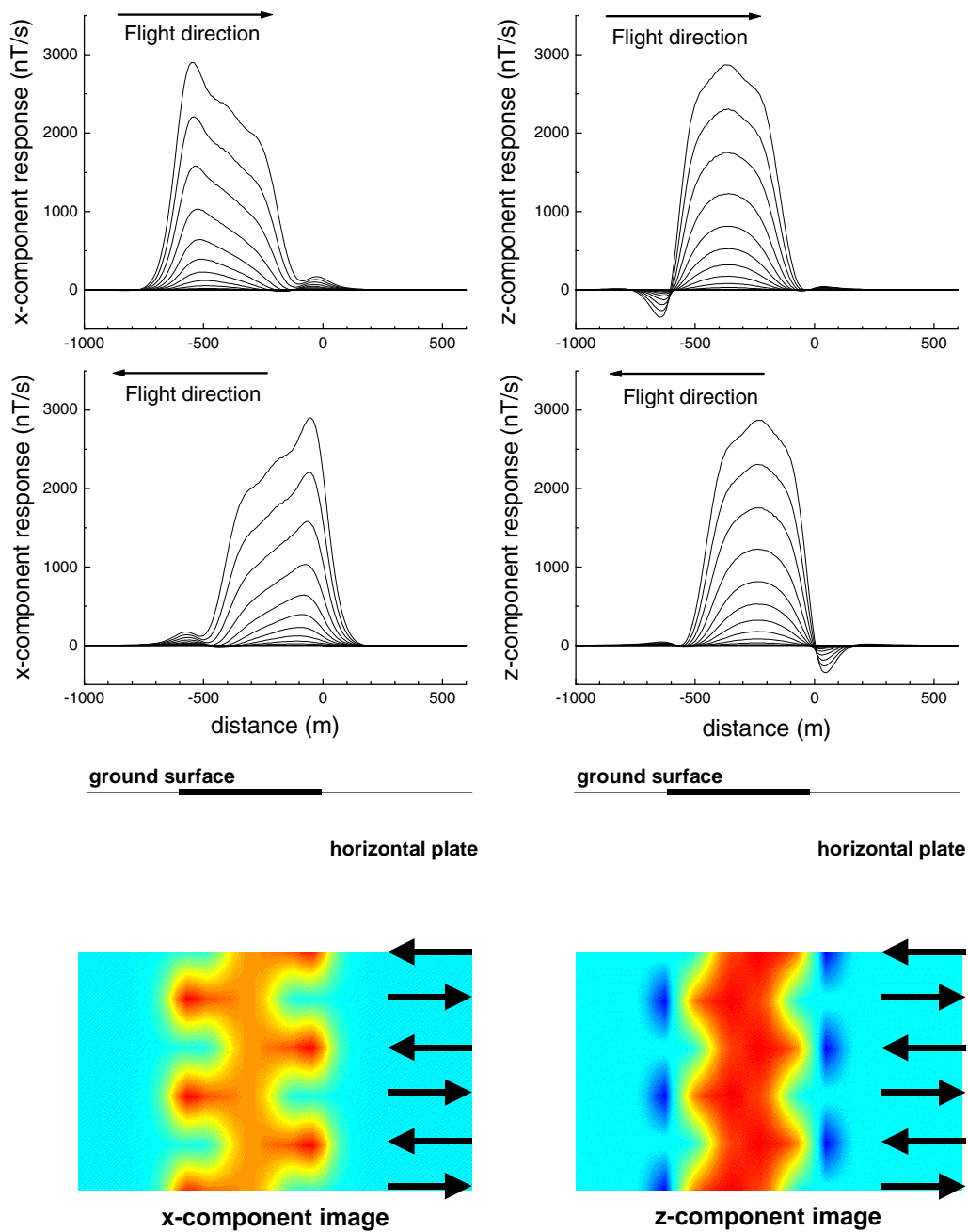
Figure 4. The response over a horizontal plate. The left panels show the x-component, the right panels the z component. The top is flying left to right, the middle is right to left, the bottom is a plan image with the alternating flight directions shown with arrows.

Appendix C

Multicomponent Modeling

Multicomponent fixed-wing airborne EM modeling

PLATE MODELING

The PLATE program has been used to generate synthetic responses over a number of plate models with varying depth of burial (0, 150 and 300 m) and dips (0, 45, 90 and 135 degrees). The geometry assumed for the fixed-wing airborne EM system is shown on the following page (Figure 1), and the transmitter waveform on the subsequent page (Figure 2). In these models, the receiver is 130 m behind and 50 m below the transmitter center.

In all cases the plate has a strike length of 600m, with a strike direction into the page. The width of the plate is 300m. As the flight path traverses the center of the plate, the y component is zero and has not been plotted.

The conductance of the plate is 20 S. In cases when the conductance is different, an indication of how the amplitudes may vary can be obtained from the nomogram included (Figure 3).

In the following profile plots (Figure 4 to 15) the plotting point is the receiver location and all of the component values are in nT/s, assuming a transmitter dipole moment of 900 000 Am^2. If the dipole moment is larger or smaller than 900 000 Am^2, then the response would be scaled up or down appropriately.

In the following profile plots (Figure 4 to 15) all components are in nT/s, for a transmitter dipole moment of 900 000 Am^2. If the dipole moment is larger or smaller, then the response should be scaled up or down appropriately.
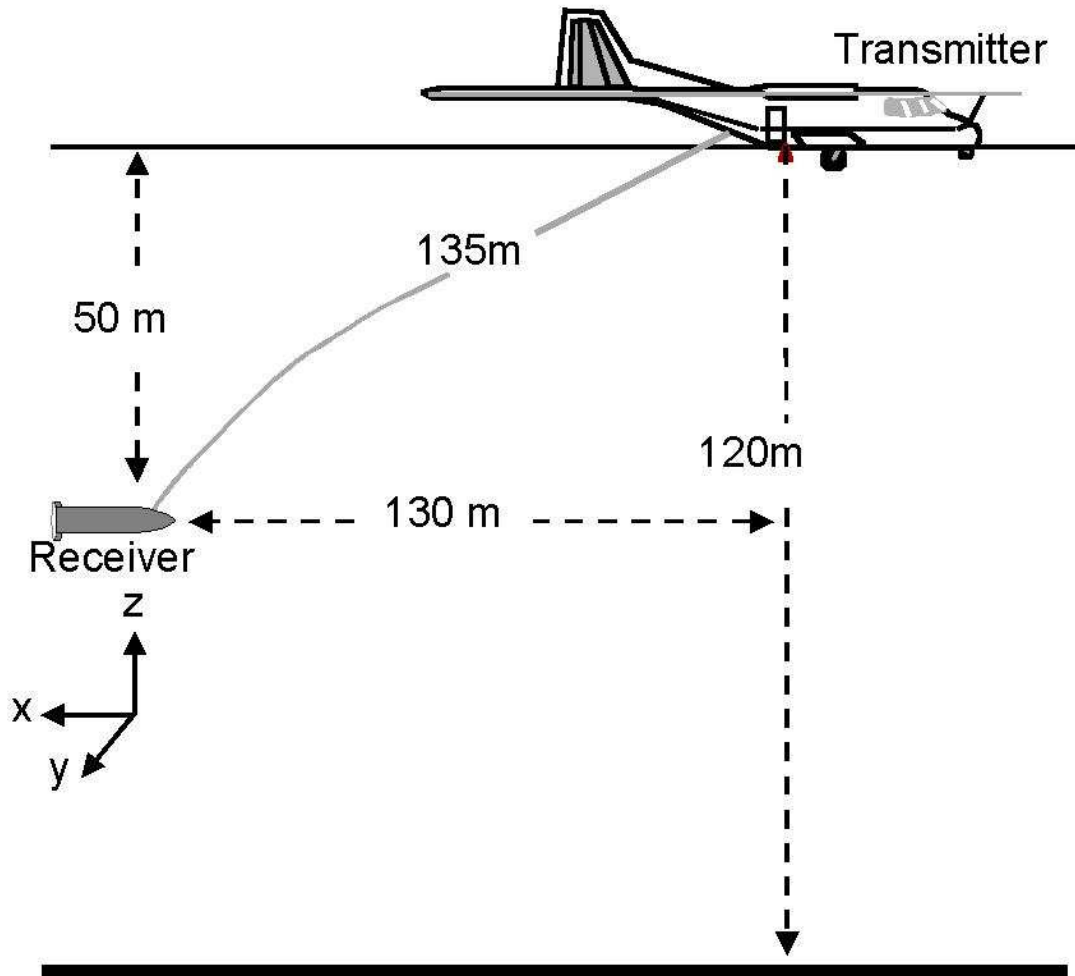
The plotting point is the receiver location.

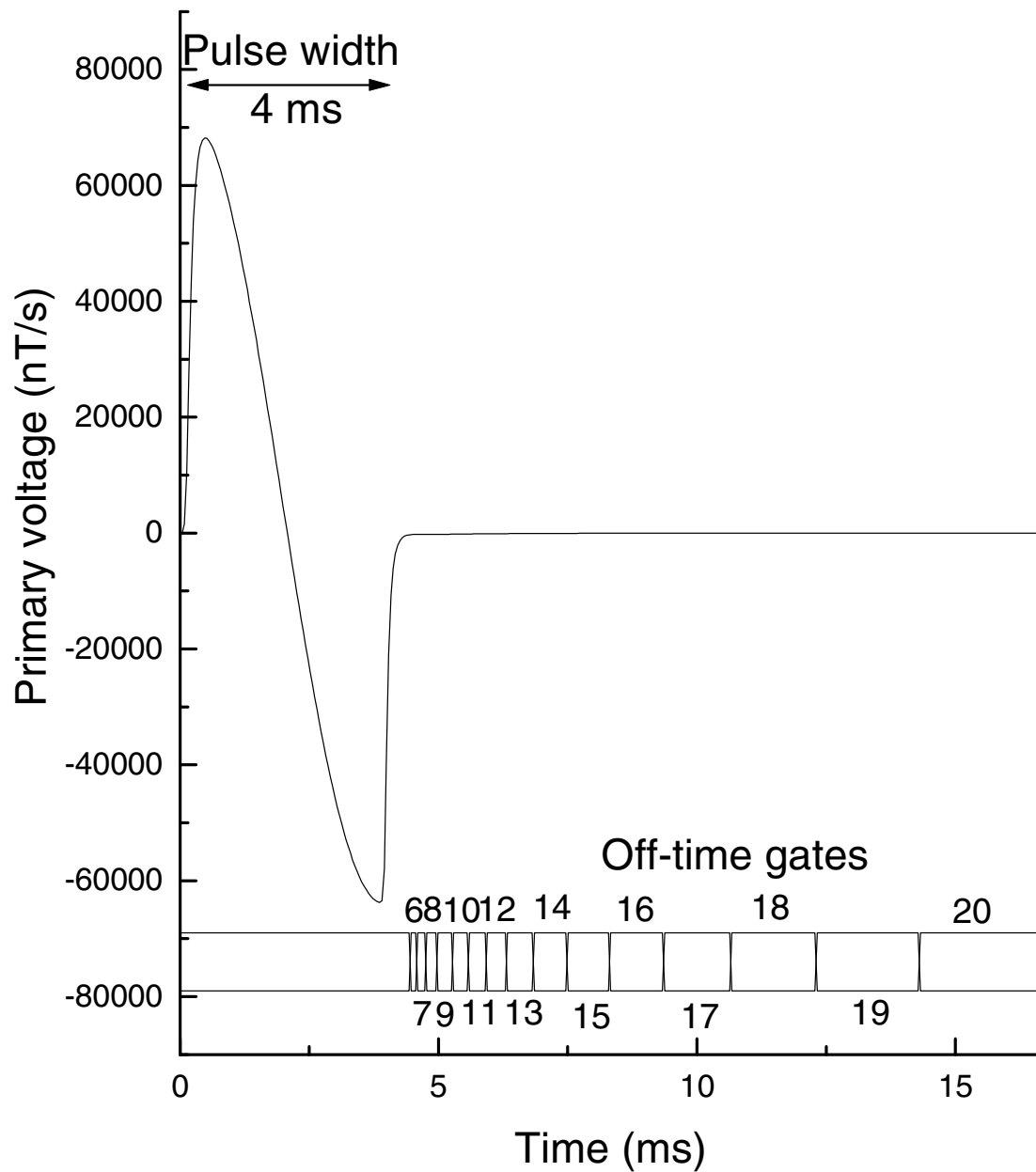Figure 1. Nominal geometry of the MEGATEM/GEOTEM system.

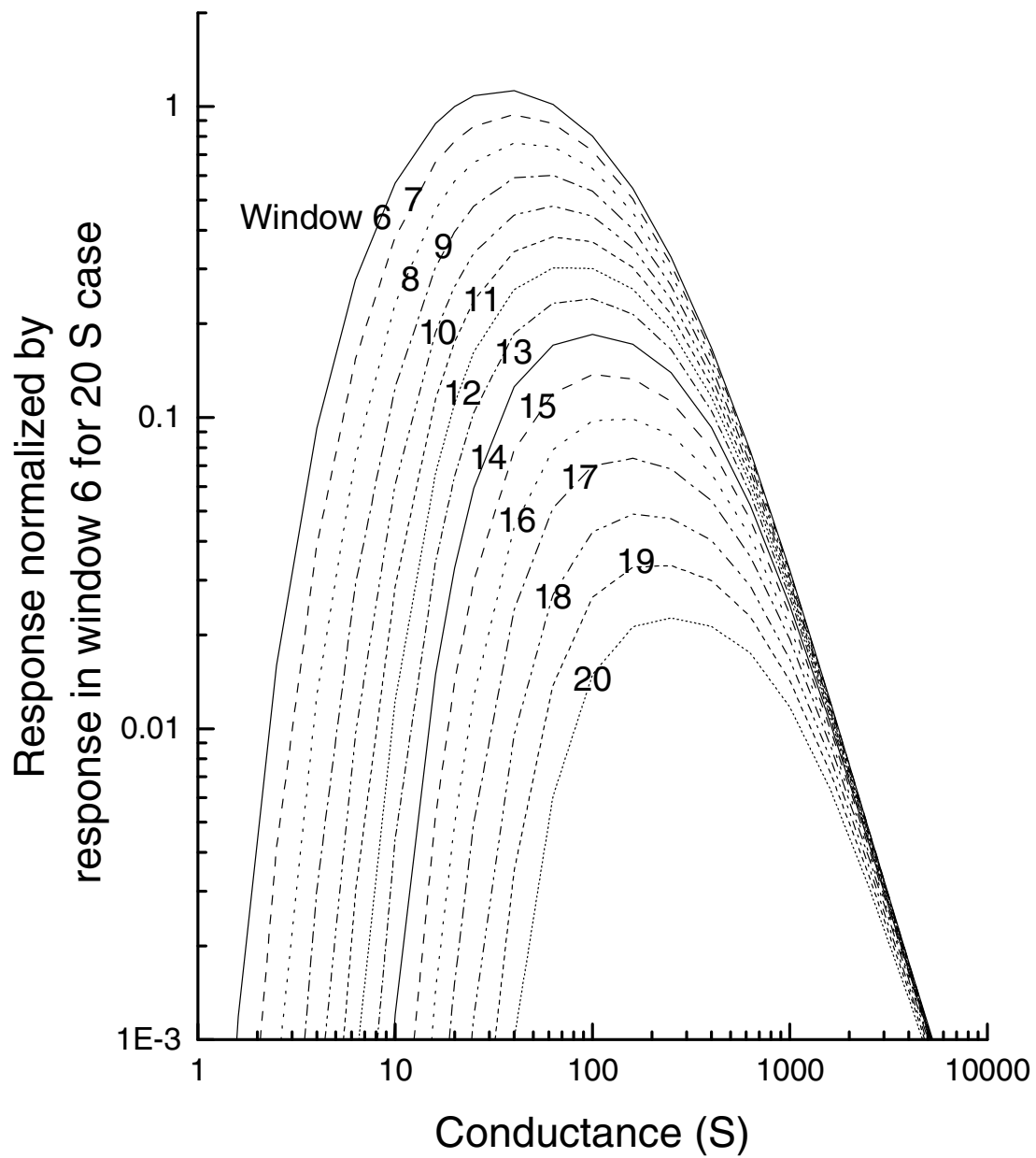Figure 2. Theoretical transmitter waveform response in the receiver.

Figure 3. Nomogram for windows 6-20 normalized to a response from a 20 Siemen conductor in window 6.
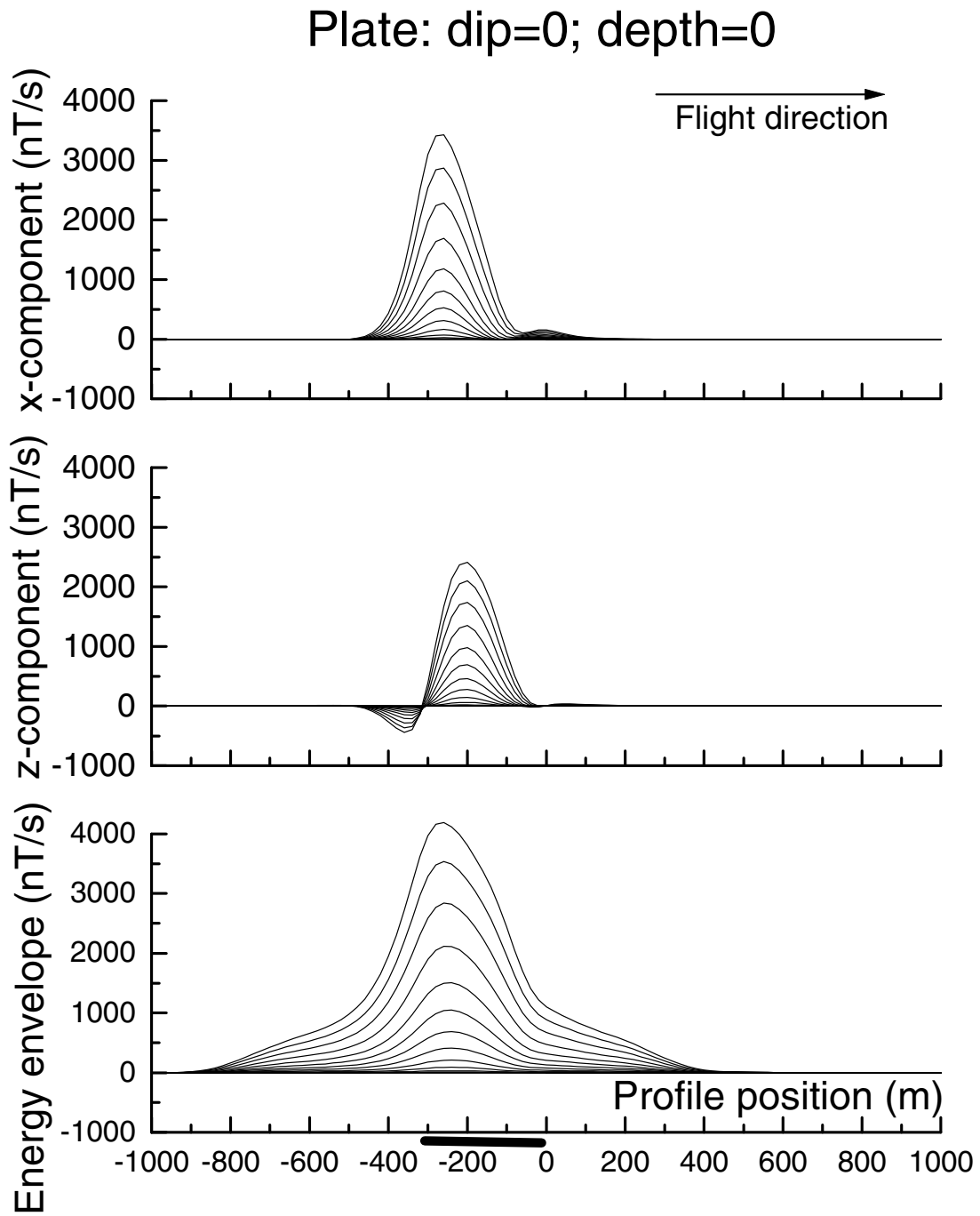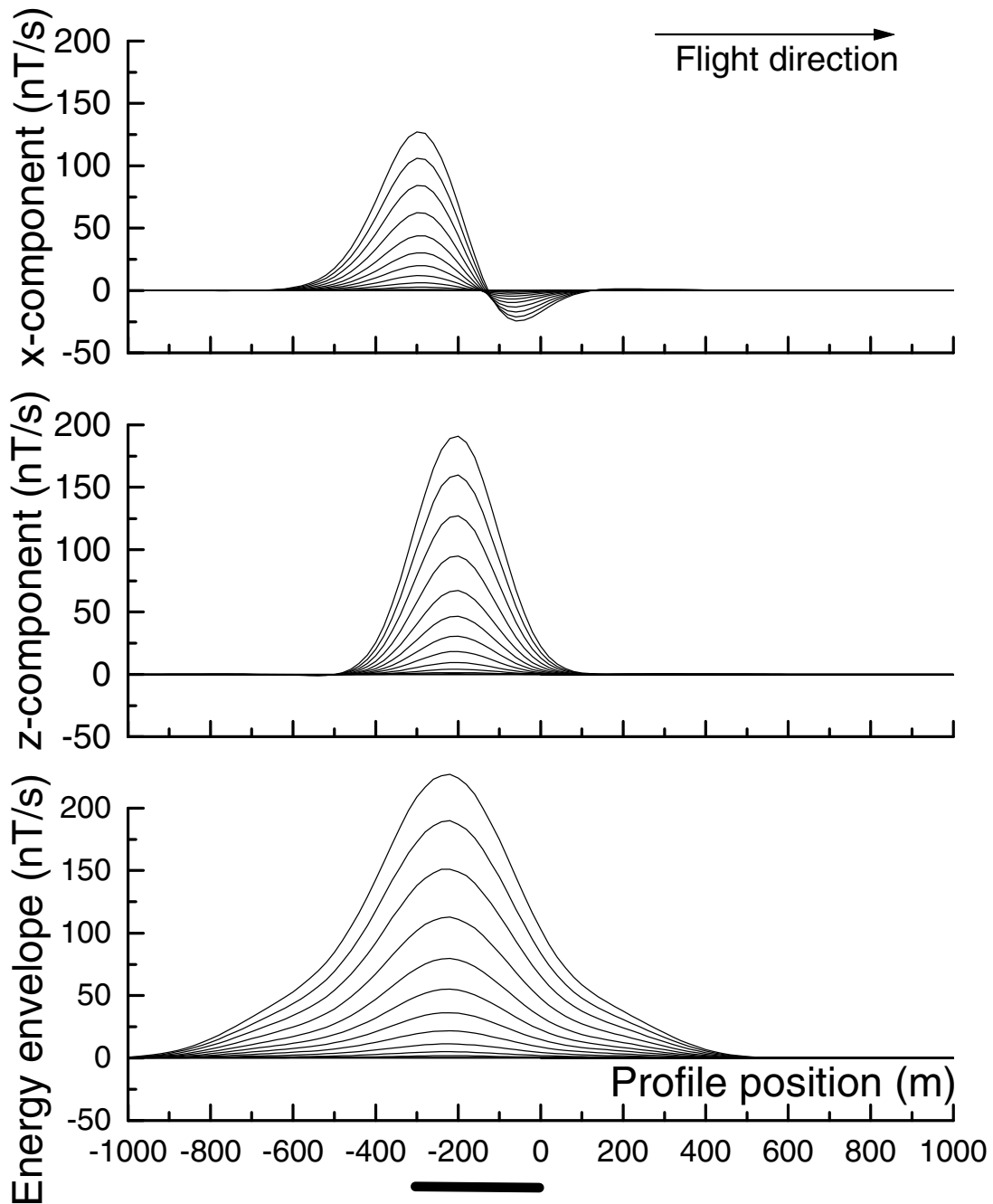
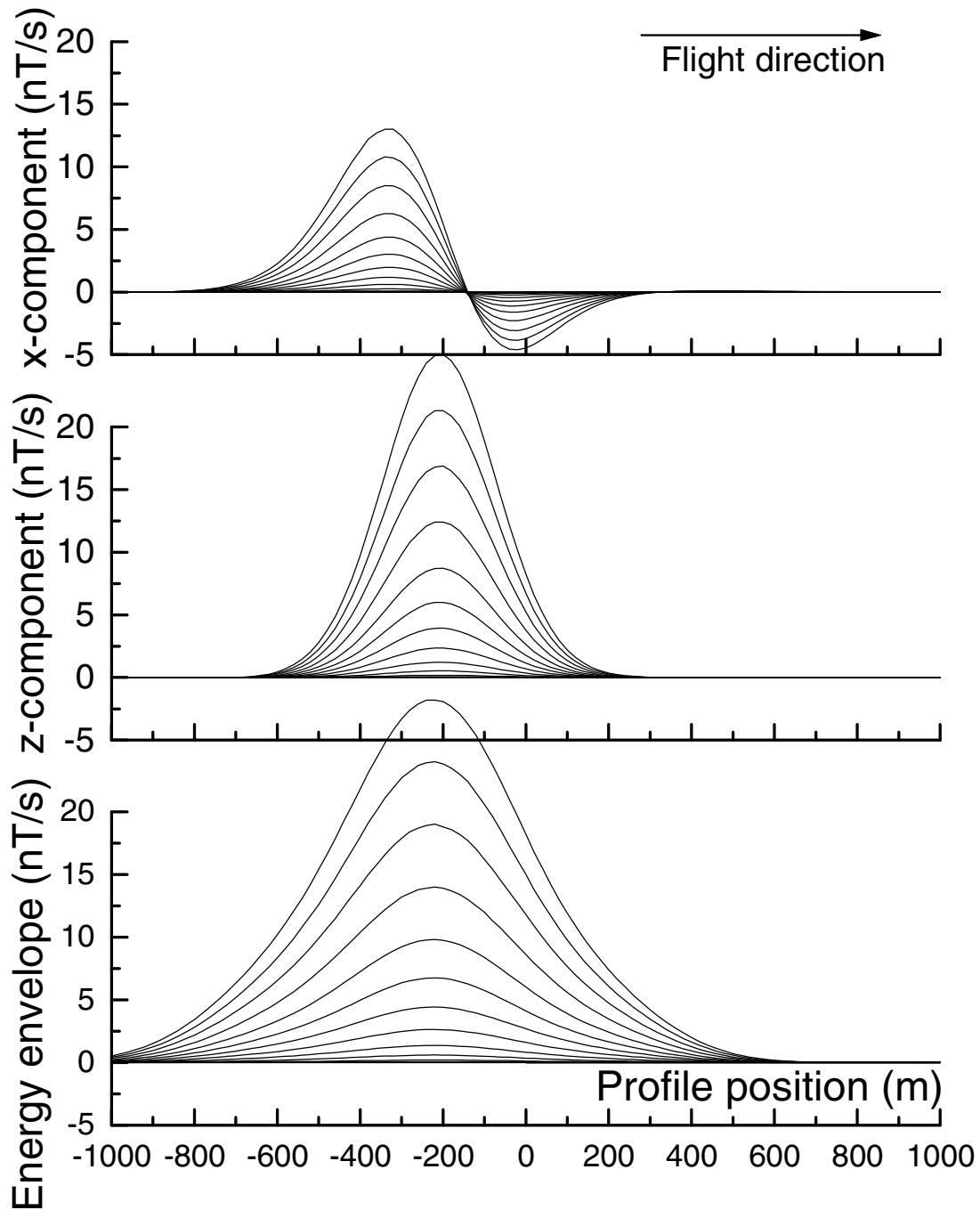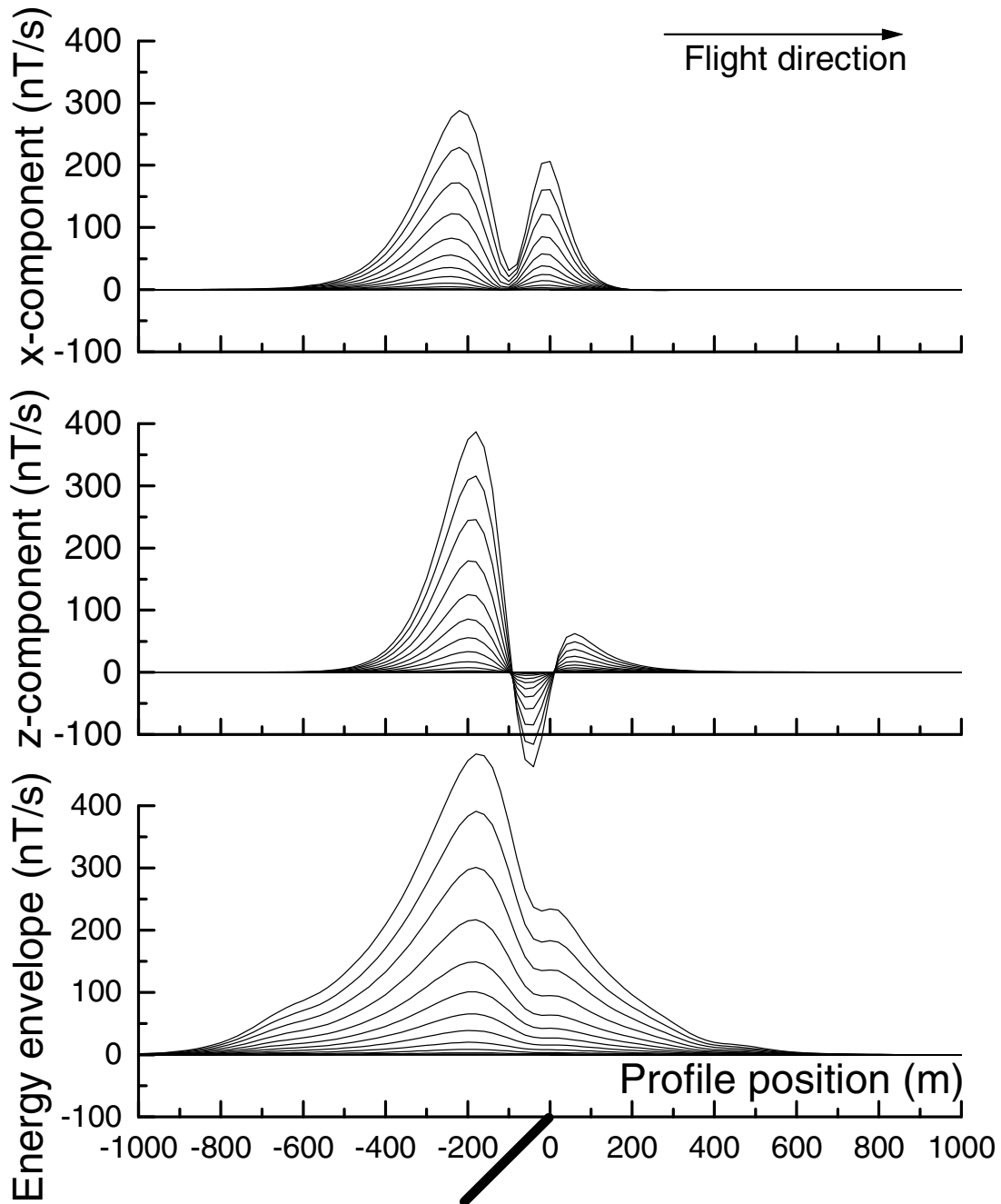# Plate: dip=0; depth=0

Figure 4.

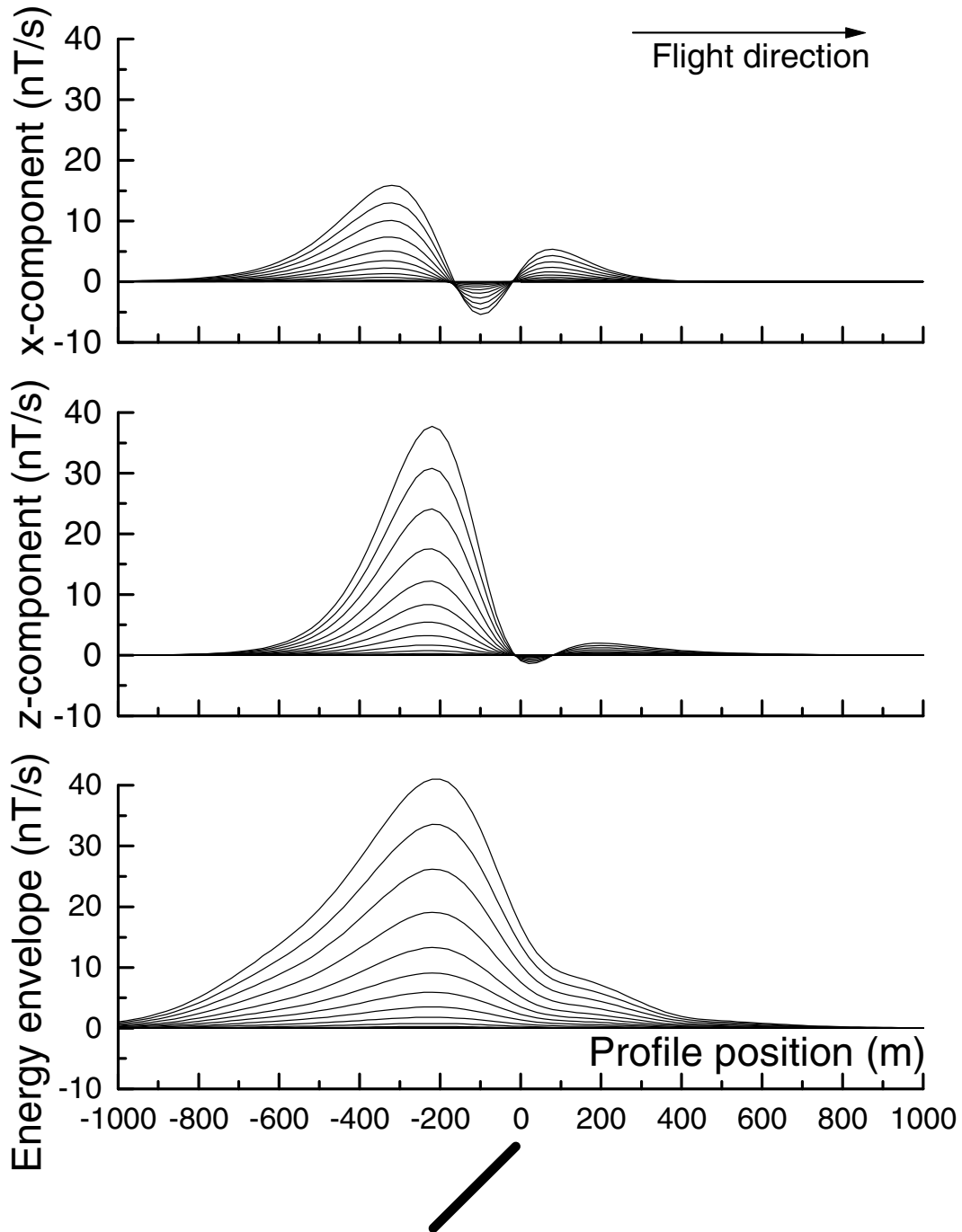# Plate: dip=0; depth=150

Figure 5.

Plate: dip=0; depth=300

Figure 6.

Plate: dip=45; depth=0

Figure 7.

Plate: dip=45; depth=150

Figure 8.
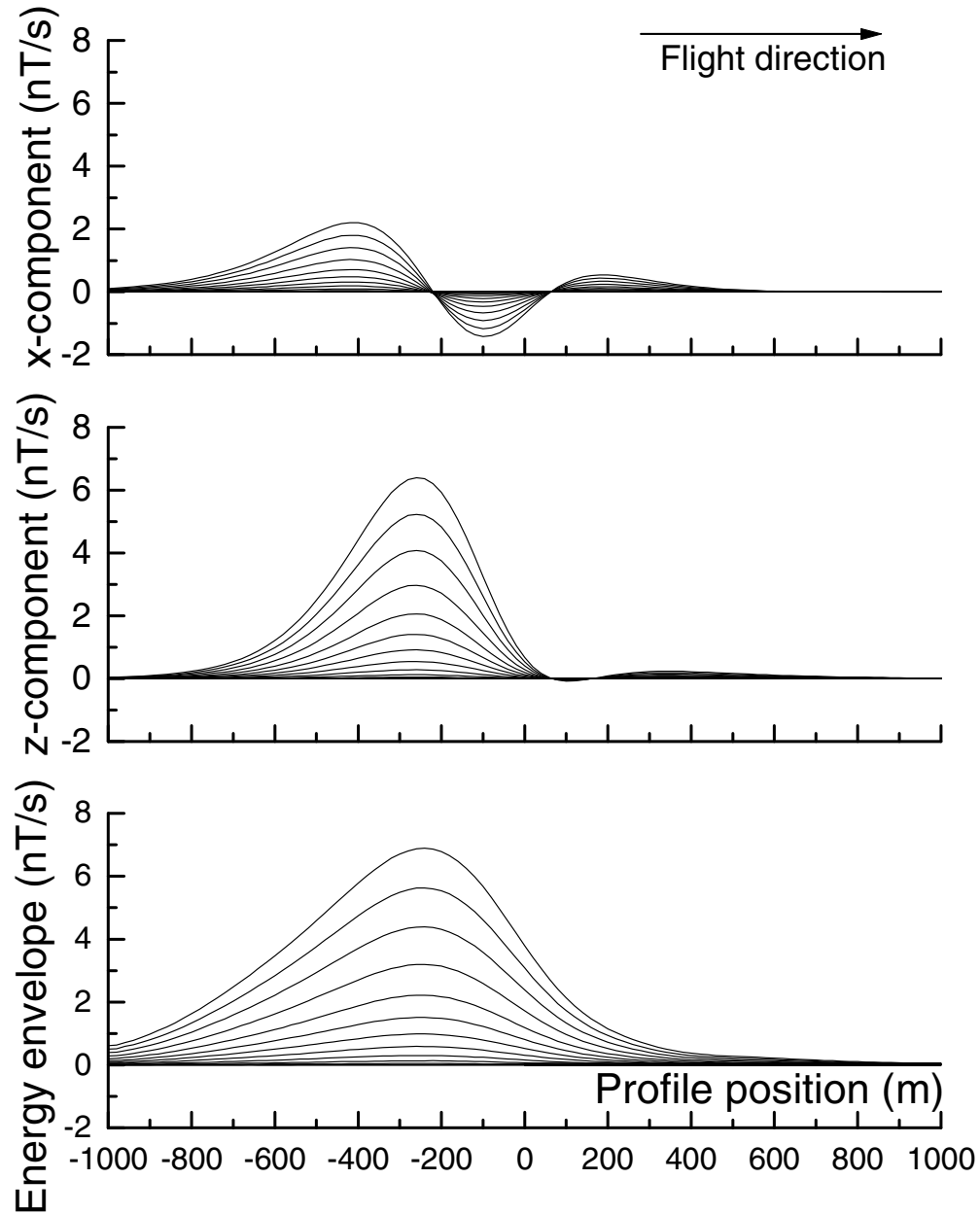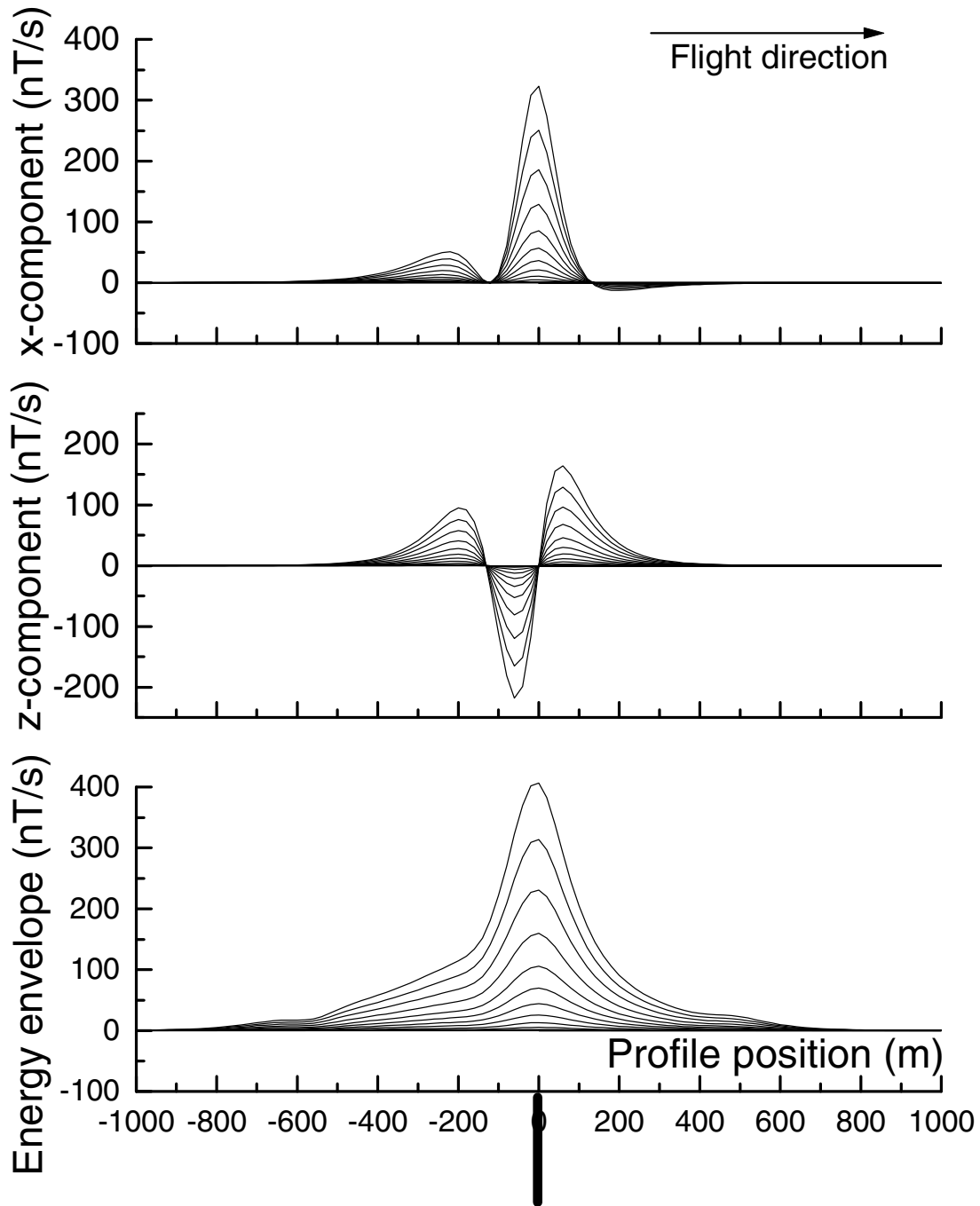
Figure 9.

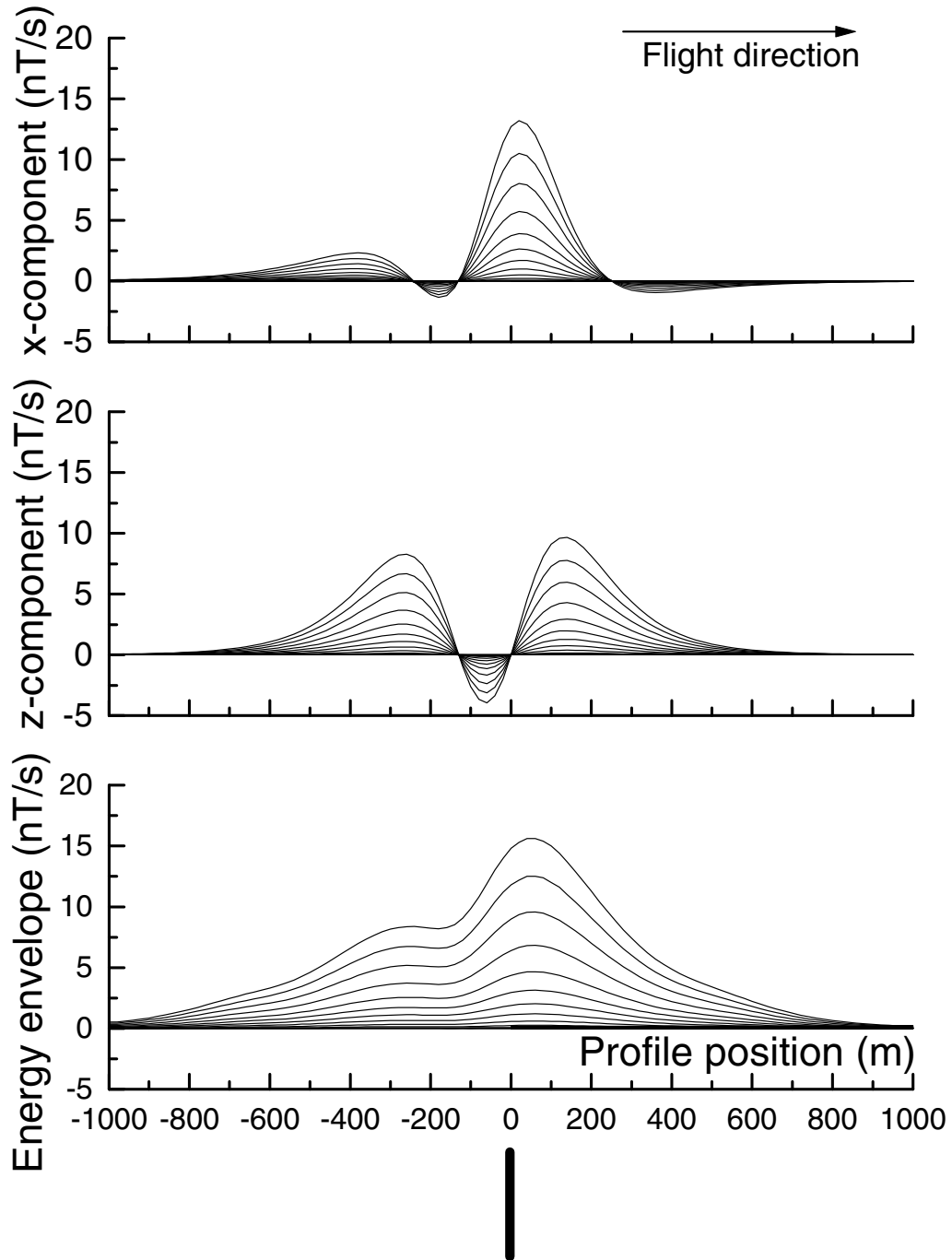Figure 10.

Plate: dip=90; depth=150
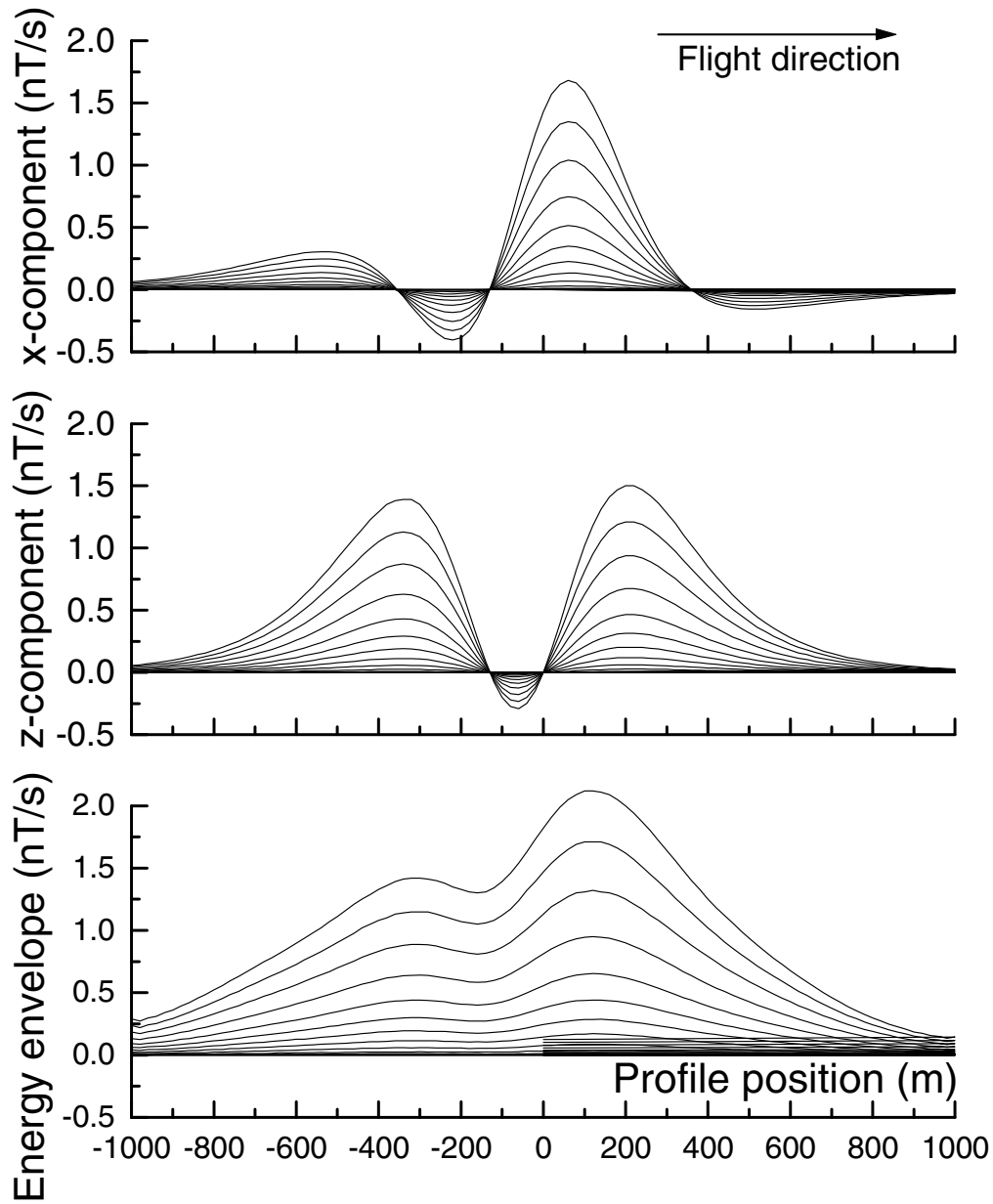

Figure 11.

Plate: dip=90; depth=300

Figure 12.
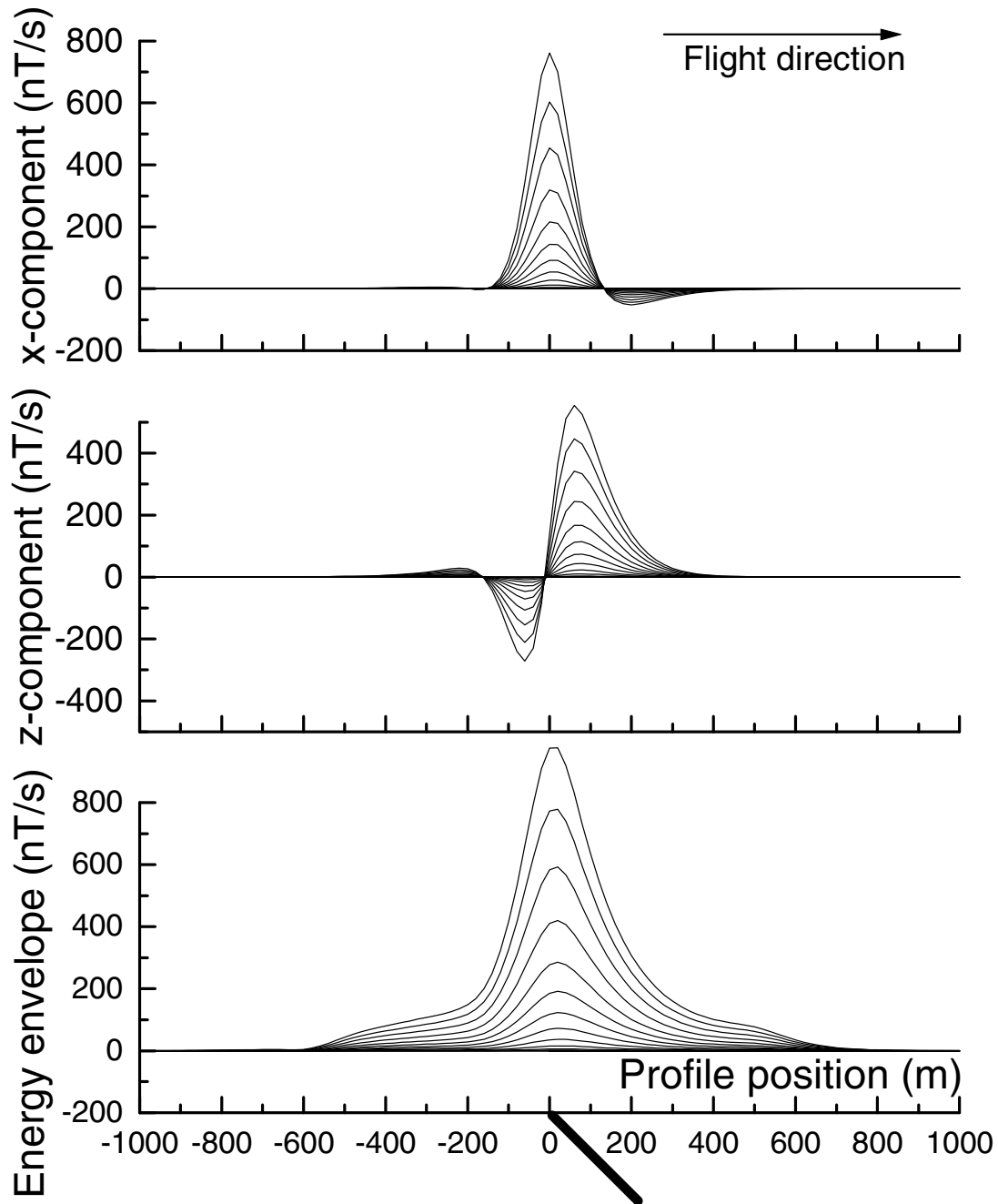
Plate: dip=135; depth=0

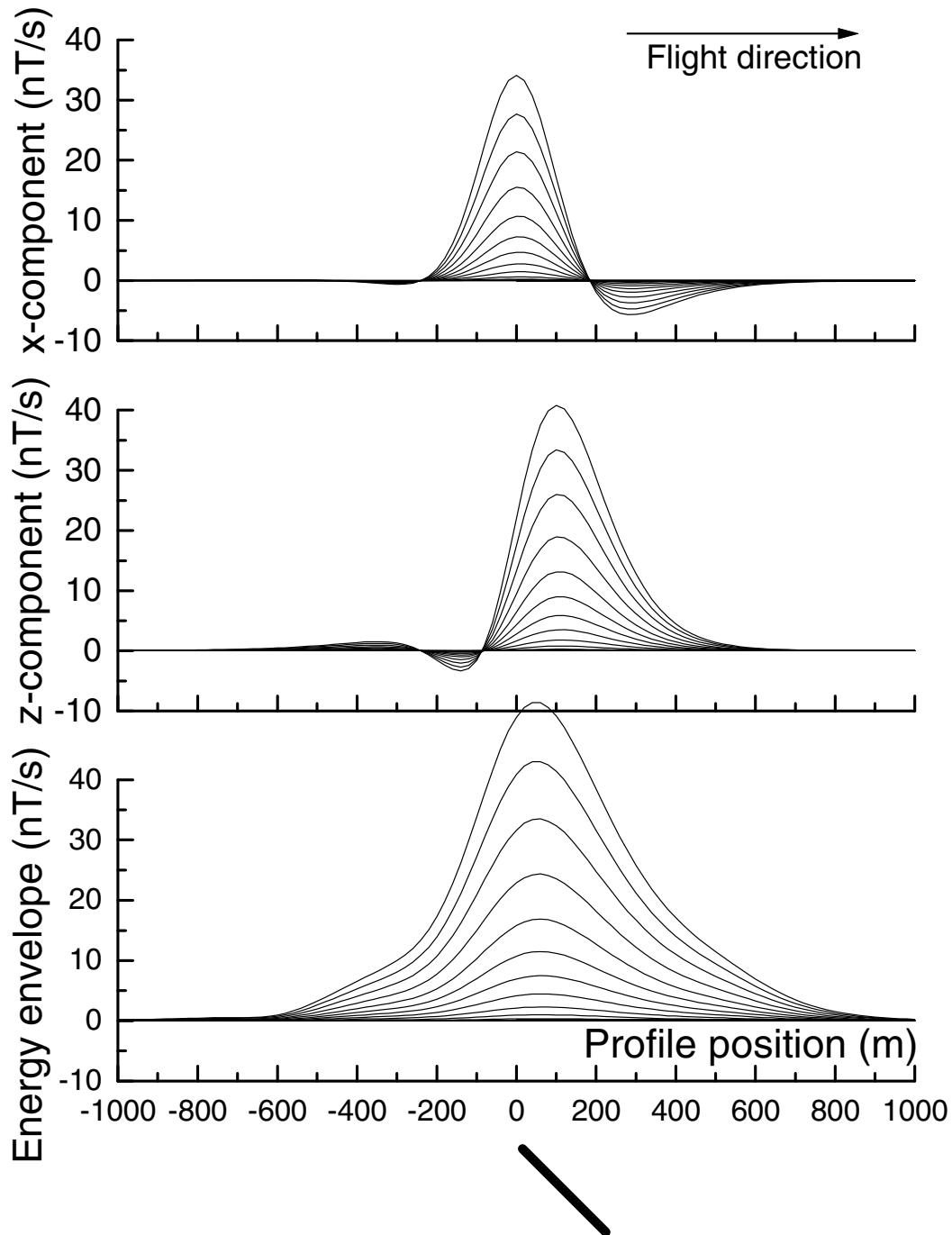
Figure 13.

Plate: dip=135; depth=150

Figure 14.

Plate: dip=135; depth=300
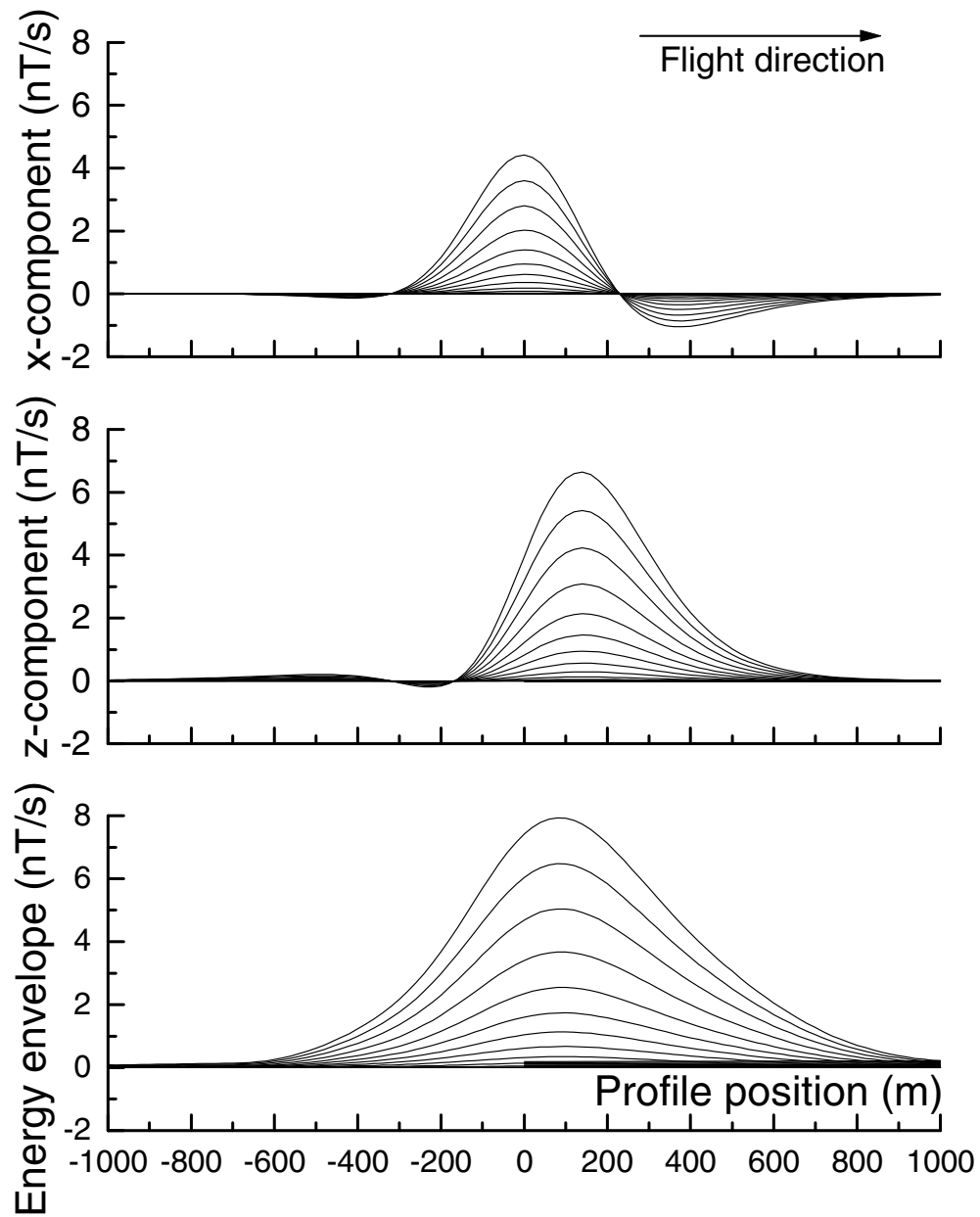
Figure 15.

SPHERE MODELING

The sphere in a uniform field program (Smith and Lee, Exploration Geophysics, 2001, pp 113-118) has been used to generate synthetic responses over a number of sphere models with varying depth of burial (0, 150 and 300 m). The geometry assumed for the fixed-wing airborne EM system and the waveform are as shown in Figures 1 and 2 above.

In all cases the sphere has a radius of 112 m. As the flight path traverses the center of the sphere, the y component is zero and has not been plotted.

The conductivity of the sphere is 1 S/m. In cases when the conductivity is different, an indication of how the amplitudes may vary can be obtained from the nomogram that follows (Figure 16).

In the following profile plots (Figure 17 to 19) all components are in nT/s, for a transmitter dipole moment of 900 000 Am^2. If the dipole moment is larger or smaller, then the response should be scaled up or down appropriately.

The plotting point is the receiver location.

Figure 16. Nomogram for windows 6-20 normalized to a response from a 1 Siemen conductor in window 6.
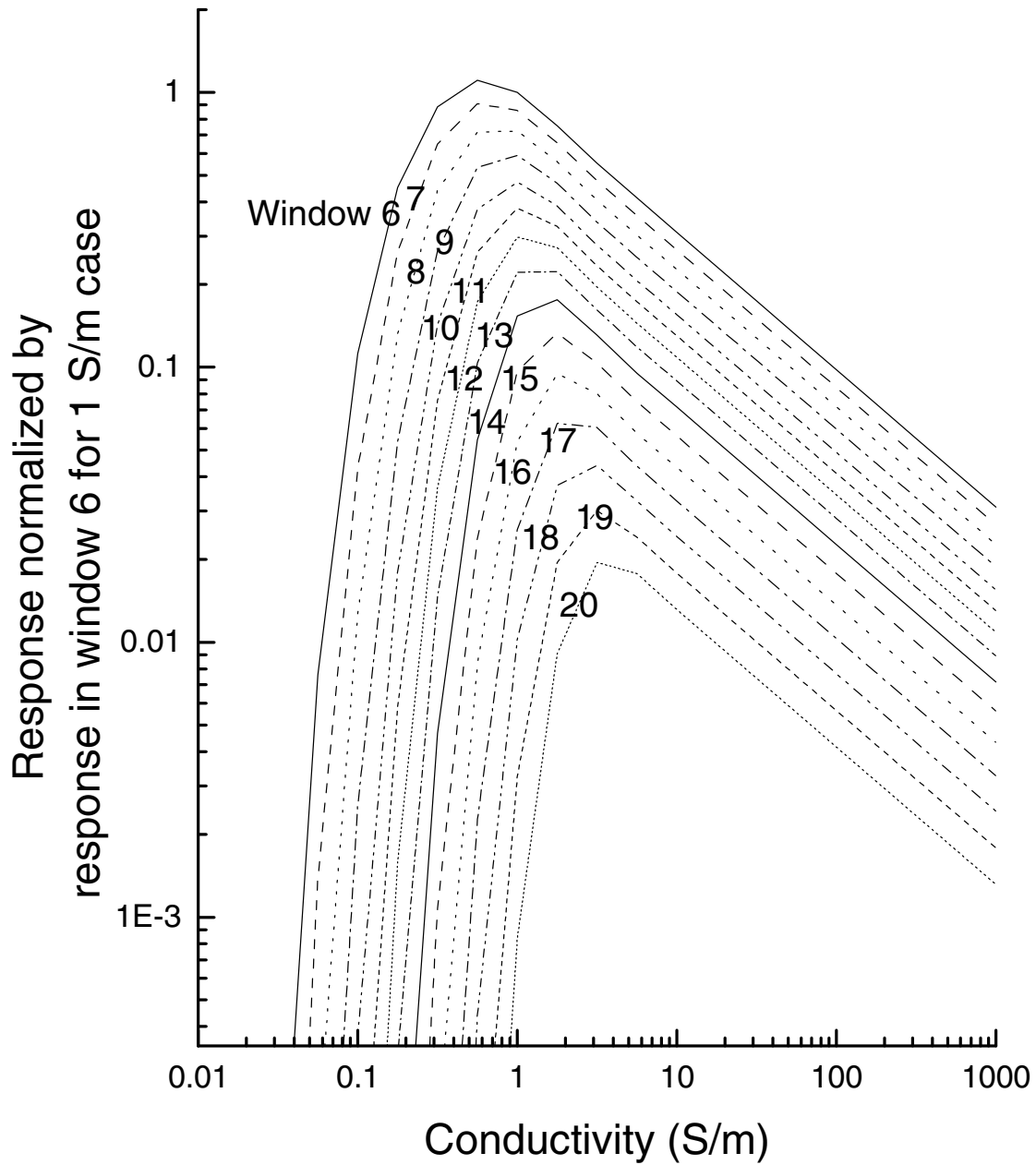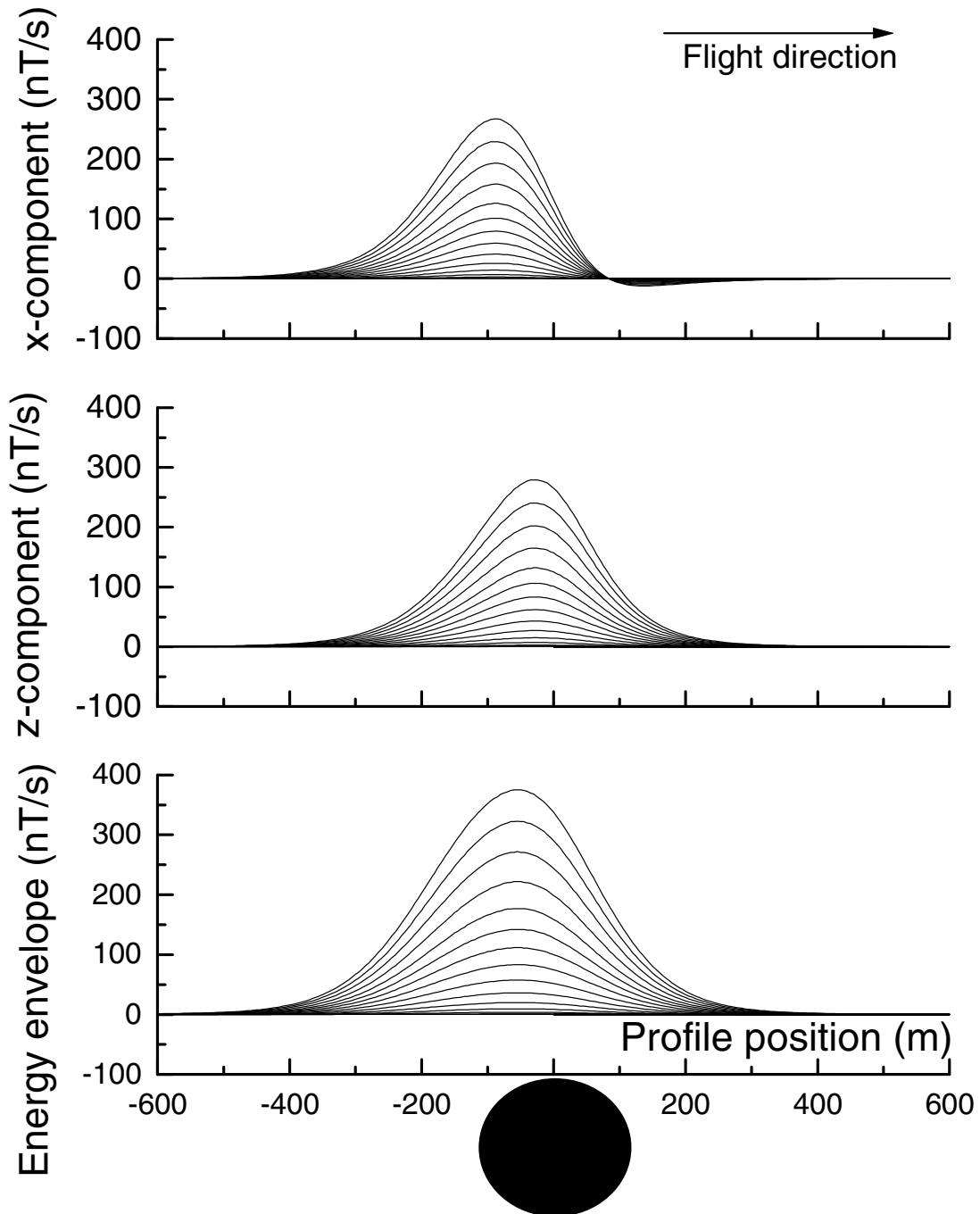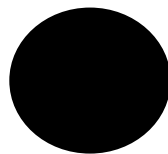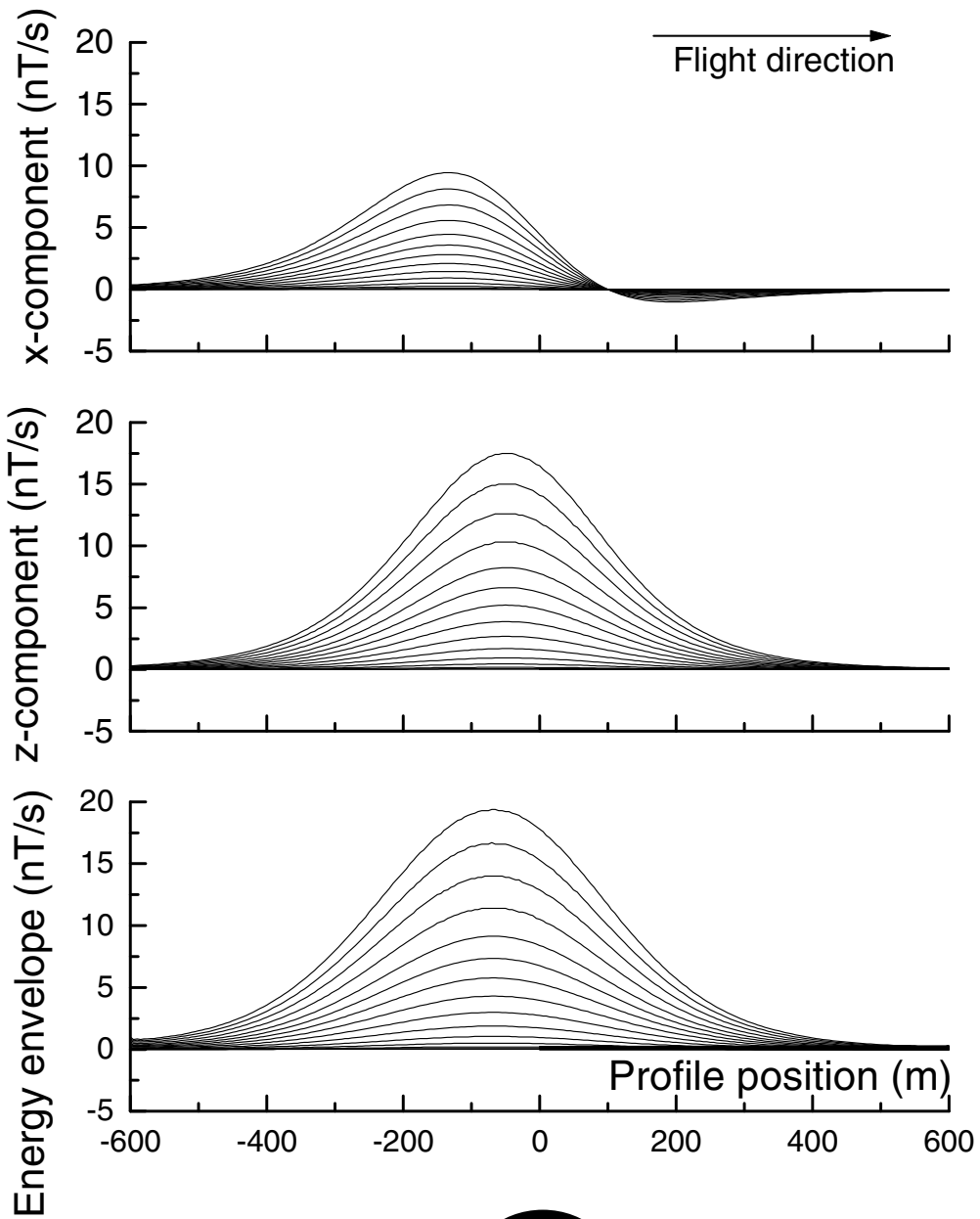
Sphere: depth to top=0

Figure 17.
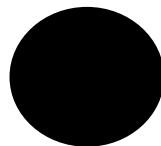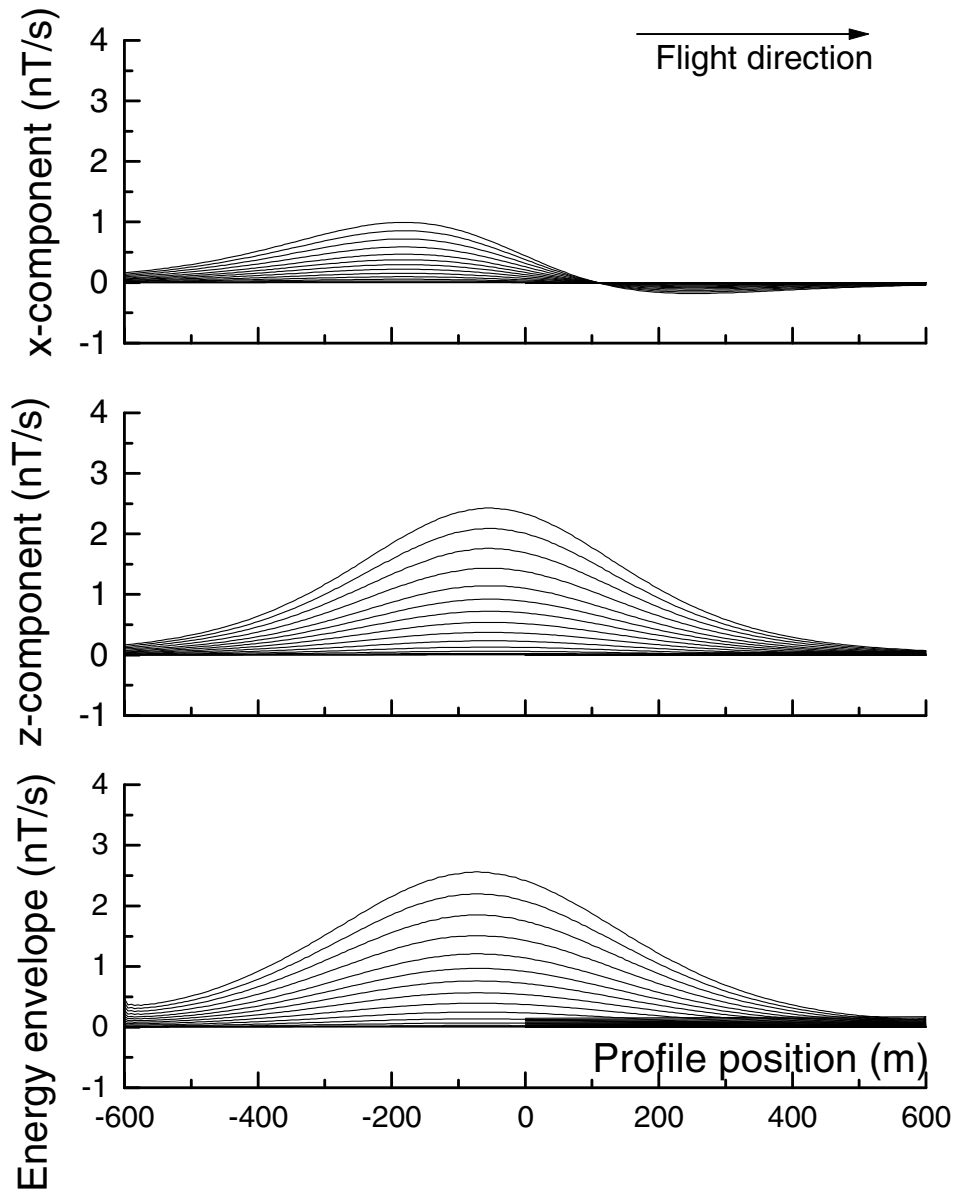
Figure 18.

Figure 19.

Appendix D

The Usefulness of Multicomponent, Time-Domain Airborne Electromagnetic Measurement

The usefulness of multicomponent, time-domain airborne electromagnetic measurements

Richard S. Smith* and Pierre B. Keating ‡

ABSTRACT

Time-domain airborne electromagnetic (AEM) systems historically measure the inline horizontal (x) component. New versions of the electromagnetic systems are designed to collect two additional components [the vertical (z) and the lateral horizontal (y) component] to provide greater diagnostic information.

In areas where the geology is near horizontal, the z-component response provides greater signal to noise, particularly at late delay times. This allows the conductivity to be determined to greater depth. In a layered environment, the symmetry implies that the y component will be zero; hence a non-zero y component will indicate a lateral inhomogeneity.

The three components can be combined to give the "energy envelope" of the response. Over a vertical plate, the response profile of this envelope has a single positive peak and no side lobes. The shape of the energy envelope is dependent on the flight direction, but less so than the shape of the x component response profile.

In the interpretation of discrete conductors, the z component data can be used to ascertain the dip and depth to the conductor using simple rules of thumb. When the profile line is perpendicular to the strike direction and over the center of the conductor, the y component will be zero; otherwise it appears to be a combination of the x and z components. The extent of the contamination of the y component by the x and z components can be used to ascertain the strike direction and the lateral offset of the target, respectively.

Having the z and y component data increases the total response when the profile line has not traversed the target. This increases the possibility of detecting a target located between adjacent flight lines or beyond a survey boundary.

INTRODUCTION

The acquisition of multiple-component electromagnetic (EM) data is becoming more commonplace. In some techniques, such as those which use the plane-wave assumption (MT, CSAMT and VLF) more than one component has been acquired as a matter of routine for some time (see reviews by Vozoff, 1990, 1991; Zonge and Hughes, 1991; McNeill and Labson, 1991). Historically, commercially available controlled-waveform finite-source systems generally measure only one component. The only systems designed to acquire multiple component data are generally experimental [e.g., those described in the appendixes of Spies and Frischknecht (1991) or proprietary (the EMP system of Newmont Exploration).

Slingram EM systems, comprising a moving dipolar transmitter and a moving receiver, generally only measure one component of the response. Although the MaxMin system was designed with a capability to measure a second (minimum coupled) component, this capability is not used extensively in practice. The only systems that use two receiver coils in practice are those that measure the wavetilt or polarization ellipse (Frischknecht et al., 1991).

Historically, time-domain EM systems have been capable of collecting multicomponent data in a sequential manner by reorienting the sensor for each component direction. The usefulness of additional components is discussed by Macnae (1984) for the case of the UTEM system. Macnae concluded that, as extra time was required to acquire the additional components, this time was better spent collecting more densely spaced vertical-component data. The vertical-component, which is less subject to sferic noise, could subsequently be converted to the horizontal components using the Hilbert transform operators.

Recent instrument developments have been towards multicomponent systems. For example, commercially available ground-EM systems such as the Geonics PROTEM, the Zonge GDP-32 and the SIROTEM have been expanded to include multiple input channels that allow three (or more) components to be acquired simultaneously. There is also a version of the UTEM system currently being developed at Lamontagne Geophysics Ltd. These multichannel receivers require complimentary multicomponent sensors -- for ground-based systems these have been developed by Geonics Ltd and Zonge Engineering and Research Organization. The interpretation of fixed-source, multi-component ground-EM data is described in Barnett (1984) and Macnae (1984).

In the past, multi-component borehole measurements have been hindered by the lack of availability of multi-component sensor probes. Following the development of two prototype probes (Lee, 1986; Hodges et al., 1991), multi-component sensors are now available from Crone Geophysics and Exploration Ltd and Geonics. Three component UTEM and SIROTEM borehole sensors are also in development at Lamontagne and Monash University (Cull, 1993), respectively. Hodges et al. (1991) present an excellent discussion of techniques that can be used to interpret three-component borehole data.

Airborne systems such as frequency-domain helicopter electromagnetic methods acquire data using multiple sensors. However, each receiver has a corresponding transmitter that either operates at a different frequency or has a different coil orientation (Palacky and West, 1991). Hence, these systems are essentially multiple single-component systems. The exception to this rule is the now superseded Dighem III system (Fraser, 1972) which used one transmitter and three receivers.

The only multicomponent airborne EM (AEM) system currently in operation is the SPECTREM system (Macnae, et al., 1991). This is a proprietary system (owned and operated by

Anglo-American Corporation of South Africa Ltd.), based on the PROSPECT system (Annan, 1986). The Prospect system was originally designed to acquire the *x, y* and *z* components, but SPECTREM is apparently only collecting two components (x and z) at the time of writing. Other multi-component systems currently in development are:

1)   the SALTMAP system,
2)   a helicopter time-domain system (Hogg, 1986), and
3)   a new version of the GEOTEM® system (GEOTEM is a registered trademark of Geoterrex).

Apart from a few type curves in Hogg (1986), there is little literature available which describes how to interpret data from these systems.

This paper is intended to give an insight into the types of responses expected with the new multi-component AEM systems, and the information that can be extracted from the data. The insight could be of some assistance in interpreting data from multicomponent moving-source ground EM systems (should this type of data be acquired).

The use of multi-component data will be discussed for a number of different applications. For illustration purposes, this paper will use the transmitter-receiver geometry of the GEOTEM system (Figure 1), which is comparable to the other fixed-wing geometries (SPECTREM and SALTMAP). The GEOTEM system is a digital transient EM system utilizing a bipolar half-sinusoidal current waveform [for more details refer to Annan and Lockwood (1991)]. The sign convention used in this paper is shown in Figure 1, with the *y* component being into the page. In a practical EM system, the receiver coils will rotate in flight. We will assume that the three components of the measured primary field and an assumed bird position have been used to correct for any rotation of the coil.
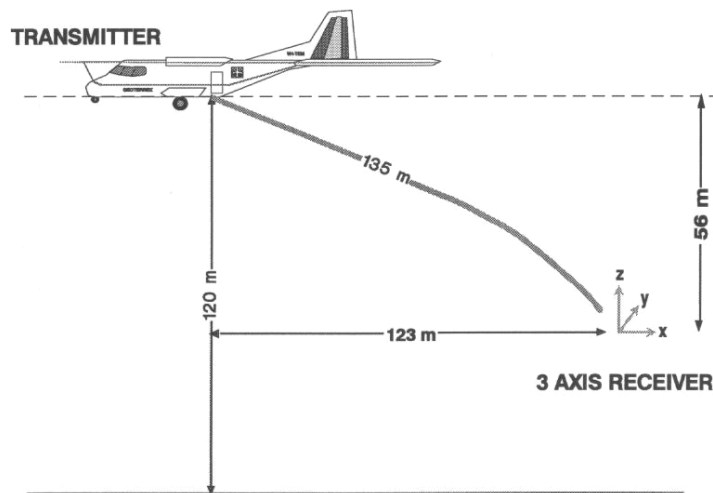

Fig. 1: The geometric configuration of the GEOTEM system. The system comprises a transmitter on the aircraft and a receiver sensor in a "bird" towed behind the aircraft. The *z* direction is positive up, *x* is positive behind the aircraft, and *y* is into the page (forming a right-hand coordinate system).

SOUNDING IN LAYERED ENVIRONMENTS

In a layered environment, the induced current flow is horizontal (Morrison et al., 1969) so the z component of the secondary response (V_z) is much larger than the x component (V_x), particularly in resistive ground and/or at late delay times. At the same time, the sferic noise in the z direction is 5 to 10 times less than in the horizontal directions (Macnae, 1984; McCracken et al., 1986), so V_z has a greater signal-to-noise ratio. Figure 2 shows theoretical curves over two different, but similar, layered earth models. One model is a half-space of 500 Ω·m and the other is a 350 m thick layer of 500 Ω·m overlying a highly resistive basement. In this plot the data have been normalized by the total primary field. The z component (V_z) is 6 to 10 times larger than V_x, and both curves are above the noise level, at least for part of the measured transient. On this plot, a noise level of 30 ppm has been assumed, which would be a typical noise level for both components when the sferic activity is low. To distinguish between the response of the half-space and thick layer, the difference between the response of one model and the response of the other model must be greater than the noise level. Figure 3 shows this difference for both components. Only the V_z difference is above the noise level. Hence for the case shown, V_z is more useful than V_x for determining whether there is a resistive layer at 350 m depth. Because V_z is generally larger in a layered environment, the vertical component will generally be better at resolving the conductivity at depth.

In the above discussion, we have assumed that corrections have been made for the coil rotation. An alternative approach is to calculate and model the magnitude of the total field, as this quantity is independent of the receiver orientation. Macnae et al. (1991) used this strategy when calculating the conductivity depth sections for SPECTREM data.

The symmetry of the secondary field of a layered environment is such that the y component response (V_y) will always be zero. In fact, the V_y component will be zero whenever the conductivity structure on both sides of the aircraft is the same. A non-zero V_y is therefore useful in identifying off-line lateral inhomogeneities in the ground.
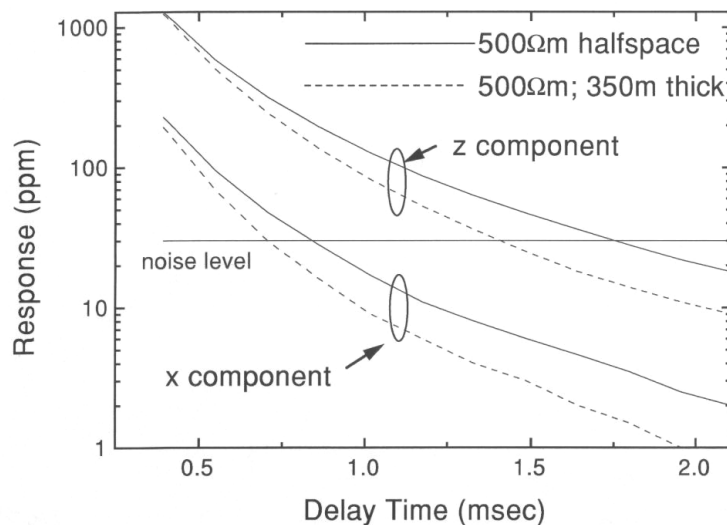
Fig. 2. The response for a 500 Ω·m half-space (solid line) and a 500 Ω·m layer of thickness 350 m overlying a resistive half-space (dashed line). The z-component responses are the two curves with the larger amplitudes and the two x-component response curves are 6 to 10 times smaller than the corresponding z component. A noise level of 30 ppm is considered to be typical of both components in the absence of strong sferics.

Halfspace and thick layer models
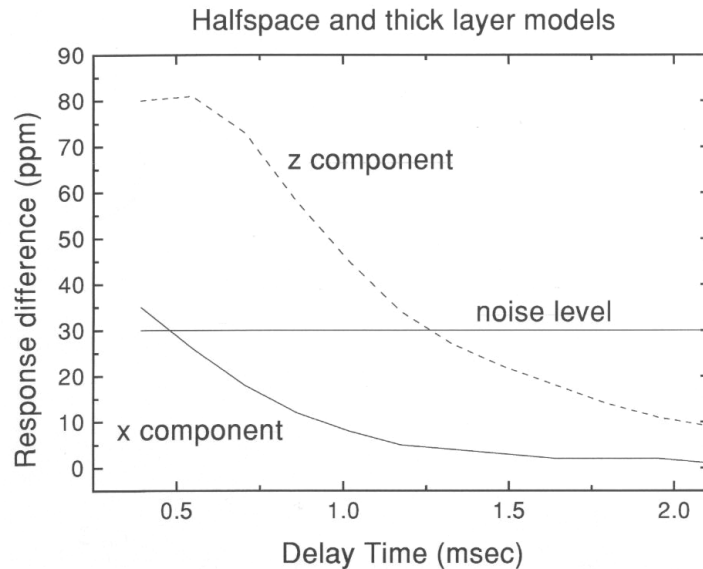
Fig. 3: The difference in the response of each component for the half-space and thick layer models of Figure 2. Only the z-component difference is above the noise level for a significant portion of the transient. Therefore, this is the only component capable of distinguishing between the responses of the two models.

DISCRETE CONDUCTORS

In our discrete conductor study, models have been calculated using a simple plate in free-space model (Dyck and West, 1984) to provide some insight into the geometry of the induced field. The extension to more complex models, such as those incorporating current gathering, will not be considered in this paper.

Historically, airborne transient electromagnetic (TEM) data have been used for conductor detection. The old INPUT system was designed to measure V_x because this component gave a large response when the receiver passed over the top of a vertical conductor. The bottom part of Figure 4 shows the response over a vertical conductor, which has been plotted at the receiver position. The V_x profile (smaller of the two solid lines) has a large peak corresponding with the conductor position. Note that there is also a peak at 200 m, just before the transmitter passes over the conductor, and a trailing edge negative to the left of the conductor. The z component (dashed line) has two peaks and a large negative trough just before the conductor. Because of the symmetry, the V_y response (dotted line) is zero.

All the peaks, troughs and negatives make the response of a single conductor complicated to display and hence interpret. The display can be simplified by plotting the "energy envelope" (EE) of the response. This quantity is defined as follows:

$$EE = \sqrt{V_x^2 + \overline{V}_x^2 + V_y^2 + \overline{V}_y^2 + V_z^2 + \overline{V}_z^2},$$

where $^-$ denotes the Hilbert transform of the quantity. The energy envelope plotted on Figure 4 (the larger of the two solid curves) is almost symmetric, and would be a good quantity to present in plan form (as contours or as an image). For flat-lying conductors, the energy envelope has a maximum at the leading edge (just after the aircraft flies onto the conductor).
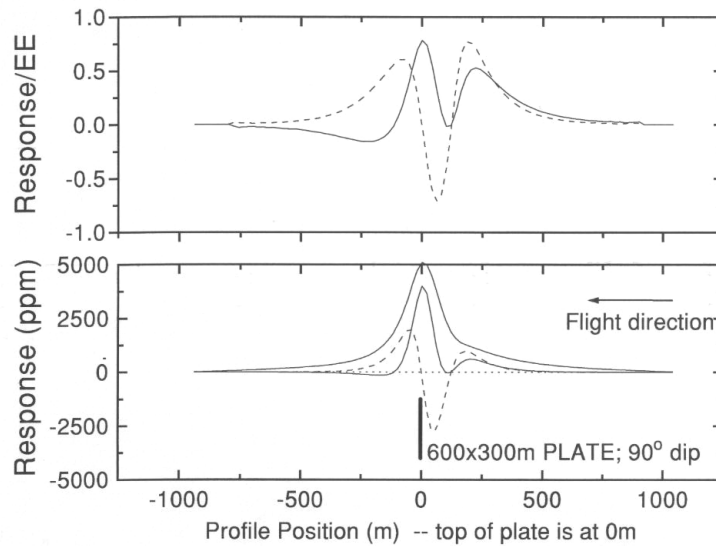
Fig. 4. (Bottom) the response of a 600 by 300 m plate 120 m below an aircraft flying from right to left. The plotting point for the response is below the receiver. The *x*-component response is the smaller amplitude solid line, the *z*-component is the dashed line, and the *y*-component response is the dotted line. The larger amplitude solid line is the "energy envelope" of all three components. (Top) the *z*- and *x*-components normalized by the energy envelope. These and all subsequent curves are for a delay time of 0.4 ms after the transmitter current is turned off.
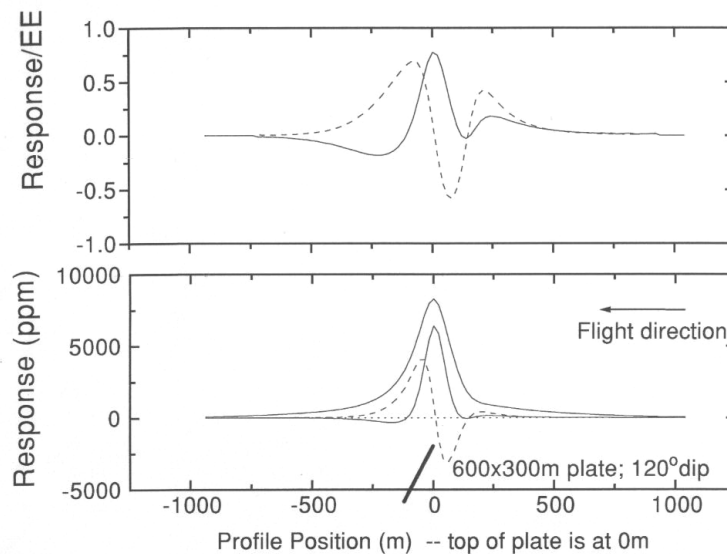
Fig. 5 (Bottom) same as Figure 4, except the plate is now dipping at 120°. On the top graph note the down-dip (left) peak on the normalized *z*-component response is larger than the right peak (c.f. Figure 4).

What little asymmetry remains in the energy envelope is a good indication of the coupling of the AEM system to the conductor. If the response profile for each component is normalized by the energy envelope, then the effect of system coupling will be removed (at least partially) and the profiles will appear more symmetric. For example, the top part of Figure 4 shows the V_x and V_z normalized by the energy envelope at each point. The size of the two *x* peaks and the two *z* peaks are now roughly comparable.

Dip determination

The response of a plate with a dip of 120º is shown on Figure 5. For the V_x/EE and V_z/EE profiles, the peak on the down dip side is larger. For shallow dips, it becomes difficult to identify both V_x/EE peaks, but the two positive V_z/EE peaks remain discernable. Plotting the ratio of the magnitudes of these two V_z/EE peaks, as has been done with solid squares on Figure 6, shows that the ratio is very close to the tangent of the dip divided by 2. Hence, calculating the ratio of the peak amplitudes (R) will yield the dip angle θ using

$$\theta = 2 \tan^{-1}(R).$$
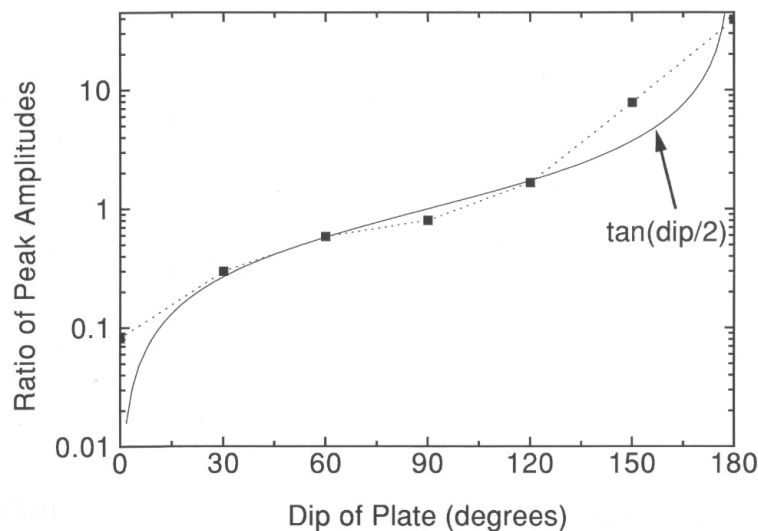
Fig. 6. The ratio of the peak amplitudes of the normalized z-component response (left/right) plotted with solid squares. The ratio plots very close to the tangent of half the dip angle θ of the plate.

Depth Determination

As the depth of the body increases, there is a corresponding increase in the distance between the two positive peaks in the V_z/EE profile. As an example of this, Figure 7 shows the case of a plate 150 m deeper than the plate of Figure 4. The peaks are now 450 m apart, as compared with 275 m on Figure 4. A plot of the peak-to-peak distances for a range of depths is shown on Figure 8 for plates with 60, 90 and 120° dips. Bec ause the points follow a straight line, it can be concluded that for near vertical bodies (60° to 120 ° dips), the depth to the top of the body d can be determined from the measured peak-to-peak distances using the linear relationship depicted in Figure 8. The expected error would be about 25 m. Such an error is tolerable in airborne EM interpretation. More traditional methods for determining d analyze the rate of decay of the measured response (Palacky and West, 1973). Our method requires only the V_z/EE response profile at a single delay time. Analyzing this response profile for each delay time allows d to be determined as a function of delay time, and hence any migration of the current system in the conductor could be tracked.
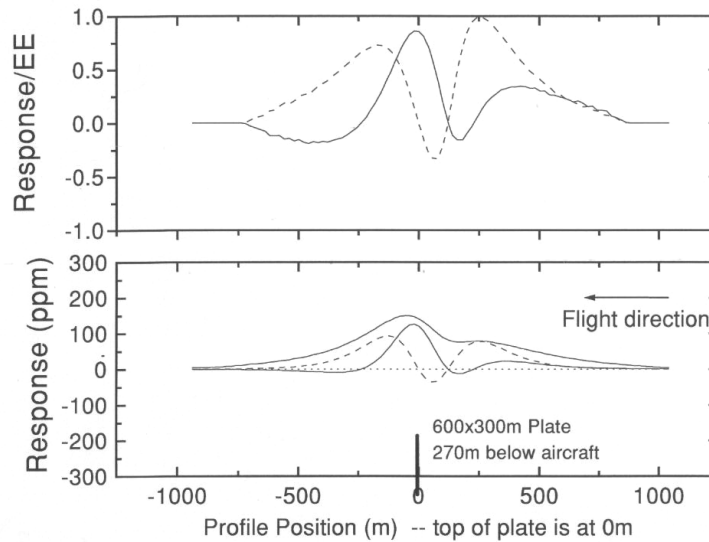
Fig. 7. The same as Figure 4, except the plate is now 270 m below the aircraft. Note that the distance between the z-component peaks is now much greater.
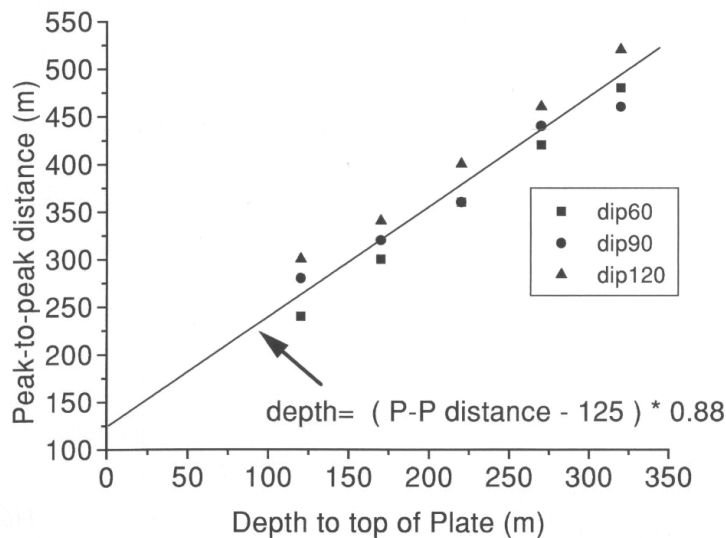
Fig. 8. The peak-to-peak distance as a function of plate depth for three different dip angles θ. A variation in dip of $\pm 30°$ does not result in a large change in the peak to peak distance.

Strike and offset determination

The response shown in Figure 4 varies in cases when the plate has a strike different from 90° or the flight path is offset from the center of the plate.

Figure 9 shows the response for a plate with zero offset and Figure 10 shows the plate when it is offset by 150 m from the profile line. The calculated voltages V_z and V_x are little changed from the no offset case, but the V_y response, is no longer zero. In fact, the shape of the V_y curve appears to be the mirror image of the V_z curve.

Profile line offset by 0m
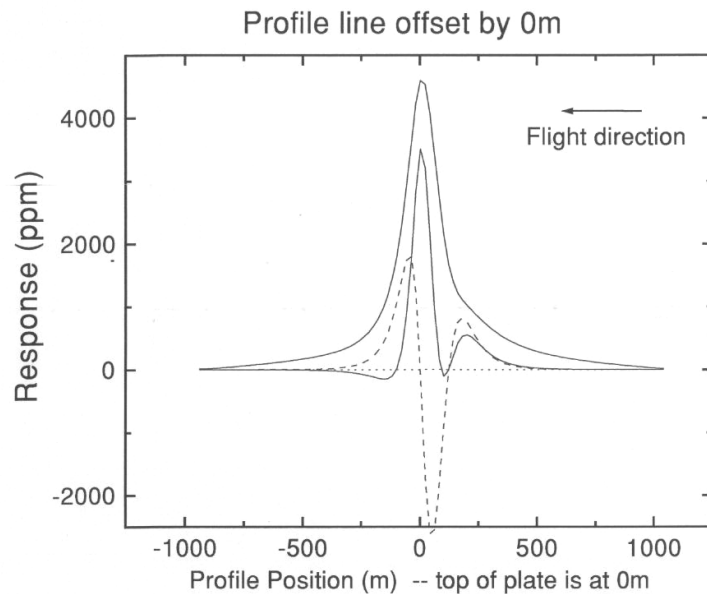
Fig. 9 The response of a 300 by 300 m plate traversed by a profile line crossing the center of the plate in a direction perpendicular to the strike of the plate (the strike angle ζ of the plate with respect to the profile line is 90°).

Profile line offset by -150m
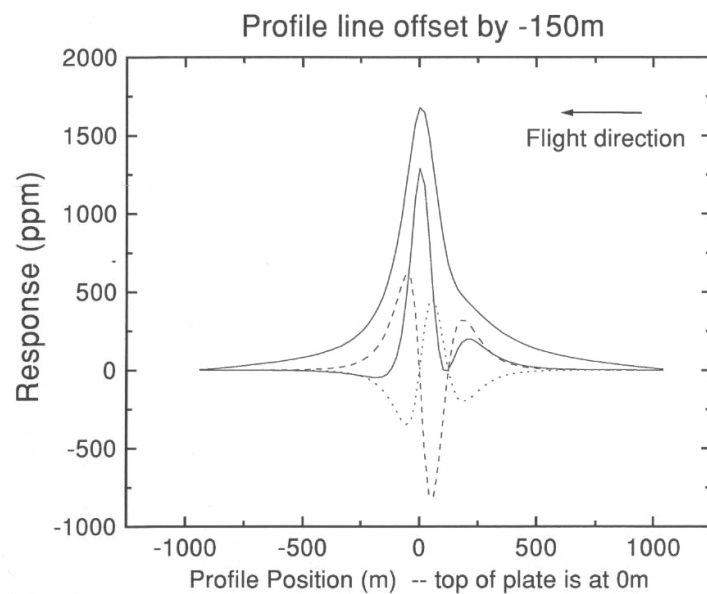
Fig. 10.   Same as Figure 9, except the profile line has been offset from the center of the plate by –150 m in the y direction (equivalent to a +150 m displacement of the plate.

In the case when the plate strikes at 45°, the *y* component is similar in shape but opposite in sign to the *x*-component response (Figure 11).
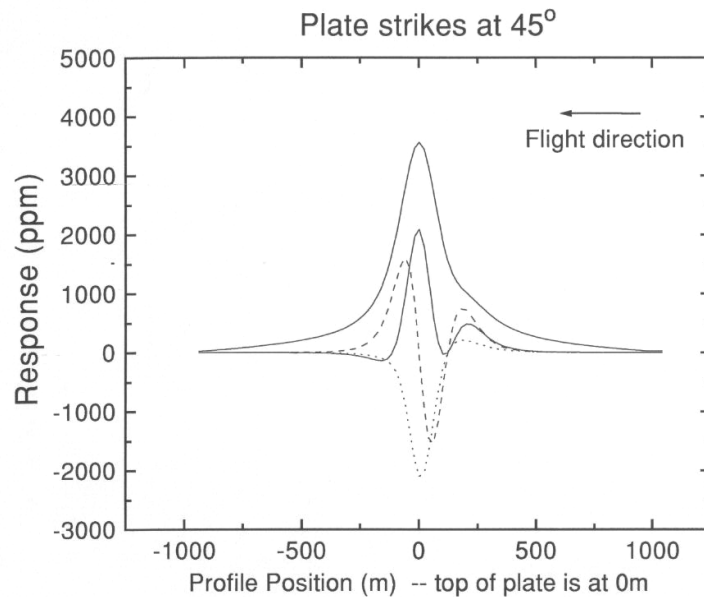
Fig. 11 Same as Figure 9, except the profile line traverses the plate such that the strike angle ζ of the plate with respect to the profile line is 45°.

These similarities can be better understood by looking at schematic diagrams of the secondary field from the plate. Figure 12 shows a plate and the field in section. For zero offset, the field is vertical (z only). As the offset increases, the aircraft and receiver moves to the right and the measured field rotates into the y-component.
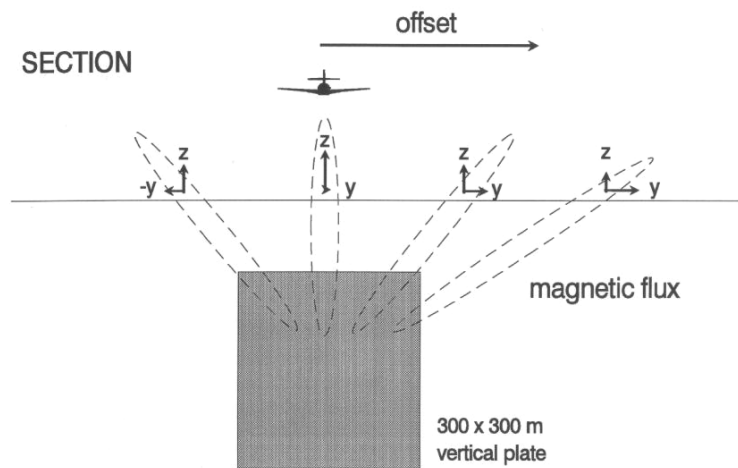
Fig. 12. A schematic diagram of the plate and the magnetic flux of the secondary field (section view). For increasing offset of the aircraft and receiver from the center of the plate, the magnetic field at the receiver rotates from the z to the y component.

The secondary field is depicted in plan view in Figure 13. Variable strike is simulated by leaving the plate stationary and changing the flight direction. When the strike of the plate is different from 90°, the effective rotation of the EM system m eans that the secondary field, which was previously measured purely in the x direction, is now also measured in the y direction.
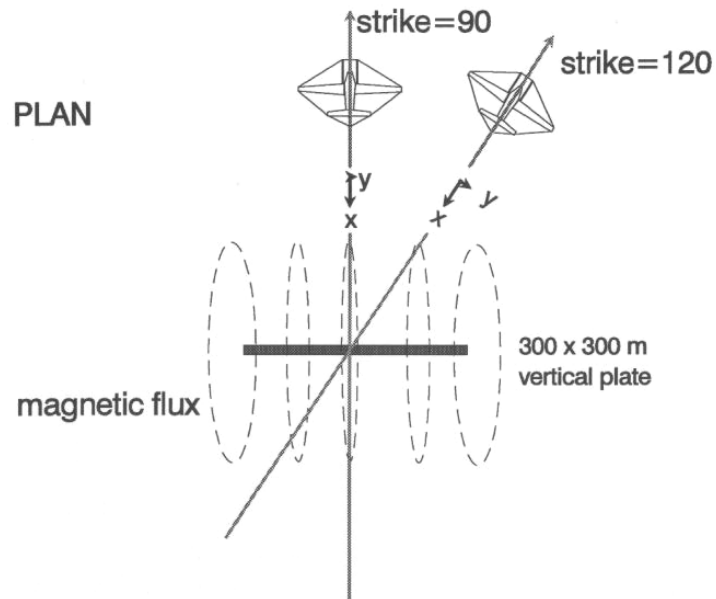
Fig. 13. A schematic diagram of the plate and the magnetic flux of the secondary field (plan view). Here varying strike is depicted by an equivalent variation of the flight direction. As the flight direction rotates from a strike angle of 90°, the receiver rotates so as to measure a greater response in the *y* direction.

The *y* component (V_y) can thus be considered to a be a mixture of V_x and V_z components, viz

$$V_y = C_{stk} V_x + C_{off} V_z ,$$

an equation that is only approximate. The response for a variety of strike angles and offset distances has been calculated and in each case the *y*-component response has been decomposed into the *x* and *z* components by solving for the constants of proportionality C_{stk} and C_{off}.

A plot of C_{stk} for the case of zero offset and varying strike direction ξ is seen on Figure 14. The values of C_{stk} determined from the data are plotted with solid squares and compared with the $\tan(90°- \xi)$. Because the agreement is so good, the formula

$$\xi = 90 - \tan^{-1} (C_{stk})$$

can be used to determine the strike. This relation was first obtained by Fraser (1972).
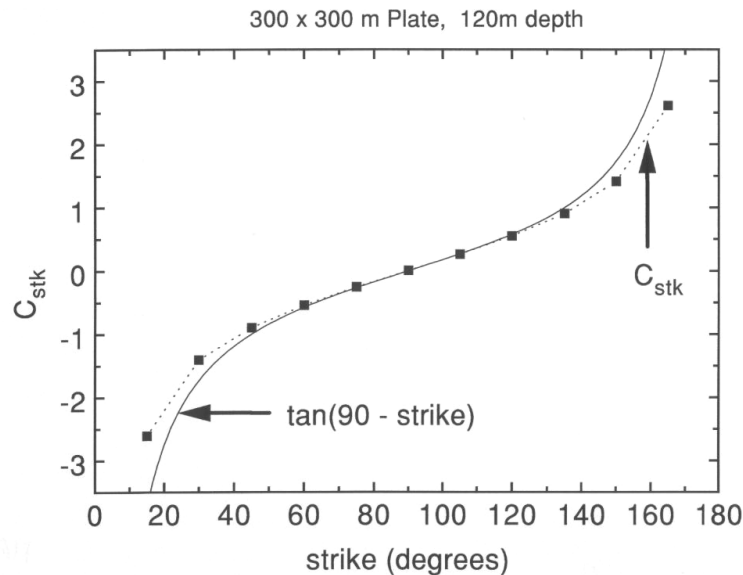
Fig. 14. The ratio $C_{stk} = V_y/V_x$ plotted as a function of varying strike angle (solid squares). The data agree very closely with the cotangent of the ζ.
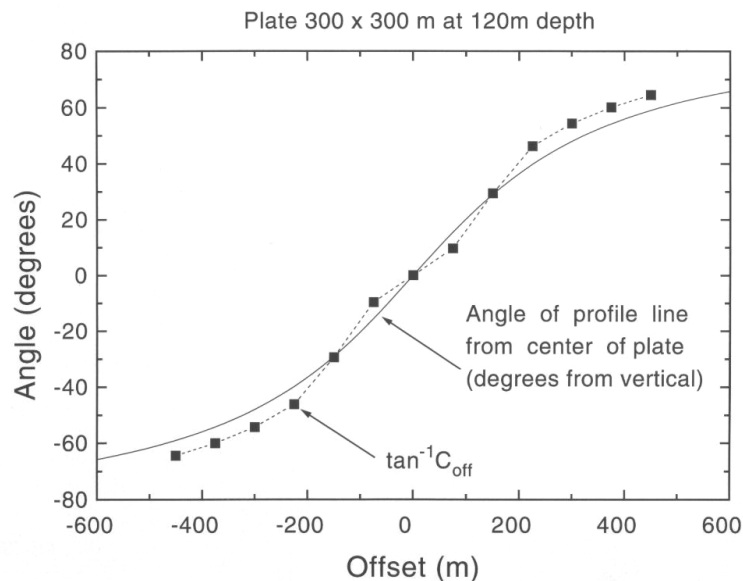
Fig. 15. The arctangent of $C_{off} = V_y/V_z$, plotted as a function of varying offset (solid squares). There is good agreement between this quantity and the angle ϕ between a vertical line and the line from the center of the top edge of the plate to the profile line.

When the strike is fixed at 90°, and the offset var ies, the corresponding values obtained for C_{off} have been plotted with solid squares on Figure 15. Again, there is good agreement with the arctangent of C_{off} and the angle ϕ between a vertical line and the line that joins the center of the top edge of the plate with the position where the aircraft traverse crosses the plane containing the plate. If an estimate of the distance to the top of the conductor D is already obtained using the method described above, or by the method described in Palacky and West (1973), then

$$D = \sqrt{(O^2 + d^2)} ,$$

(where d is the depth below surface). Hence, the offset distance O can be written as follows

$$O = d \tan (\phi)$$
$$= d\, C_{off}$$
$$= C_{off} \sqrt{(D^2 - O^2)}$$

which can be rearranged to give

$$O = C_{off}\, D / \sqrt{(1 + C_{off}^2)} .$$

Lateral delectability

Figure 12 illustrates that V_y becomes relatively strong as the lateral displacement from the conductor is increased. Thus, if V_y is measured, then the total signal will remain above the noise level at larger lateral displacements of the traverse line from the conductor. This has been illustrated by assuming a flat-lying conductor, here approximated by a wire-loop circuit of radius 125 m (Figure 16). The x, y and z components of the response have been computed using the formula for the large-loop magnetic fields in Wait (1982). The results are plotted on Figure 17 as a function of increasing lateral displacement L of the transmitter/receiver from the center of the conductor. The transmitter and receiver are separated in a direction perpendicular L to simulate the case when the system is maximal coupled to the conductor, but the flight line misses the target by an increasing amount. The effect of varying the conductance or measurement time has been removed by normalizing the response to the total response measured when the system is at zero displacement. At displacements greater than 80 m, the y component is clearly larger than any other component. Assuming the same sensitivity and noise level for each component (which is a realistic assumption if the data are corrected for coil rotation and the sferic activity is low), it is clearly an advantage to measure V_y, as this will increase the chances of detecting the target when the flight line has not passed directly over the conductor.
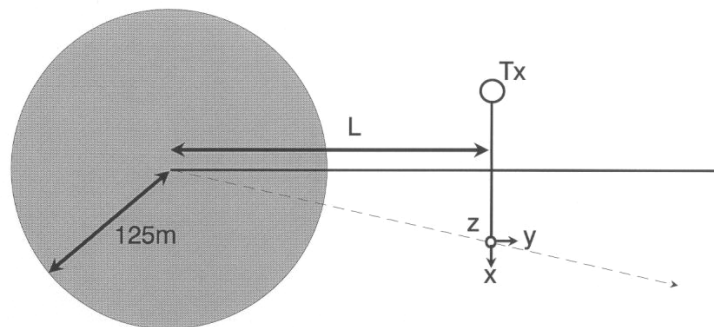
Fig. 16. Plan view of a flat-lying conductor (a circular loop with a radius of 125 m). The AEM system is offset a distance L from the center of the conductor in a direction perpendicular to the traverse direction. The traverse direction of the system is from the bottom to the top of the figure.
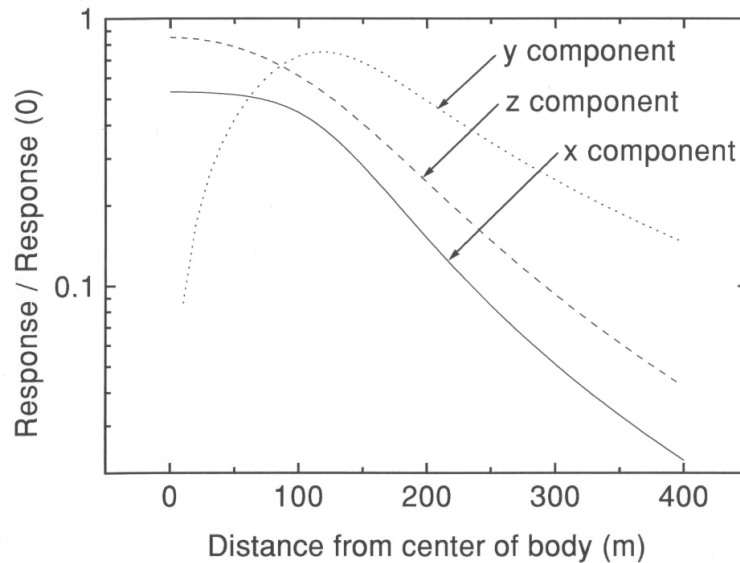
Fig. 17. The normalized response of the EM system plotted as a function of increasing offset distance *L*. The *x* component falls off most rapidly and the y component most slowly with increasing offset distance.

CONCLUSIONS

AEM systems measuring three components of the response can be used to infer more and/or better information than those systems that measure with only one component, i.e., V_x.

The *z*-component data enhances the ability of the AEM system to resolve layered structures as the *z*-component has a larger signal and a smaller proportion of sferic noise than any other component. If all the components are employed to correct for coil rotation, then the data quality and resolving power is increased further, as individual components are not contaminated by another component. Having better signal-to-noise and greater fidelity in the data will allow deeper layers to be interpreted with confidence.

A non-zero *y* component is helpful in identifying when the conductivity structure has a lateral inhomogeneity that is not symmetric about the flight line.

All components can be used to calculate the energy envelope, which is a valuable quantity to image. The energy envelope has a single peak over a vertical conductor and two peaks over a dipping conductor (one at either end). The asymmetry in the response profile of each individual component can be reduced by normalizing each profile by the energy envelope.

All three components are of great use in determining the characteristics of discrete conductors. For example, the distance between the two positive peaks in the V_z/EE profile can be employed to determine the depth. Also, the ratio of the magnitude of the two V_z/EE peaks helps to ascertain the dip of the conductor. The *x* component has been used in the past for these purposes, but is not as versatile, as it requires the data at all delay times, or an ability to identify a very small peak.

The *y* component can be utilized to extract information about the conductor that cannot be

obtained from single component AEM data. The degree of mixing between the *y* and *z* components can give the lateral offset of the conductor (provided the depth is known), while the mixing between the *y* and *x* component gives the strike of a vertical conductor.

Finally, because the *y* component decreases most slowly with increasing lateral offset, this component gives an enhanced ability to detect a conductor positioned at relatively large lateral distances from the profile line, either between lines or beyond the edge of a survey boundary.

ACKNOWLEDGMENTS

REFERENCES

Annan, A. P., 1986, Development of the PROSPECT I airborne electromagnetic system, in Palacky. G. J., Ed., Airborne resistivity mapping : Geol. Surv. Can. Paper **86-22**, 63-70.

Annan, A. P., and Lockwood, R., 1991, An application of airborne GEOTEM in Australian conditions: Expl., Geophys., **22**, 5-12.

Barnett, C. T., 1984, Simple inversion of time-domain electromagnetic data: Geophysics, **49**, 925-933.

Cull, J. P., 1993, Downhole three component TEM probes: Expl. Geophys., **24**, 437-442.

Dyck, A. V., and West G. F., 1984, The role of simple computer models in interpretations of wide-band, drill-hole electromagnetic surveys in mineral exploration: Geophysics, **49**, 957-980.

Fraser, D. C., 1972, A new multicoil aerial electromagnetic prospecting system: Geophysics, **37**, 518-537.

Frischknecht, F. C., Labson, V. F., Spies, B. R., and Anderson, W. L., 1991, Profiling methods using small sources, in Nabighian M. N., Ed., Electromagnetic methods in applied geophysics, Vol. 2, Applications: Soc. Expl. Geophys. Investigations in geophysics, no. 3, 105-270.

Hodges, D. G., Crone, J. D., and Pemberton, R., 1991, A new multiple component downhole pulse EM probe for directional interpretation: Proc. 4th Int. MGLS/KEGS Sym. on Borehole Geophys. For Min. Geotech. And Groundwater Appl.

Hogg, R. L. S., 1986, The Aerodat multigeometery, broadband transient helicopter electromagnetic system, in Palacky. G. J., Ed., Airborne resistivity mapping: Geol. Surv. Can. Paper **86-22**, 79-89.

Lee, J., 1986, A three component drill-hole EM receiver probe: M.Sc. thesis, Univ. of Toronto.

Macnae, J. C., 1984, Survey design for multicomponent electromagnetic systems: Geophysics, **49**, 265-273.

Macnae, J. C., Smith, R. S., Polzer, B. D., Lamontagne, Y., and Klinkert, P. S., 1991, Conductivity-depth imaging of airborne electromagnetic step-response data: Geophysics, **56**, 102-114.

McCracken, K. G., Oristaglio, M. L., and Hohmann, G. W., 1986, Minimization of noise in electromagnetic exploration systems: Geophysics, **51**, 819-132.

McNeill, J.D., and Labson, V., 1991, Geological mapping using VLF radio fields, in Nabighian M. N., Ed., Electromagnetic methods in applied geophysics, Vol. 2, Applications: Soc. Expl.

Geophys. Investigations in geophysics, no. 3, 521-640.

Morrison, H.F., Phillips, R.J., and O'Brien, D.P., 1969, Quantitative interpretation of transient electromagnetic fields over a layered earth: Geophys. Prosp. **17**, 82-101.

Palacky, G. J., and West, G. F., 1973, Quantitative measurements of Input AEM measurements: Geophysics, **38**, 1145-1158.

Palacky, G. J., and West, G. F., 1991, Airborne electromagnetic methods, in Nabighian M. N., Ed., Electromagnetic methods in applied geophysics, Vol. 2, Applications: Soc. Expl. Geophys. Investigations in geophysics, no. 3, 811-879.

Spies, B. R., and Frischknecht, F. C., 1991, Electromagnetic sounding, in Nabighian M. N., Ed., Electromagnetic methods in applied geophysics, Vol. 2, Applications: Soc. Expl. Geophys. Investigations in geophysics, no. 3, 285-425.

Vozoff, K., 1990, Magnetotellurics: Principles and practices: Proc. Indian Acad. Sci., **99**, 441-471.

Vozoff, K., 1991, The magnetotelluric method, in Nabighian M. N., Ed., Electromagnetic methods in applied geophysics, Vol. 2, Applications: Soc. Expl. Geophys. Investigations in geophysics, no. 3, 641-711.

Wait, J. R., 1982, Geo-electromagnetism: Academic Press Inc.

Zonge K. L., and Hughes, L. J., 1991, Controlled-source audio-magnetotellurics, in Nabighian M. N., Ed., Electromagnetic methods in applied geophysics, Vol. 2, Application: Soc. Expl. Geophys. Investigations in geophysics, no. 3, 713-809.

Appendix E

Data Archive Description

Data Archive Description:

Survey Details

Survey Area Name:	Edmonton - Red Deer Area
Job number:	09401
Client:	Alberta Energy Resources Conservation Board
Survey Company Name:	Fugro Airborne Surveys
Flown Dates:	January 27th – February 20th, 2009
Archive Creation Date:	March, 2009

Survey Specifications

Traverse Line Azimuth:	150º-330º
Traverse Line Spacing:	800 m
Tie Line Azimuth:	065º-245º
Tie Line Spacing:	14500 m
Flying Elevation:	120 m Mean Terrain Clearance
Average Aircraft Speed:	65 m/s

Geodetic Information for map products

Projection:	Alberta 10TM Projection
Datum:	NAD83
Central meridian:	115° West
False Easting:	500000 metres
False Northing:	0 metres
Scale factor:	0.9992
I.G.R.F. Model:	2005
I.G.R.F. Correction Date:	2009.1

Equipment Specifications:

Navigation

GPS Receiver:	NovAtel OEM4, 12 Channels
Aircraft:	Casa (Twin Turbo Propeller)
Video Camera:	Panasonic WV-CL302

Magnetics

Type:	Scintrex CS-2 Cesium Vapour
Installation:	Towed bird
Sensitivity:	0.01 nT
Sampling:	0.1 s

Electromagnetics

Type:	GEOTEM®, 20 channel multicoil system
Installation:	Vertical axis loop (231m^2 area with 6 turns) mounted on the aircraft. Receiver coils in a towed bird.
Coil Orientation:	X, Y and Z
Frequency:	30 Hz
Pulse width:	4036 µs
Off-time:	12590 µs
Geometry:	Tx-Rx horizontal separation of ~130 m Tx-Rx vertical separation of ~45 m
Sampling:	0.25 s

Data Windows:

Channel	Start (p)	End (p)	Width (p)	Start (ms)	End (ms)	Width (ms)	Mid (ms)
1	6	20	15	0.041	0.163	0.122	0.102
2	21	177	157	0.163	1.440	1.278	0.802
3	178	336	159	1.440	2.734	1.294	2.087
4	337	493	157	2.734	4.012	1.278	3.373
5	494	508	15	4.012	4.134	0.122	4.073
6	509	520	12	4.134	4.232	0.098	4.183
7	521	535	15	4.232	4.354	0.122	4.293
8	536	555	20	4.354	4.517	0.163	4.435
9	556	580	25	4.517	4.720	0.203	4.618
10	581	615	35	4.720	5.005	0.285	4.862
11	616	660	45	5.005	5.371	0.366	5.188
12	661	715	55	5.371	5.819	0.448	5.595
13	715	785	71	5.811	6.388	0.578	6.099
14	786	870	85	6.388	7.080	0.692	6.734
15	871	970	100	7.080	7.894	0.814	7.487
16	971	1095	125	7.894	8.911	1.017	8.403
17	1096	1245	150	8.911	10.132	1.221	9.521
18	1246	1445	200	10.132	11.759	1.628	10.946
19	1446	1695	250	11.759	13.794	2.035	12.777
20	1696	2048	353	13.794	16.667	2.873	15.230

ASCII and Geosoft Line Archive File Layout (AREA_ascii.xyz & AREA.gdb):

Field	Variable	Description	Units
1	Line	Line Number	
2	Fiducial	Seconds after Midnight	sec.
3	Flight	Flight Number	-
4	Date	Date of the Survey Flight	ddmmyy
5	Lat_NAD83	Latitude in NAD83	degrees
6	Long_NAD83	Longitude in NAD83	degrees
7	X_NAD83	Easting (X) in NAD83 Alberta 10TM Projection	m
8	Y_NAD83	Northing (Y) in NAD83 Alberta 10TM Projection	m
9	GPS_Z	GPS Elevation (above WGS84 datum)	m
10	Radar	Radar Altimeter	m
11	DTM	Terrain (above WGS84 datum)	m
12	Diurnal	Ground Magnetic Intensity	nT
13	TMI_raw	Raw Airborne Total Magnetic Intensity	nT
14	IGRF	International Geomagnetic Reference Field	nT
15	RMI	Final Airborne Residual Magnetic Intensity	nT
16	Primary_field	Electromagnetic Primary Field	µV
17	Hz_monitor	Powerline Monitor (60 Hz)	µV
18-37	x01-x20	Final dB/dt X-Coil Channels 1-20	pT/s
38-57	y01-y20	Final dB/dt Y-Coil Channels 1-20	pT/s
58-77	z01-z20	Final dB/dt Z-Coil Channels 1-20	pT/s
78-97	Bx01-Bx20	Final B-Field X-Coil Channels 1-20	fT
98-117	By01-By20	Final B-Field Y-Coil Channels 1-20	fT
118-137	Bz01-Bz20	Final B-Field Z-Coil Channels 1-20	fT
138-157	Raw_x01-Raw_x20	Raw dB/dt X-Coil Channels 1-20	pT/s
158-177	Raw_y01-Raw_y20	Raw dB/dt Y-Coil Channels 1-20	pT/s
178-197	Raw_z01-Raw_z20	Raw dB/dt Z-Coil Channels 1-20	pT/s
198-217	Raw_Bx01-Raw_Bx20	Raw B-Field X-Coil Channels 1-20	fT
218-237	Raw_By01-Raw_By20	Raw B-Field Y-Coil Channels 1-20	fT
238-257	Raw_Bz01-Raw_Bz20	Raw B-Field Z-Coil Channels 1-20	fT
258	VD1	First Vertical Derivative of RMI	nT/m
259	Res_hs_z	Apparent Resistivity (Half Space Model) from dB/dt Z	ohm-m

Note – The null values in the ASCII archive are displayed as –9999999.000000

ASCII and Geosoft RDI File Layout (AREA_RDI_ascii.xyz and AREA_RDI.gdb):

Field	Variable	Description	Units
1	Line	Line Number	
2	Fiducial	Seconds after Midnight	sec.
3	X_NAD83	Easting (X) in NAD83 Alberta 10TM Projection	m
4	Y_NAD83	Northing (Y) in NAD83 Alberta 10TM Projection	m
5	GPS_Z	GPS Elevation (above WGS84 datum)	m
6	Radar	Radar Altimeter	m
7	DTM	Terrain (above WGS84 datum)	m
8	Hz_monitor	Powerline Monitor (60 Hz)	µV
9 – 159	Resistivity	Resistivity at Depth Below Surface from 0 – 300 m at 2 m intervals	ohm-m
	Depth*	Depth Below Surface (0 – 300 m)	m
	Distance*	Distance Along Line	m

Note – The Depth and Distance fields are in the Geosoft database only.

The null values in the ASCII archive are displayed as –9999999.000000

Grid Archive File Description:

The grids are in Geosoft format. A grid cell size of 200m was used for all area grids.

File	Description	Units
ERDA_AREA_RMI.grd	Residual Magnetic Intensity	nT
ERDA_AREA_VD1(_deh).grd	First Vertical Derivative	nT/m
ERDA_AREA_Res_z.grd	Apparent Resistivity from dB/dt Z	ohm-m
ERDA_AREA_RDI_Slice_(0 to 120)m(_deh).grd	Resistivity Depth Slices for 0 to 120 m depths	ohm-m
ERDA_COMBINED_RMI.grd	Residual Magnetic Intensity merged with previous surveys	nT
ERDA_COMBINED_VD1(_deh).grd	First Vertical Derivative merged with previous surveys	nT/m
ERDA_COMBINED_30Hz_Res_z.grd	Apparent Resistivity from dB/dt Z merged with previous surveys	ohm-m
ERDA_90Hz_Res_z.grd	Apparent Resistivity from dB/dt Z for the 90Hz area only	ohm-m
ERDA_COMBINED_RDI_Slice_(0 to 120)m(_deh).grd	Resistivity Depth Slices for 0 to 120m depths merged with previous surveys	ohm-m

The *_deh files are the grid files corrected for asymmetry ("de-herringboned"). This was also applied to the First Vertical Derivative as a method of smoothing the high frequency content.

Resistivity Depth Section grid archive Description:

The resistivity depth section grids are named according to the following convention:

rdi*LINE(_trc)*.grd

where **LINE** is the line number of the section grid and **trc** refers to sections that are terrain

corrected. Grids are in Geosoft binary format with units in ohm-metres.

SEG-Y Archive Description:

Two sets of the resistivity SEG-Y files were archived. One set relative to surface and one set shifted to be referenced to a datum of 1865 metres (West) and 1085 (East), above the WGS84 spheroid. Both the shifted and non-shifted SEG-Y files have identical names and are differentiated by the directories in which they are contained (surface, datum). The SEG-Y files are named according to the following convention:

sgy***LINE***.sgy

where ***LINE*** is the survey line number.
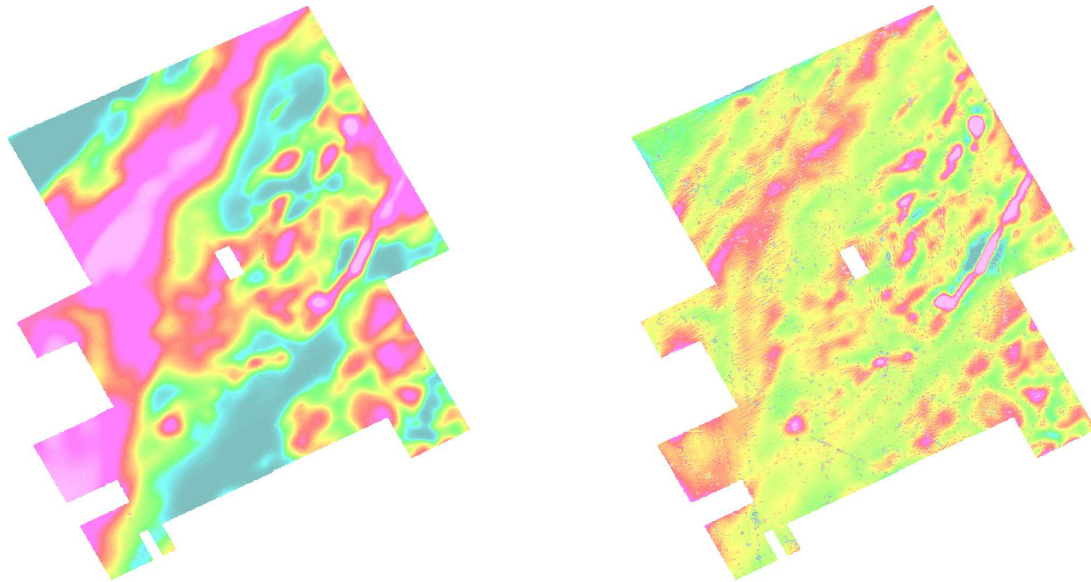
Appendix F

Map Product Grids

Figure 1. Residual Magnetic Intensity (left) and First Vertical Derivative of Residual Magnetic Intensity (right)
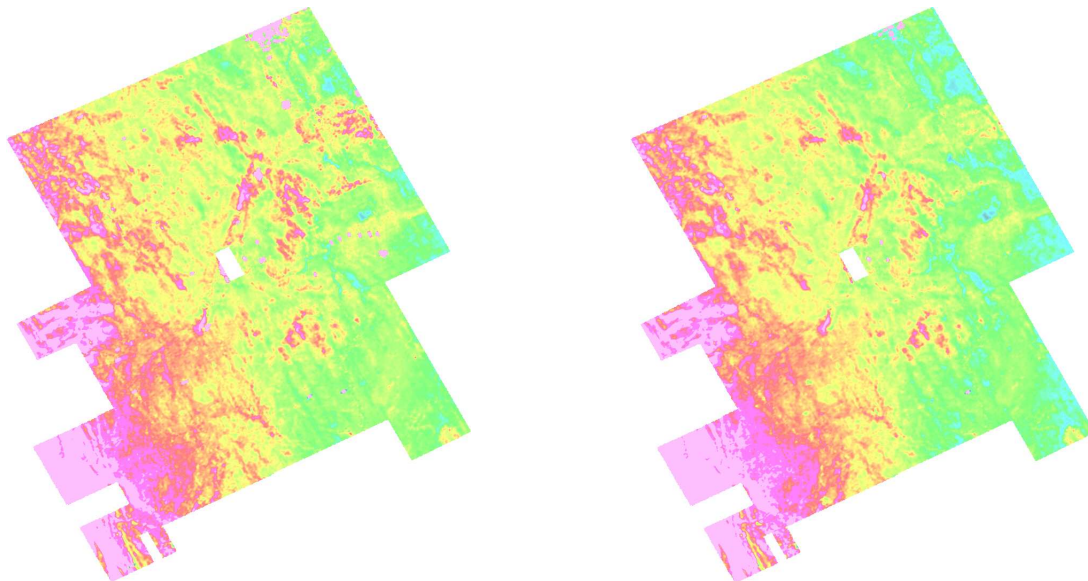

Figure 2. Resistivity Depth Slices at 10 metres (left) and 30 metres (right)
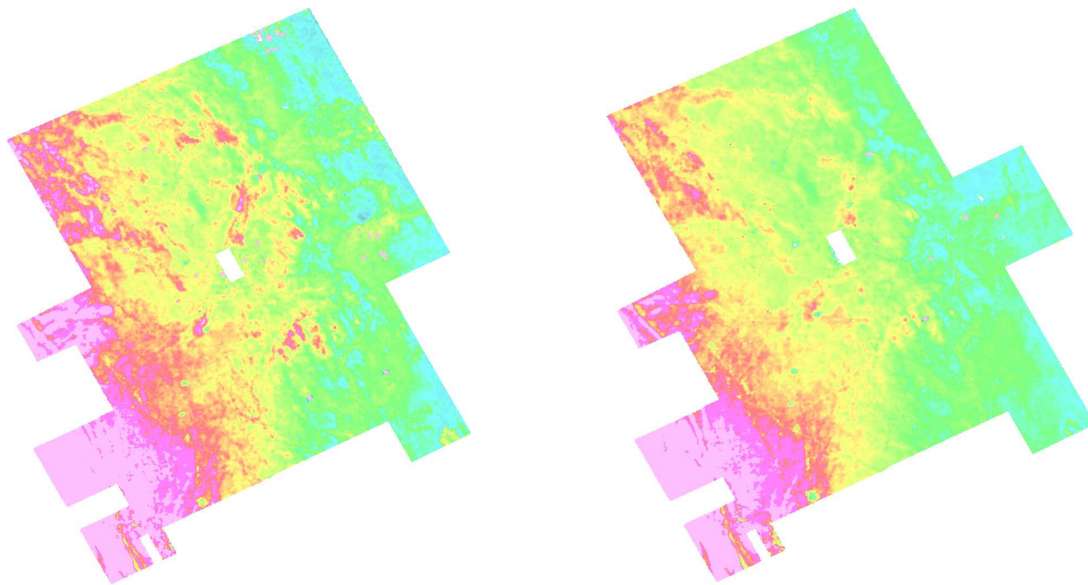
Figure 3. Resistivity Depth Slices at 60 metres (left) and 120 metres (right)

Figure 4. Apparent Resistivity Derived from dB/dt Z Coil Channels 1 to 20

Reference Waveform Descriptor:

The information shown is only an example. The actual reference waveforms are provided on CD-ROM or DVD and will have been renamed to ptaFLTpre.out / ptaFLTpost.out, "FLT" represents the flight number.

The reference waveform can be divided into four main sections, which are described below.

Section 1

This section contains the name of the raw reference waveform file (i.e. D0050704.002). The approximate horizontal and vertical offsets (i.e. 125 m and 50 m) of the EM bird position in meters are listed. These are followed by the base frequency (i.e. 90Hz) in Hertz and the sample interval (i.e. 43.4 µs) in microseconds.

```
GEOTEM Calibration Data - Version 31 July 1998
 'D0050704.002' = Name of original saved parameter table file
      125.000000000000000 = Horizontal TX-RX separation in meters
       50.000000000000000 = Vertical   TX-RX separation in meters
       90.000000000000000 = Base Frequency in Hertz
       43.402777777777779 = Sample Interval in micro-seconds
```

Section 2

This section displays the gate configuration for channels 1 to 20.

```
       20 Time Gates:  First and Last Sample number, RMS chart position:

          Start & end samples of each channel

     1          4          11          1
     2         12          25          2
     3         26          39          3
     4         40          53          4
     5         54          59          5
     6         60          61          6
     7         62          64          7
     8         65          67          8
     9         68          71          9
    10         72          75         10
    11         76          79         11      Channels 1 to 20
    12         80          83         12
    13         84          87         13
    14         88          92         14
    15         93          97         15
    16         98         102         16
    17        103         108         17
    18        109         114         18
    19        115         121         19
    20        122         128         20
```

Section 3

This section contains the different types of conversion factors for each of the components. If the data is provided in ppm the standard procedure is to normalize the data based on the individual components. Three different conversion factors are provided. The first factor converts the data to ppm based on the peak voltages of each individual component. The second factor converts the data to ppm based on the "total" peak voltage which is actually the RMS value of the 3 components. The third factor converts each component to standard SI units, which are Teslas per second for the dB/dt data and Teslas for the B-field data.

Component:	dBx/dt	dBy/dt	dBz/dt	Bx	By	Bz
IndivPPM_per_DataUnit:	0.1112428E-01	1.106797	0.2890714E-01	0.1519028E-01	1.670836	0.3945841E-01
TotalPPM_per_DataUnit:	0.1038160E-01	0.1038160E-01	0.1038160E-01	0.1417559E-01	0.1417559E-01	0.1417559E-01
SI_Units_per_DataUnit:	0.1000000E-11	0.1000000E-11	0.1000000E-11	0.1000000E-14	0.1000000E-14	0.1000000E-14

Section 4

The last section contains the reference waveform. Each column represents a component (i.e. dBx/dt). The data units (i.e. pT/s) for each component are displayed in the second row. The first column is the sample number. The transmitter channel (TX) values have been converted to transmitter moment value (transmitter current x loop area x number of turns)

For this example there are 128 samples.

Component:	TX	dBx/dt	dBy/dt	dBz/dt	Bx	By	Bz
DataUnits:	Am^2	pT/s	pT/s	pT/s	fT	fT	fT

128 Samples:

	TX	dBx/dt	dBy/dt	dBz/dt	Bx	By	Bz
1	1161.572	38526.84	924.7899	14929.63	-164386.1	447.8830	-57789.91
2	1182.870	37266.81	431.6681	14992.79	-162768.6	466.6186	-57139.19
3	2471.644	130950.8	4966.128	46394.08	-157085.0	682.1624	-55125.55
4	18579.32	3142793.	4921.018	1117837.	-20679.01	895.7482	-6608.309
125	-1089.137	-41458.52	-304.3134	-15670.09	166886.3	-413.2204	58736.67
126	-1000.563	-40324.45	-44.37050	-14808.83	165136.1	-415.1462	58093.93
127	-1006.226	-39601.37	61.07057	-14660.24	163417.3	-412.4956	57457.63
128	-1134.029	-39423.19	-546.7703	-15091.65	161706.2	-436.2269	56802.61